



Kinetics and Mechanism of Oxidation of Neomycin and Streptomycin Antibiotics by Alkaline Permanganate

Ahmed Fawzy^{a,b,*}, Metwally Abdallah^{a,c} and Nada Alqarni^{a,d,*}

^a Chemistry Department, Faculty of Applied Sciences, Umm Al-Qura University, Makkah, Saudi Arabia

^b Chemistry Department, Faculty of Science, Assiut University, Assiut, Egypt

^c Chemistry Department, Faculty of Science, Benha University, Benha, Egypt

^d Chemistry Department, Faculty of Science, Bisha University, Bisha, Saudi Arabia

ARTICLE INFO

Article History:

Submission date: 05/05/2020

Accepted date: 22/06/2020

Keywords:

Kinetics, Mechanism, Permanganate, Oxidation, Antibiotics.

ABSTRACT

The kinetics and mechanistic aspects of oxidation of two aminoglycoside antibiotics, namely, neomycin and streptomycin by permanganate ion (MnO_4^-) in alkaline solutions were examined spectrophotometrically. The stoichiometry of the reactions between the investigated antibiotics and MnO_4^- were set to be 8.0 ± 0.3 mol. The reactions exhibited first order dependence regarding to $[MnO_4^-]$ and less-than unit order dependences with respect to antibiotics and OH^- concentrations. Under the same investigational conditions, the rate of oxidation of streptomycin was found to be about seven times more than that of neomycin. The impact of ionic strength of the reactions medium was explored which revealed that as the ionic strength increases the oxidation rates are also increased. Also, the influence of temperature was studied and the activation parameters were calculated and discussed. The plausible reactions mechanism was proposed and the appropriate rate-law expression consisted with the acquired investigational kinetic results was derived.

1. Introduction

Antibiotics, a kind of pharmaceutical drugs, are composed of synthetic or natural organic compounds employed to cure, treat or prevent human and animal diseases. However, antibiotics are regarded as one of the dangerous pollutants for the environment and human health if they reach to the environment because they contain complex organic compounds in their structures [1]. It was reported [2-10] that antibiotics are greatly susceptible to oxidation which can be a relatively common technique for antibiotics degradation [3,6]. Hence, oxidation of antibiotics is regarded as a presumed way for removal of antibiotics from the environment to care for the human health. During the oxidation process, oxidizing agents convert the polluted substances to less harmful ones that are safe to be discharged into the environment [3,5,7,10]. Furthermore, study of the kinetics of oxidation of antibiotics have significantly help in identifying the mechanism of conversions of such organic compounds in biological systems. A detailed literature review revealed little published studies on the kinetics of oxidative removal of antibiotics in different media [2-5,8-10].

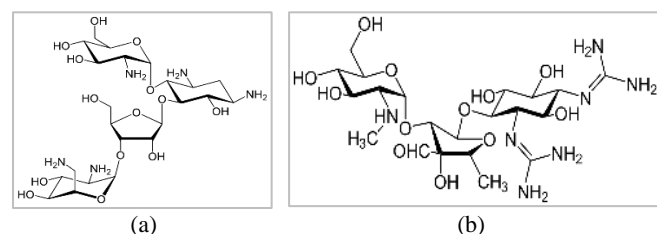


Figure 1: Chemical structures of (a) streptomycin (STR) and (b) neomycin (NOM).

In the light of the above mentioned aspects, this investigation deals with the kinetics and mechanism of oxidation of two aminoglycoside antibiotics, viz. neomycin and streptomycin, (their structures are illustrated in Figure 1) using one of the supreme significant, powerful, cheap and green oxidants, namely, permanganate ion (MnO_4^-) [11-15] in alkaline solutions. This investigation aimed to explore the

selectivity of the examined antibiotics towards permanganate ion oxidant and to comprehend the reactive species of both reactants in alkaline solutions. The activation parameters were planned to determine and discuss. Furthermore, the study is extended to propose a plausible reactions mechanism as well as to establish the rate-law expression consistent with the obtained kinetic results.

2. Results and Discussion

2.1. Spectral Changes

Spectral changes during the oxidation of neomycin (NOM) and streptomycin (STP) by permanganate ion are shown in Figure 2 (a) and (b), respectively. These figures showed a continuous decay of MnO_4^- ion band at $\lambda = 526$ nm as the reactions advanced. This behavior indicated reduction of permanganate ion as a result of oxidation of such antibiotics. From Figure 2, it can be observed that the rate of oxidation of streptomycin was significantly higher than that of neomycin under the same investigational conditions which may be due to the structural difference between the two antibiotics and presence of two very reactive guanidine groups ($-NH=C(NH_2)_2$) in streptomycin. A careful examination of the spectral scans in case of neomycin antibiotic, shown in Figure 3(a,b), confirmed construction of Mn^{VI} intermediate by detecting the new peak at 606 nm [13]. Also, additional proof of the construction of Mn^{VI} transient species was the continued appearance of the green color as the oxidation reactions proceeded [11,12,15].

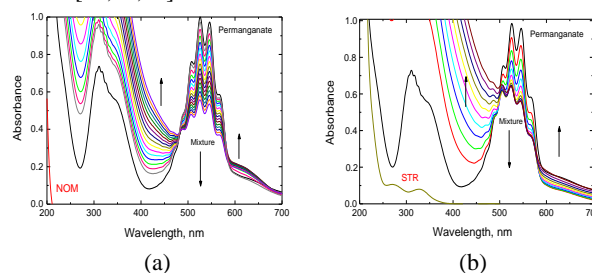


Figure 2: Spectral changes during oxidation of: (a) neomycin (NOM) and (b) streptomycin (STP) by alkaline permanganate. $[MnO_4^-] = 4.0 \times 10^{-4}$, $[A] = 5.0 \times 10^{-3}$, $[OH^-] = 5.0 \times 10^{-3}$ and $I = 0.1$ mol dm^{-3} at $T = 298$ K.

* Corresponding Author

Chemistry Department, Faculty of Applied Sciences, Umm Al-Qura University, Makkah, Saudi Arabia.

E-mail address: sfsaad13@yahoo.com (A. Fawzy), alqarni.nada@yahoo.com (N. Alqarni)

1685-4732 / 1685-4740 © 2020 UQU All rights reserved.

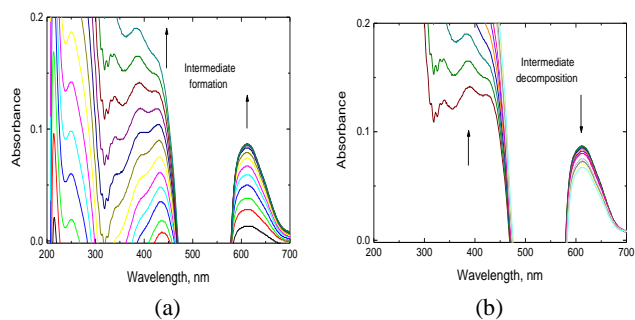


Figure 3: Spectral changes during: (a) construction, and (b) decay of Mn^{VI} intermediate complex in the oxidation of neomycin by alkaline permanganate. $[MnO_4^-] = 4.0 \times 10^{-4}$, $[NOM] = 5.0 \times 10^{-3}$ and $I = 0.1 \text{ mol dm}^{-3}$ at $T = 298 \text{ K}$.

2.2. Reactions Stoichiometry

A set of reaction mixtures containing various ratios of antibiotic, $[A] / [MnO_4^-]$, were equilibrated in a dark place for about 24 h until completion of the reactions in all mixtures at constant $[OH^-]$ and at room temperature. Determination of unreacted $[MnO_4^-]$ spectrophotometrically at $\lambda_{max} = 526 \text{ nm}$ indicated that the stoichiometric ratios of $([MnO_4^-] / [A]_0)$, were set to be $8.0 \pm 0.3 \text{ mol}$, i.e. each mole of antibiotic was consumed eight moles of permanganate ion.

2.3. Effect of Permanganate Oxidant

The oxidation reactions of both neomycin (NOM) and streptomycin (STR) with permanganate ion in alkaline solutions were investigated at different $[MnO_4^-]_0$, while other reactants concentrations were kept constant. The investigational results showed that the first order rate constant plots were straight lines for more than two half-lives of the reactions completion as illustrated in Figure 4. In addition, change of the initial concentration of the oxidant was set to have no significant effect on the observed first order rate constant values (k_{obs}) as listed in Table 1. These results indicated that such reactions were first order regarding to $[MnO_4^-]$.

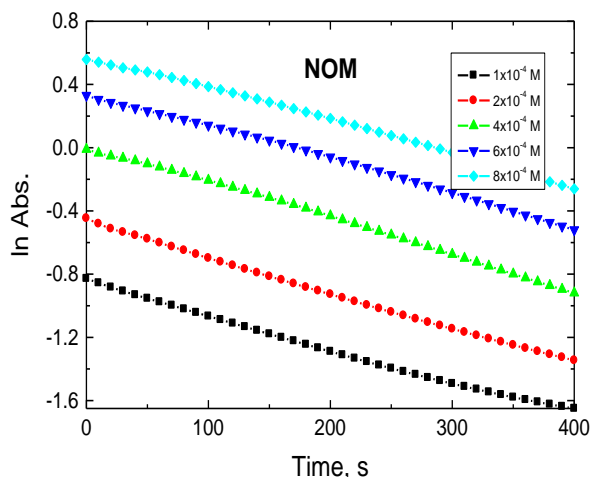


Figure 4: Effect of $[MnO_4^-]$ on the first order plot in the alkaline permanganate oxidation of neomycin (NOM) at $[NOM] = 5.0 \times 10^{-3}$, $[OH^-] = 5.0 \times 10^{-3}$, $I = 0.1 \text{ mol dm}^{-3}$ and $T = 298 \text{ K}$.

2.4. Effect of Antibiotics

In this context, the kinetics experiments were performed at variety of concentrations of the investigated antibiotics, $[A]$, at constant concentrations of MnO_4^- and OH^- , ionic strength and temperature. The values of k_{obs} listed in Table 1 indicated that the reaction rates were set to increase with increasing $[A]$. The plots of k_{obs} versus $[A]$ were linear with positive intercepts on the k_{obs} axes as shown in Figure 5(a). Also, the plots of $\log [A]$ versus $\log k_{obs}$ gave good straight lines with slopes of less-than unity as illustrated in Figure 5(b) indicating the fractional-first order credences with respect to $[A]$.

2.5. Effect of $[OH^-]$

To clarify the reactions mechanism, the oxidation rates of the examined antibiotics by alkaline permanganate was measured at various $[OH^-]$. The experimental results indicated that the reaction rates were increased with rising $[OH^-]$ as manifested from the acquired

values k_{obs} listed in Table 1. The plots of k_{obs} versus $[OH^-]$ gave straight lines with positive intercepts on the k_{obs} axes as shown in Figure 6(a). Also, the plots of $\log k_{obs}$ versus $\log [OH^-]$ were set to be straight lines with slopes of 0.894 and 0.883 for neomycin and streptomycin, respectively, as illustrated in Figure 6(b), indicating that these reactions were less-than unit order dependences in $[OH^-]$.

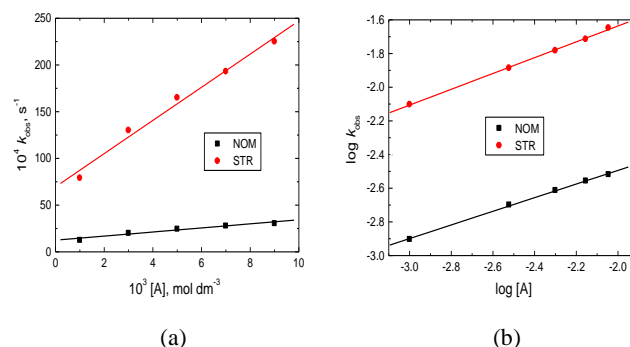


Figure 5: (a) Plots of k_{obs} vs. $[A]$, and (b) plots of $\log k_{obs}$ vs. $\log [A]$ in the alkaline permanganate oxidation of antibiotics at $[MnO_4^-] = 4.0 \times 10^{-4}$, $[OH^-] = 5.0 \times 10^{-3}$, $I = 0.1 \text{ mol dm}^{-3}$ and $T = 298 \text{ K}$.

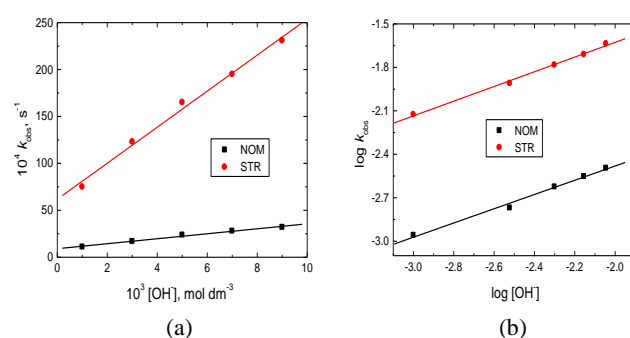


Figure 6: (a) Plots of k_{obs} vs. $[OH^-]$, and (b) plots of $\log k_{obs}$ vs. $\log [OH^-]$ in the alkaline permanganate oxidation of antibiotics at $[A] = 5.0 \times 10^{-4}$, $[MnO_4^-] = 4.0 \times 10^{-4}$, $I = 0.1 \text{ mol dm}^{-3}$ and $T = 298 \text{ K}$.

2.6. Effect of Ionic Strength

To explore the nature of the reactive species and, therefore, to the suggested reactions mechanism, kinetic measurements were performed at firm alkali and antibiotic concentrations while the concentration of sodium perchlorate was increased. The results indicated that the rates of the oxidation reactions were increased as the ionic strength (I) of the reactions media increased as observed from the values of k_{obs} listed in Table 1. The Debye-Hückel plots were set to be linear with positive slopes as illustrated in Figure 7. These results suggested that oxidation reactions occurred between ions of similar charges [16].

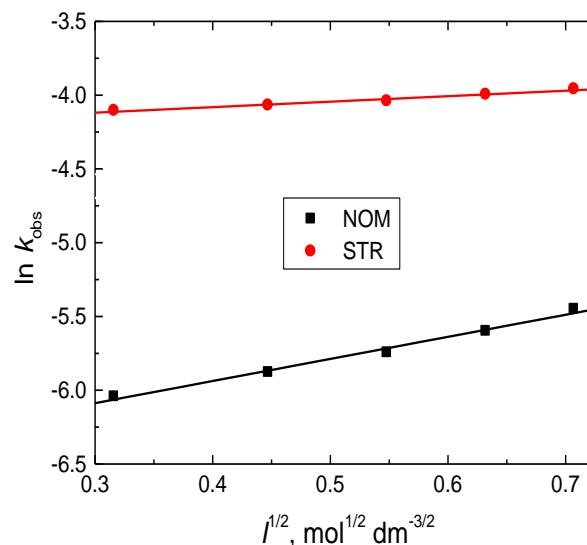


Figure 7: Debye-Hückel plots in the alkaline permanganate oxidation of antibiotics at $[A] = 5.0 \times 10^{-3}$, $[MnO_4^-] = 4.0 \times 10^{-4}$, $[OH^-] = 5.0 \times 10^{-3} \text{ mol dm}^{-3}$ and $T = 298 \text{ K}$.

Table 1: Effect of $[\text{MnO}_4^-]$, $[\text{A}]$, $[\text{OH}^-]$ and I on the values of k_{obs} in the alkaline permanganate oxidation of antibiotics at $T = 298 \text{ K}$.

$10^4 [\text{MnO}_4^-]$ (mol dm^{-3})	$10^3 [\text{A}]$ (mol dm^{-3})	$10^3 [\text{OH}^-]$ (mol dm^{-3})	I (mol dm^{-3})	$10^4 k_{\text{obs}}$ (s^{-1})	
				NOM	STR
1.0	5.0	5.0	0.1	24.07	161.21
2.0	5.0	5.0	0.1	23.21	162.04
4.0	5.0	5.0	0.1	23.75	160.32
6.0	5.0	5.0	0.1	23.27	161.94
8.0	5.0	5.0	0.1	22.98	159.82
4.0	1.0	5.0	0.1	12.50	79.35
4.0	3.0	5.0	0.1	19.79	129.88
4.0	5.0	5.0	0.1	23.75	160.32
4.0	7.0	5.0	0.1	27.78	193.08
4.0	9.0	5.0	0.1	30.30	221.99
4.0	5.0	1.0	0.1	11.33	75.30
4.0	5.0	3.0	0.1	17.21	123.17
4.0	5.0	5.0	0.1	23.75	160.32
4.0	5.0	7.0	0.1	28.24	194.96
4.0	5.0	9.0	0.1	31.99	231.12
4.0	5.0	5.0	0.1	23.75	160.32
4.0	5.0	5.0	0.2	28.11	171.41
4.0	5.0	5.0	0.3	32.27	176.04
4.0	5.0	5.0	0.4	37.07	184.00
4.0	5.0	5.0	0.5	43.15	191.16

2.7. Effect of Temperature

In order to evaluate the activation parameters, the reactions were conveyed out at different temperatures at firm other variables. The experimental results indicated that the rates of the reactions were set to speed up by rising temperature as listed in Table 2. On the other hand, both Eyring and Arrhenius plots of the second order rate constant values (k_2) were linear as shown in Figures 8(a) and (b), correspondingly. The activation parameters were evaluated from these plots and are inserted in Table 3.

2.8. Polymerization Test

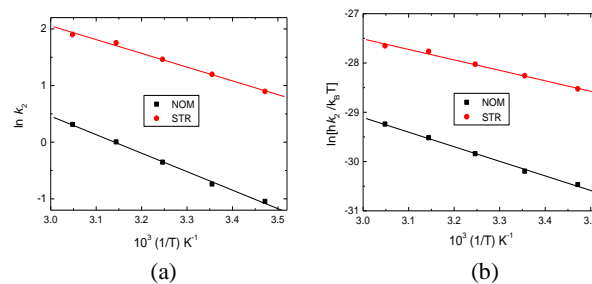
The possibility of formation of free radicals in the existing oxidation reactions was explored by acrylonitrile test. This test was conveyed out by the addition of a definite acrylonitrile quantity to the reaction mixture in an inert atmosphere for about 4 hours. No polymerization appeared in all reaction mixtures (as no white precipitates were formed) indicating that the present oxidation reactions did not proceed via intervention of free radicals.

Table 2: Effect of temperature on the values of k_{obs} in the alkaline permanganate oxidation of antibiotics at $[\text{A}] = 5.0 \times 10^{-3}$, $[\text{MnO}_4^-] = 4.0 \times 10^{-4}$, $[\text{OH}^-] = 5.0 \times 10^{-3}$ and $I = 0.1 \text{ mol dm}^{-3}$.

T (K)	$10^4 k_{\text{obs}}$ (s^{-1})	
	NOM	STR
288	17.51	122.07
298	23.75	160.32
308	34.92	215.31
318	49.83	288.14
328	68.06	332.93

Table 3: Activation parameters of k_2 in the alkaline permanganate oxidation of antibiotics at $[\text{A}] = 5.0 \times 10^{-3}$, $[\text{MnO}_4^-] = 4.0 \times 10^{-4}$, $[\text{OH}^-] = 5.0 \times 10^{-3}$ and $I = 0.1 \text{ mol dm}^{-3}$.

Antibiotic	ΔS^\ddagger $\text{J mol}^{-1}\text{K}^{-1}$	ΔH^\ddagger kJ mol^{-1}	ΔG^\ddagger_{298} kJ mol^{-1}	E_a^\ddagger kJ mol^{-1}
NOM	-169.07	24.61	74.99	27.10
STR	-175.41	18.02	70.29	19.89

**Figure 8:** (a) Eyring plots, and (b) Arrhenius plots of k_2 in the alkaline permanganate oxidation of antibiotics at $[\text{A}] = 5.0 \times 10^{-3}$, $[\text{MnO}_4^-] = 4.0 \times 10^{-4}$, $[\text{OH}^-] = 5.0 \times 10^{-3}$ and $I = 0.1 \text{ mol dm}^{-3}$.

2.9. Suggested Reactions Mechanism

In the light of the investigational kinetic outcomes, the appreciable reactions mechanism was suggested and can be discussed as follows. The first step is the rapid deprotonation of antibiotic molecules (A) according to the following equation:



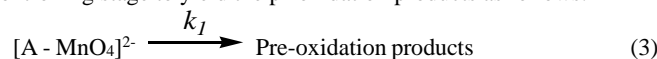
The deprotonated form (A^-) appears to be the reactive species in the rate-controlling stage of the proposed reactions mechanism. This suggested step is based on increasing the oxidation rates upon increasing alkali concentration as well as the structures of the examined antibiotics [17].

The second step of the suggested mechanism is the attack of MnO_4^- on the deprotonated antibiotic to construct a complex, $[\text{A} - \text{MnO}_4]^{2-}$ (C), Eq. (2):



Complex construction during the oxidation reactions by MnO_4^- in alkaline solutions was reported earlier [18-21]. Furthermore, such complexation was approved spectrophotometrically by the achieved UV-Vis spectra as shown in Figures 2 and 3, as well as kinetically as the plots of $1/k_{\text{obs}}$ vs. $1/[\text{A}]$ were linear with positive slopes [22] as shown in Figure 9(a).

Then, the formed transient complex (C) decomposed in the rate-controlling stage to yield the pre-oxidation products as follows:



The latter interacts with other seven MnO_4^- ions in subsequent fast steps to yield the final oxidation products of the antibiotics.

According to the suggested mechanism, the rate law expressing the relationship between the reaction rate and the concentrations of antibiotic, OH^- and oxidant was derive as in Eq. (4):

$$\text{Rate} = \frac{k_1 K_1 K_2 [\text{A}][\text{OH}^-][\text{MnO}_4^-]}{1 + K_1[\text{OH}^-] + K_1 K_2 [\text{OH}^-][\text{A}]} \quad (4)$$

Also, k_{obs} equation was derived, Eq. (5):

$$k_{\text{obs}} = \frac{k_1 K_1 K_2 [\text{A}][\text{OH}^-]}{1 + K_1[\text{OH}^-] + K_1 K_2 [\text{OH}^-][\text{A}]} \quad (5)$$

Rearranging Eq. (5) led to the following two equations:

$$\frac{1}{k_{\text{obs}}} = \left(\frac{1 + K_1[\text{OH}^-]}{k_1 K_1 K_2 [\text{OH}^-]} \right) \frac{1}{[\text{A}]} + \frac{1}{k_1} \quad (6)$$

$$\frac{1}{k_{\text{obs}}} = \left(\frac{1}{k_1 K_1 K_2 [\text{A}]} \right) \frac{1}{[\text{OH}^-]} + \left(\frac{1}{k_1 K_2 [\text{A}]} + \frac{1}{k_1} \right) \quad (7)$$

Regarding to Eqs. (6) and (7), the plots of $1/k_{\text{obs}}$ versus $1/[\text{A}]$ at constant $[\text{OH}^-]$ and $1/k_{\text{obs}}$ versus $1/[\text{OH}^-]$ at constant $[\text{A}]$ must be linear with positive intercepts on the $1/k_{\text{obs}}$ axes as were experimentally found to be so as illustrated in Figures 9(a) and (b), respectively. The values of the slow step of the proposed reactions mechanism (k_1) and the equilibrium constants (K_1 and K_2) were calculated from these plots and are inserted in Table 4.

Table 4: Values of k_1 , K_1 and K_2 in the alkaline permanganate oxidation of antibiotics. $[A] = 5.0 \times 10^{-3}$, $[MnO_4^-] = 4.0 \times 10^{-4}$, $[OH^-] = 5.0 \times 10^{-3}$, $I = 0.1$ mol dm^{-3} at $T = 298$ K.

Antibiotic	Constant		
	$10^2 k_1, s^{-1}$	$K_1, dm^3 mol^{-1}$	$10^2 K_2, dm^3 mol^{-1}$
NOM	0.35	16.4	52.37
STR	2.65	30.00	25.13

2.10. Activation Parameters

The calculated activation parameters listed in Table 3 were found to be in a good accord with the suggested oxidation reactions mechanism. The acquired higher negative values of ΔS^\ddagger suggested formation of complexes amongst the reacting species. Also, the positive values of both ΔH^\ddagger and ΔG^\ddagger indicated that such complexes formation was endothermic and non-spontaneous, respectively [16]. The higher values of E_a^\ddagger proposed that the rate-determining step was the decomposition of the formed complexes.

3. Conclusions

The kinetics of oxidation of neomycin and streptomycin by permanganate ion in alkaline solution were studied. Under the same investigational conditions, the rate of oxidation of streptomycin was found to be about seven times more than that of neomycin. The activation parameters were calculated and discussed. The appreciable reactions mechanism was proposed. The rate-law expression in consistent with the obtained results was derived.

4. Experimental

4.1. Materials and Methods

All employed chemicals were from Merck or Sigma in spectroscopic grade and were used as supplied. Doubly distilled water was utilized to prepare all the solutions. Fresh solutions of neomycin and streptomycin antibiotics were prepared by dissolving their weighted samples in doubly distilled water. Potassium permanganate solution was prepared and standardized as reported earlier [14]. The reactions temperature were equilibrated within ± 0.1 °C.

Kinetic experiments were conveyed out at pseudo-first order conditions where the concentrations of the examined antibiotics were presented in excess higher than that of permanganate concentration at constant ionic strength and temperature. A Shimadzu UV-1800 PC automatic scanning double-beam spectrophotometer was utilized to measuring the absorbance readings of the existing reactions. The reactions were followed by recording the decrease of permanganate ion absorbance at its absorption maximum, $\lambda = 526$ nm, with time. All experiments were carried out at least two times and the rate constants were found to be reproducible in the range of ± 3 %.

Author Contributions: All authors contributed to the study conception and design. Material preparation, data collection and analysis were performed by [Nada Alqarni], [Ahmed Fawzy] and [Metwally Abdallah]. The first draft of the manuscript was written by [Ahmed Fawzy] and all authors commented on previous versions of the manuscript. All authors read and approved the final manuscript.

Acknowledgments: Authors strongly acknowledge Chemistry Department, Faculty of Applied Sciences and Umm Al-Qura University in Makkah, Saudi Arabia, for the facilities and providing the chemicals and apparatus.

Conflicts of Interest: The authors declare no conflict of interest.

References

[1] D. Ann-Marie. Pharmaceuticals in industrial wastewater and their removal using photo-Fenton's oxidation Ph.D. Research Thesis. School of Biotechnology Dublin City University Dublin 9 Ireland, **2011**. <http://doras.dcu.ie/16453/>

[2] A. K. Durgannavar, M. B. Patgar, S. A. Chimatadar. Oxidation of amoxicillin by hexacyanoferrate (III) in aqueous alkaline medium - a kinetic and mechanistic approach. *Indian J. Chem.*, **2015**, 1085-1091. <http://hdl.handle.net/123456789/32224>

[3] A. Fawzy. Removal of toxic tellurium (IV) compounds via bioreduction using flucloxacillin in aqueous acidic medium: A kinetic and mechanistic approach. *Journal of Molecular Liquids*. **2019**, 111436. <https://doi.org/10.1016/j.molliq.2019.111436>

[4] R. V. Hosahalli, K. S. Byadagi, S. T. Nandibewoor, S. A. Chimatadar. Kinetics and mechanism of ruthenium(III) catalyzed oxidation of chloramphenicol - an antibiotic drug by diperiodatocuprate(III) in aqueous alkaline medium. *Kinetics and Catalysis*, **2012**, 53, 65–74. <https://doi.org/10.1134/S0023158411060085>

[5] R. R. Hosamani, N. P. Shetti, S. T. Nandibewoor. Mechanistic investigation on the oxidation of ampicillin drug by diperiodatoargentate (III) in aqueous alkaline medium. *J. Org. Phys. Chem.*, **2009**, 22, 234-240. <https://doi.org/10.1002/poc.1460>

[6] O. S. Keen, K. G. Linden. Degradation of antibiotic activity during UV/H₂O₂ advanced oxidation and photolysis in wastewater effluent. *Environ. Sci. Technol.*, **2013**, 47, 13020–13030. <https://doi.org/10.1021/es402472x>

[7] N. P. Shetti, N. P. Hegde, S. T. Nandibewoor. Structure reactivity and thermodynamic analysis on the oxidation of ampicillin drug by copper(III) complex in aqueous alkaline medium (stopped-flow technique). *J. Mol. Str.*, **2009**, 930, 180-186. <https://doi.org/10.1016/j.molstruc.2009.05.013>

[8] A. K. Singh, R. Negi, B. Jain, Y. Katre, S. P. Singh, V. K. Sharma. Kinetics and mechanism of Ru(III)-catalyzed oxidation of paracetamol by chloramine-T in aqueous acidic medium. *Catal. Letters*, **2009**, 132, 285–291. <https://doi.org/10.1007/s10562-009-0107-8>

[9] A. K. Singh, M. Singh, S. Rahmani, J. Srivastava, J. Singh. Kinetics of the oxidation of tetracycline hydrate by copper(II) complexed with bipyridyl in alkaline medium using chloro-complex of palladium(II) as homogeneous catalyst. *Ind. Eng. Chem. Res.*, **2012**, 51, 5728-5736. <https://doi.org/10.1021/ie300306a>

[10] A. K. Singh, R. Yadav, J. Srivastava, R. S. Bala, R. Pradhan, S. Rahmani. Kinetics of Ir (III)-catalysed oxidation of ampicillin by Cu (Bip)₂²⁺ in alkaline medium: a spectrophotometric study. *Int. J. ChemTech Res.*, **2017**, 10, 514-524. [http://sphinx.sai.com/2017/ch_vol10_no9/2/\(514-524\)V10N9CT.pdf](http://sphinx.sai.com/2017/ch_vol10_no9/2/(514-524)V10N9CT.pdf)

[11] G. A. Ahmed, A. Fawzy, R. M. Hassan. Spectrophotometric evidence for the formation of short-lived hypomanganate(V) and manganate(VI) transient species during the oxidation of K-carrageenan by alkaline permanganate. *Carbohydr. Res.*, **2007**, 342, 1382-1386. <https://doi.org/10.1016/j.carres.2007.03.022>

[12] R. M. Hassan, A. Fawzy, A. Alarifi, G. A. Ahmed, I. A. Zaafarany, H. D. Takagi. Base-catalyzed oxidation of some sulfated macromolecules: Kinetics and mechanism of formation of intermediate complexes of short-lived manganate(VI) and/or hypomanganate (V) during oxidation of iota- and lambda-carrageenan polysaccharides by alkaline permanganate. *J. Mol. Catal.*, **A. 2011**, 335, 38-45. <https://doi.org/10.1016/j.molcata.2010.11.011>

[13] L. I. Simandi, M. Jacky, Z. A. Schelly. Short-lived manganate(VI) and manganate(V) intermediates in the permanganate oxidation of sulfite ion. *J. Am. Chem. Soc.*, **1984**, 106, 6866-6867. <https://doi.org/10.1021/ja00334a079>

[14] I. A. Vogel, A Text book of quantitative inorganic analysis, 4th edn. ELBS and Longman, New York, pp. 352, **1978**.

[15] I. A. Zaafarany, A. Fawzy, G. A. Ahmed, S. A. Ibrahim, R. M. Hassan, H. D. Takagi. Further evidence for detection of short-lived transient hypomanganate(V) and manganate(VI) intermediates during oxidation of some sulfated polysaccharides by alkaline permanganate using conventional spectrophotometric techniques. *Carbohydr. Res.*, **2010**, 345, 1588-1593. <https://doi.org/10.1016/j.carres.2010.04.013>

[16] K. J. Laidler, "Chemical Kinetics", McGraw-Hill, New York, **1965**.

[17] V. F. Chemie, Ph D Thesis, Duisburg University, Germany, **2005**.

[18] L. L. Halligudi, S. M. Desai, A. K. Mavalangi, S. T. Nandibewoor. Kinetics of the oxidative degradation of rac-serine by aqueous alkaline permanganate. *Monatshefte für Chemie*, **2000**, 131, 321–332. <https://doi.org/10.1007/PL00022942>

- [19] L. L. Halligudi, S. M. Desai, A. K. Mavalangi, S. T. Nandibewoor. Free radical intervention, deamination and decarboxylation in the ruthenium(III)-catalysed oxidation of L-arginine by alkaline permanganate—a kinetic study. *Transit. Met. Chem.*, **2000**, 26, 28–35. <https://doi.org/10.1023/A:1007195304258>
- [20] T. P. Jose, S.T. Nandibewoor, S. M. Tuwar. Mechanism of oxidation of L-histidine by heptavalent manganese in alkaline medium. *E-Journal of Chemistry*, **2005**, 2, 75–85. <https://doi.org/10.1155/2005/206147>
- [21] A. K. Kini, S. A. Farokhi, S. T. Nandibewoor. A comparative study of ruthenium(III) catalyzed oxidation of L-leucine and L-isoleucine by alkaline permanganate. A kinetic and mechanistic approach. *Transit. Met. Chem.*, **2002**, 27, 532–540. <https://doi.org/10.1023/A:1015641231236>
- [22] L. Michaelis, M. L. Menten. The kinetics of invertase action. *Biochemische Zeitschrift*. **1913**, 49, 333–369.



Fingerprinting analysis using crystal based mid-infrared spectroscopy to differentiate between Saudi Dates Fruits for food adulteration

Ali Sayqal

Chemistry Department, Faculty of Applied Science, Umm Al-Qura University, Makkah, Saudi Arabia.

ARTICLE INFO

Article History:

Submission date: 06/10/2020

Accepted date: 21/10/2020

Keywords:

ATR-FT-IR; Dates; PC-DFA; Food adulteration.

ABSTRACT

Date palm is a commonly edible fruit and has been known widely by the society in the Gulf countries. Dates can be used within the diet of many people due to its contribution in benefits of health and its functions treat various diseases. Date fruits are rich in many valuable elements such as minerals, fatty acids, carbohydrates, vitamins and amino acids. Although there are many varieties of Date fruit, Ajwa Date can be considered to be the most well-known type of dates. In addition, the medicinal and religious value of Ajwa is also known within Muslim populations. Due to the importance value of Dates, it is highly susceptible to adulteration. One of the many forms of adulteration is packing and mixing low quality of Dates for promotion purposes of the known brand to delude the consumers of their high quality. The present study demonstrated that attenuated total reflectance fourier transform infrared (ATR-FT-IR) spectroscopy as a qualitative method for the classification and determination of Date fruit adulteration. Several types of palm Dates (e.g. Ajwa, Rabiah, Sagiel, Meshrg, Khdiry and Safawy) were purchased from local markets in Al Madina Al Monawara. Fruit and seed samples were subjected to ATR-FT-IR spectroscopy for analysis. For discrimination of Date samples, supervise method such as principal components-discriminant function analysis was conducted on raw spectral data. Results exhibited that infrared spectra contained valuable information could allow the differentiation between different types of Dates. Therefore, employing metabolic fingerprinting and supervised chemometric analysis is a proper procedure for food adulteration detects.

1. Introduction

Date palm is a commonly edible fruit and has been known widely by the society of Kingdom of Saudi Arabia (KSA) and other Gulf countries. In KSA, there might be more than five hundred cultivars, and about five thousand species of Date palms grown in various regions globally [1,2]. The production of Dates of several excellent commercial cultivars in KSA is more than one million tons annually. Dates fruit are consumed by large populations in the Middle East and its consumption tends to increase during Ramadan and Al-Hajj seasons. In general, it is consumed either eaten immediately or it might be added to different types of foods and beverages (e.g. pie, cake, jam and juice). Dates can be used within the diet of many people due to its beneficial health and its functions for the protection from poisons according to the statement of prophet Mohammed [3,4]. Although there are many varieties of Date fruit, Ajwa Date can be considered to be the most well-known types of Dates as well as the medicinal and religious value of Ajwa is also known within Muslim populations. In addition, it has been reported that extract of Date fruits is considered as anticancer, antioxidant, antibacterial and antifungal properties and several other competencies in disease protection [5,6]. Date fruits have several nutritional values as it is rich in vitamins, fatty acids, carbohydrates, amino acids and minerals such as magnesium, potassium, calcium, iron and zinc [7-9].

In recent times, food authenticity is growing globally, and the authentication issue in Date fruits is most likely to occur in Date fruit origin. Due to the importance value of Dates, it is highly susceptible to adulteration. Detecting food authenticity for accurate labeling and quality control is the usual respecting religious and economic viewpoint. Therefore, the introduction of convenient analytical approaches for Food authenticity is required. Several analytical methods exist to determine food adulteration, which are mostly based on physicochemical, DNA-based and chromatographic methods [10]. Most of these approaches are expensive, highly time-consuming and require laboratory sample preparations. Recently, chemometric tools coupled with vibrational spectroscopy techniques such as Raman and

infrared spectroscopy have been established [11]. Spectroscopic techniques with appropriate chemometric analysis have the ability to investigate multiple objectives employing food fingerprinting [12]. Furthermore, attenuated total reflection-Fourier transform infrared (ATR-FTIR) spectroscopy is an inexpensive, non-destructive, simple, short analysis time and accurate methods [13,14]. It is also used to generate information about the composition and molecular structure (fingerprints) of the sample [15]. FT-IR spectroscopy can be used in various fields; for instance, pharmaceutical research [16], food [17,18], agricultural applications [19] and metabolomics [20-22].

2. Results and discussion

FTIR was conducted to evaluate and compare the fingerprinting of seven types of Dates. In order to achieve a better classification of samples, experiments were performed for Date fruits and seeds samples. The FTIR spectra of Date fruit and seed sample is shown in Fig. 1A and B. Several bands in the mid-infrared region between 4000-650 cm⁻¹ were observed which are attributed to a functional group and vibration mode of proteins, lipids and carbohydrate, as Date fruits are rich in proteins, fatty acids, carbohydrates and vitamins. Vibrational assignments of the mid-infrared regions are provided in Table 1 [23].

It was clearly noticed that a slight spectral difference among Dates samples was observed as shown in (Fig 1), however, FT-IR spectra are difficult to interpret visually. Thus, a supervised clustering approach such as DFA were performed for data analysis. DFA allows to visualize the samples distribution on the basis of their infrared fingerprint [24]. Therefore, ATR-FTIR data were subjected to PC-DFA in order to generate the first and second discriminant function (DF) scores which allow to identify variation among samples. The resultant DFA scores plots is shown in Fig 2 A and B. It is clearly to be seen that a clear separation among Meshrg, Rabiah, Sagiel, Khdiry and Safawy Date fruits samples is achieved in the first discriminant function that explain the majority of variance among samples. Additionally, similar observations were found the Date seed samples. In addition, it is evident that Ajwa Aliya and Ajwa Madina Date fruits cluster together significantly and separately from other type of Date

*** Corresponding Author**

Chemistry Department, Faculty of Applied Science, Umm Al-Qura University, Makkah, Saudi Arabia.

E-mail address: aasayqal@uqu.edu.sa (Ali Sayqal).

1685-4732 / 1685-4740 © 2020 UQU All rights reserved.

fruits, and also a noticeable slight shift was observed between Ajwa Aliya and Ajwa Madina Date fruits. Although these two types are similar, this variance could be due to harvesting the Date fruits from different palm farms in Al Madina Al-Monawara. Ajwa Aliya Dates fruits are harvested from certain palm farms which was established since the time of prophet Mohammed. Whereas, Ajwa Madina Date fruits is collected from other palm farms in Al-Madina AL-Monawara. This clustering pattern would suggest that different types of Dates fruits can be distinguished from each other due to its fruit origins or nutritional values, indicating the ability of ATR-FTIR coupled with appropriate multivariate analysis as a fingerprinting tool to discriminate between different types of Date fruits and detecting Date fruits adulteration.

To study which spectral regions that caused the discrimination among different types of Dates fruits and Date seeds, the loading plots for PC-DFA and wavenumbers were conducted (Fig 3 A and B). It was clearly observed that some changes take place within these loading plots and the major infrared spectra variances being observed at $\nu = 2925, 2848, 1555, 1025 \text{ cm}^{-1}$. In addition, it was noticed that the most major infrared spectra variances being observed only $\nu = 1025 \text{ cm}^{-1}$ for Date seeds. These peaks could be associated with chemical groups of components that might present in the Date fruits. The bands at 2925 and 2848 cm^{-1} are responsible for C-H stretching vibrations of fatty acids, whereas these two peaks are not significant and contributing in the separation of Date seed samples. This would suggest that the lipid contents are an important factor to classify Date fruit but not for seed samples. The peaks at 1555 cm^{-1} can be attributed to carbonyl stretching (primary amide) and N-H bending (Secondary amide) vibrations related to the components of protein. Additionally, the band at 1024 cm^{-1} could arise from C-O stretching in the carbohydrate (polysaccharides). Therefore, the noticeable large variations in carbohydrates, proteins and lipids among seven diverse types of Dates could be due to different nutritional contents presents in the Date fruits.

Table 1. Wavenumber and assignment for mid-infrared region.

Wavenumber (cm^{-1})	Mode of IR vibration	Vibrational assignment
2960-2850	Asymmetric and symmetric stretches for CH_2 and CH_3 group	lipids
3399-3299	N-H stretching	Amide A of proteins
1691-1619	carbonyl group stretching	proteins (primary amide)
1591-1529	N-H bending and C-N	Proteins (secondary amide)
1450-1200	Carboxyl group of protein	
1200-900	C-O or OH stretching	Carbohydrate

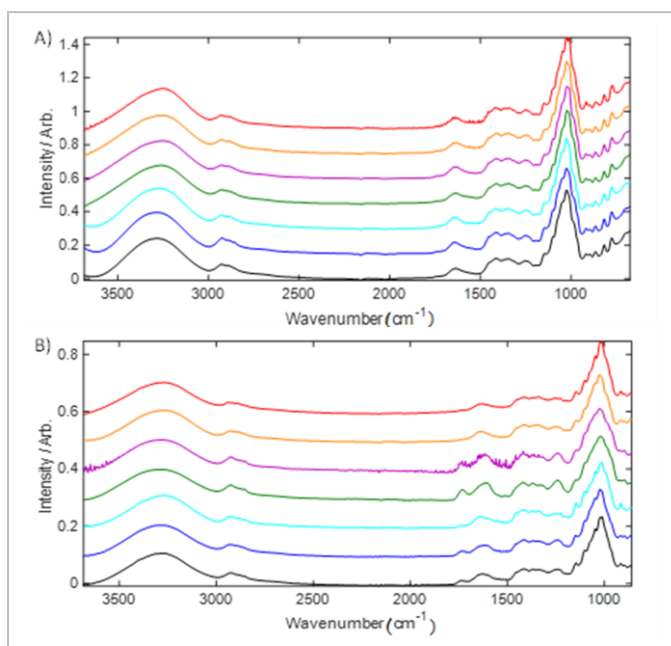


Figure 1. FT-IR spectra collected for (A) date fruits samples and (B) date seed samples. Colours represent different types of dates. Ajwa Aliya (red), Ajwa Madina (orange), Rabiah (pink), Sagiell (green), Meshrg (light blue), Khdiry (dark blue) and Safawy (black).

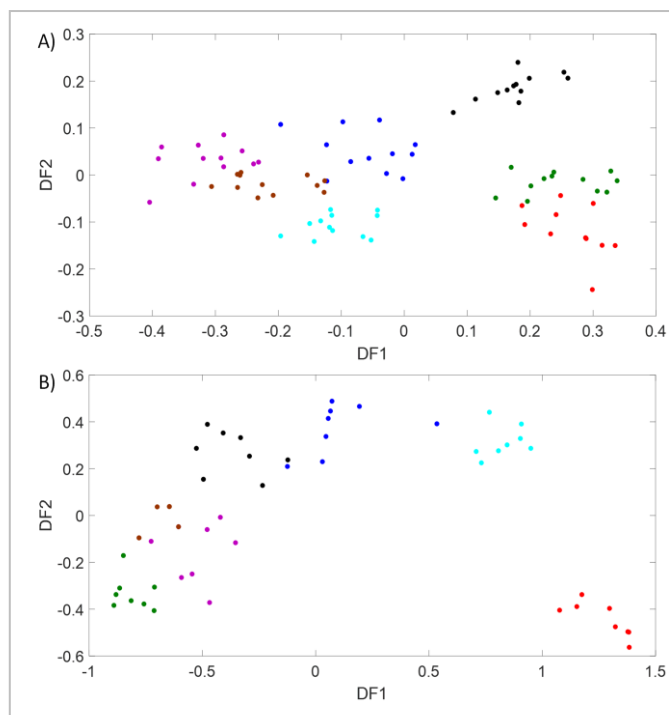


Figure 2. PC-DFA scores plots FT-IR data for (A) date fruits samples and PCs 1-30 with a total explained variance (TEV) of 99.93% were used for the discriminant function analysis (DFA), while (B) date seed samples and PCs 1-21 with TEV of 99.87% were employed for the DFA. Colours represent different types of dates. Ajwa Aliya (red), Ajwa Madina (Green), Rabiah (pink), Sagiell (brown), Meshrg (black), Khdiry (dark blue) and Safawy (light blue).

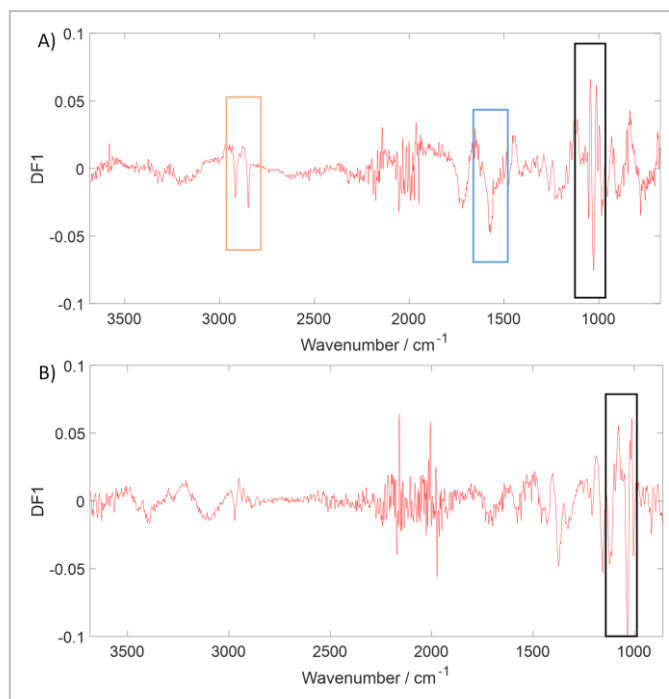


Figure 3. PC-DFA loadings plots from DF1 of (A) date fruits samples and (B) date seed samples. Significant loadings were assigned to carbohydrates, proteins and lipids

3. Conclusions

Our study shows the ability of ATR-FTIR instrument to discriminate between different types of Date samples. Even though many observed bands were similar in Fruit and seed Date samples, their units of absorbance were different because of the variation in the origin and nutritional contents present in the sample. The IR data obtained by ATR-FTIR exhibits that PC-DFA plots demonstrate excellent separations among several types of Dates sample, and the first function (DF1) loading vector demonstrate that several regions derived from carbohydrates, proteins and lipids contribute to this separation.

To sum up, it has been demonstrated that ATR-FTIR technique with a suitable chemometric tool can be a valuable fingerprinting method for classification and detecting Date adulteration according to its origin or nutritional contents.

4. Materials and Methods

4.1 samples collection and preparation for instrumental analysis

Seven types of palm Dates fruits (e.g. Ajwa Aliya, Ajwa Madina, Rabiah, Sagi, Meshrg, Khdir and Safawy) were purchased from local Dates central market in Al Madina Al Monawara. Date fruit samples were cut in small round pieces in order to fit the crystal surface. Whereas, Date seed samples were placed on the ATR crystal surface without any modification. Finally, Pressure Clamp was used to press the samples to the crystal surface.

4.2 ATR-FTIR spectra acquisition

Infrared spectra were acquired by using a Nicolet iS50 FTIR spectrometer (Thermo Scientific, Dreiech, Germany) equipped with an ATR crystal (Diamond MIRacle; PIKE Technologies, USA). Measurements were recorded employing a deuterated triglycine sulfate (DTGS) detector from 4000 to 650 cm^{-1} at ambient temperature, with a resolution of 4 cm^{-1} . Finally, 32 scans were co-added and then the mean was calculated in order to enhance signal to noise ratio (SNR) according to the method proposed by Svecnjak *et al* [25]. All measurements were performed in triplicate for each Date fruit sample, therefore, a total of 84 spectra were collected. The resulting obtained spectra are presented as a graph of absorbance spectra. ATR crystal was carefully cleaned with isopropyl alcohol and then dried prior to analysis.

4.3 spectral pre-processing and data analysis

Initially, raw acquired IR spectra were converted to ASCII files and then imported into Matlab software, version R2016b for operations of multivariate analysis. Prior to analysis, extended multiplicative signal correction (EMSC) were conducted in order to scale the spectra [26].

For cluster analysis, an unsupervised method such as principal component analysis (PCA) was performed on the data for dimension reduction of multivariate data and maintaining the variance [27]. Additionally, a supervised method such as discriminant function analysis (DFA) was then performed in order to separate groups. DFA attempts to increase the differences between the known groups whilst decreasing the differences within the same group [28,29]. PC-DFA was conducted using PCs 1-30 and 1-21 for Date fruits and Date seed respectively.

Acknowledgments: I would like to thank The Custodian of the Two Holy Mosques Institute for Hajj and Umrah Research for using their laboratory.

Conflicts of Interest: "The author declare no conflict of interest."

References

- [1] S. Al Jaouni, S. Selim, S. H. Hassan, H. S. H. Mohamad, M. A. M. Wadaan, W. N. Hozzein, H. Asard, H. AbdElgawad. Vermicompost Supply Modifies Chemical Composition and Improves Nutritive and Medicinal Properties of Date Palm Fruits From Saudi Arabia. *Front. Plant Sci.*, **2019**, 10. <https://doi.org/10.3389/fpls.2019.00424>
- [2] J. S. M. Sabir, S. Abo-Aba, S. Bafeel, T. A. Zari, S. Edris, A. M. Shokry, A. Atef, N. O. Gadalla, A. M. Ramadan, M. A. Al-Kordy, F. M. El-Domyati, R. K. Jansen, A. Bahieldin. Characterization of ten date palm (*Phoenix dactylifera* L.) cultivars from Saudi Arabia using AFLP and ISSR markers. *Comptes Rendus Biologies*, **2014**, 337, 6-18. <https://doi.org/10.1016/j.crv.2013.11.003>
- [3] M. Wahini. Exploration of making date seed's flour and its nutritional contents analysis, in International Conference on Innovation in Engineering and Vocational Education, *IOP Conf. Series: Materials Science and Engineering*, **2016**, 128, 012031 doi:10.1088/1757-899X/128/1/012031
- [4] S. K. Marwat, M. A. Khan, I. U. Bhatti. Aromatic plant species mentioned in the holy Qura'n and Ahadith and their ethnomedicinal importance. *Pakistan J. Nutrition*, **2009**, 8, 1472-1479. <https://www.cabdirect.org/cabdirect/abstract/20093305175>
- [5] S. Selim, S. Alfay, M. Al-Ruwaili, A. Abdo, S. Jaouni. Susceptibility of imipenem-resistant *Pseudomonas aeruginosa* to flavonoid glycosides of date palm (*Phoenix dactylifera* L.) tamar growing in Al Madinah, Saudi Arabia. *African J. biotechnology*, **2012**, 11, 416-422. DOI: [10.5897/AJB11.1412](https://doi.org/10.5897/AJB11.1412)
- [6] I. Hamad, H. AbdElgawad, S. Al Jaouni, G. Zinta, H. Asard, S. Hassan, M. Hegab, N. Hagagy, S. Selim. Metabolic Analysis of Various Date Palm Fruit (*Phoenix dactylifera* L.) Cultivars from Saudi Arabia to Assess Their Nutritional Quality. *Molecules*, **2015**, 20, 13620-13641. DOI: [10.3390/molecules200813620](https://doi.org/10.3390/molecules200813620)
- [7] W. Al-Shahib, R. J. Marshall. The fruit of the date palm: its possible use as the best food for the future? *International J. Food Sciences and Nutrition*, **2003**, 54, 247-259. DOI: [10.1080/09637480120091982](https://doi.org/10.1080/09637480120091982)
- [8] S. Khalid, A. Ahmad, T. Masud, M. J. Asad, M. Sandhu. Nutritional assessment of Ajwa dates flesh and pits in comparison to local varieties. *J. Animal and Plant Sciences*, **2016**, 26, 1072-1080.
- [9] H. A. Almana, R. M. Mahmoud. Palm date seeds as an alternative source of dietary fiber in Saudi bread. *Ecology of Food and Nutrition*, **1994**, 32, 261-270. <https://doi.org/10.1080/03670244.1994.9991406>
- [10] E. Hong, S. Y. Lee, J. Y. Jeong, J. M. Park, B. H. Kim, K. Kwon, H. S. Chun. Modern analytical methods for the detection of food fraud and adulteration by food category. *J. Science of Food and Agriculture*, **2017**, 97, 3877-3896. <https://doi.org/10.1002/jsfa.8364>
- [11] K. M. Nunes, M. V. O. Andrade, A. M. P. Santos, M. C. Lasmar, M. M. Sena. Detection and characterisation of frauds in bovine meat in natura by non-meat ingredient additions using data fusion of chemical parameters and ATR-FTIR spectroscopy *Food Chemistry*, **2016**, 205, 14-22. <https://doi.org/10.1016/j.foodchem.2016.02.158>
- [12] S. Esslinger, J. Riedel, C. Fahl-Hassek. Potential and limitations of non-targeted fingerprinting for authentication of food in official control. *Food Res. Int.*, **2014**, 60, 189-204. <https://doi.org/10.1016/j.foodres.2013.10.015>
- [13] M. Lucarini, A. Durazzo, J. S. del Pulgar, P. Gabrielli, G. Lombardi-Boccia. Determination of fatty acid content in meat and meat products: The FTIR-ATR approach. *Food Chem.*, **2018**, 267, 223-230. <https://doi.org/10.1016/j.foodchem.2017.11.042>
- [14] E. L. Kendix, S. Prati, E. Joseph, G. Sciuotto, R. Mazzeo. ATR and transmission analysis of pigments by means of far infrared spectroscopy. *Anal. Bioanal. Chem.*, **2009**, 394, 1023-1032. <https://doi.org/10.1007/s00216-009-2691-2>
- [15] N. Cebi, M. T. Yilmaz, O. Sagdic. A rapid ATR-FTIR spectroscopic method for detection of sibutramine adulteration in tea and coffee based on hierarchical cluster and principal component analyses. *Food Chem.*, **2017**, 229, 517-526. <https://doi.org/10.1016/j.foodchem.2017.02.072>
- [16] R. Nikzad-Langerodi, K. Arth, V. Klatte-Asselmeyer, S. Bressler, J. Saukel, G. Reznicek, C. Dobes. Quality Control of *Valeriana Radix* by Attenuated Total Reflection Fourier Transform Infrared (ATR-FTIR) Spectroscopy. *Planta Medica*, **2018**, 84, 442-448. DOI: [10.1055/s-0043-122239](https://doi.org/10.1055/s-0043-122239)
- [17] T. Czaja, E. Kuzawinska, A. Sobota, R. Szostak. Determining moisture content in pasta by vibrational spectroscopy. *Talanta*, **2018**, 178, 294-298. <https://doi.org/10.1016/j.talanta.2017.09.050>
- [18] P. Jaiswal, S. N. Jha, J. Kaur, A. Borah, H. G. Ramya. Detection of aflatoxin M1 in milk using spectroscopy and multivariate analyses. *Food Chemistry*, **2018**, 238, 209-214. <https://doi.org/10.1016/j.foodchem.2016.07.150>
- [19] A. Fernandez-Gonzalez, J. M. Montejó-Bernardo, H. Rodríguez-Prieto, C. Castano-Monllor, R. Badia-Laino, M. E. Diaz-Garcia. Easy-to-use analytical approach based on ATR-FTIR and chemometrics to identify apple varieties under Protected Designation of Origin (PDO). *Computers and Electronics in Agriculture*, **2014**, 108, 166-172. <https://doi.org/10.1016/j.compag.2014.07.009>

- [20] A. Sayqal, Y. Xu, D. K. Trivedi, N. AlMasoud, D. I. Ellis, R. Goodacre. Metabolic Fingerprinting of *Pseudomonas putida* DOT-T1E Strains: Understanding the Influence of Divalent Cations in Adaptation Mechanisms Following Exposure to Toluene *Metabolites*, **2016**, 6, 14. DOI: [10.3390/metabo6020014](https://doi.org/10.3390/metabo6020014)
- [21] A. Sayqal, Y. Xu, D. K. Trivedi, N. AlMasoud, D. I. Ellis, H. Muhamadali, N. J. W. Rattray, C. Webb, R. Goodacre. Metabolic analysis of the response of *Pseudomonas putida* DOT-T1E strains to toluene using Fourier transform infrared spectroscopy and gas chromatography mass spectrometry. *Metabolomics*, **2016**, 12, 112. DOI: [10.1007/s11306-016-1054-1](https://doi.org/10.1007/s11306-016-1054-1)
- [22] A. Sayqal, Y. Xu, D. K. Trivedi, N. AlMasoud, D. I. Ellis, N. J. W. Rattray, R. Goodacre. Metabolomics Analysis Reveals the Participation of Efflux Pumps and Ornithine in the Response of *Pseudomonas putida* DOT-T1E Cells to Challenge with Propranolol. *Plos One*, 2016, 11, e0156509. DOI: [10.1371/journal.pone.0156509](https://doi.org/10.1371/journal.pone.0156509)
- [23] D. H. Kim, R. M. Jarvis, Y. Xu, A. W. Oliver, J. W. Allwood, L. Hampson, I. N. Hampson, R. Goodacre Combining metabolic fingerprinting and footprinting to understand the phenotypic response of HPV16 E6 expressing cervical carcinoma cells exposed to the HIV anti-viral drug lopinavir. *Analyst*, **2010**, 135, 1235-1244. <https://doi.org/10.1039/B923046G>
- [24] D. I. Ellis, R. Goodacre. Metabolic fingerprinting in disease diagnosis: biomedical applications of infrared and Raman spectroscopy. *Analyst*, **2006**, 131, 875-885. DOI: [10.1039/b602376m](https://doi.org/10.1039/b602376m)
- [25] L. Svecnjak, L. A. Chesson, A. Gallina, M. Maia, M. Martinello, F. Mutinelli, M. N. Muz, F. M. Nunes, F. Saucy, B. J. Tipple, K. Wallner, E. Was, T. A. Waters. Standard methods for *Apis mellifera* beeswax research. *J. Apicultural Research*, **2019**, 58, 1-108. <https://doi.org/10.1080/00218839.2019.1571556>
- [26] H. Martens, J. P. Nielsen, S. B. Engelsen. Light scattering and light absorbance separated by extended multiplicative signal correction. Application to near-infrared transmission analysis of powder mixtures. *Analytical Chem.*, **2003**, 75, 394-404. <https://doi.org/10.1021/ac020194w>
- [27] S. Wold, K. Esbensen, P. Geladi. Principal component analysis. *Chemometrics and Intelligent Laboratory Systems*, **1987**, 2, 37-52. [https://doi.org/10.1016/0169-7439\(87\)80084-9](https://doi.org/10.1016/0169-7439(87)80084-9)
- [28] P. S. Gromski, H. Muhamadali, D. I. Ellis, Y. Xu, E. Correa, M. L. Turner, R. Goodacre. A tutorial review: Metabolomics and partial least squares-discriminant analysis - a marriage of convenience or a shotgun wedding. *Analytica Chimica Acta*, **2015**, 879, 10-23. <https://doi.org/10.1016/j.aca.2015.02.012>
- [29] H. J. H. Macfie, C. S. Gutteridge, J. R. Norris. Use of canonical variates analysis in differentiation of bacteria by pyrolysis gas-liquid-chromatography. *J. General Microbiology*, **1978**, 104, 67-74. DOI: [10.1099/00221287-104-1-67](https://doi.org/10.1099/00221287-104-1-67)



Hydrochemical Evaluation for Al-Sada Area Wells and their Suitability for Agricultural Usages

Kotayba T. Al-Youzbakey*, Ali M. Sulaiman.

Dams and Water Resources Researches Center, University of Mosul, Mosul, Iraq.

ARTICLE INFO

Article History:

Submission date: 12/09/2020

Accepted date: 02/12/2020

Keywords:

Hydrochemical evaluation, groundwater, water quality, Al-Sada area, agricultural usages.

ABSTRACT

The present study is concerned with the impact of the geological nature of Al-Fat'ha Formation rock beds and soil on the well water quality of the Al-Sada area (about 2 Km. from the border of Mosul city toward the north). Groundwater passes through different depths dissolving gypsum within their passages between gypsum fractures, which is assumed as the major constituents of Al-Fat'ha Formation. It was found that water resources had significant concentrations of total dissolved solids (TDS), total hardness (TH), calcium (Ca^{2+}), magnesium (Mg^{2+}), sodium (Na^+), sulphate (SO_4^{2-}), bicarbonate (HCO_3^-) and chloride (Cl^-).

Cations and anions are ordered as $Na^+ > Ca^{2+} > Mg^{2+} > K^+$ and $SO_4^{2-} > Cl^- > HCO_3^- > NO_3^-$ in shallow wells (1 and 2) and $Ca^{2+} > Mg^{2+} > Na^+ > K^+$ and $SO_4^{2-} > HCO_3^- > Cl^- > NO_3^-$ in deep wells (3, 4 & 5) as well as the well No. 6. The deep wells classified as high salinity water and shallow wells as very high salinity, all wells could be used for plants that bearing salinity with continuous leaching in permeable soils.

1. Introduction

Al-Sada area is located near Mosul city, about 2 Km. from the border of the city toward the north. There are many farms distributed in the area around the road (Mosul – Tel Kaif) (Figure 1). Most farms nearly planting many kinds of trees, as well as vegetables and the people drill many wells in the area for agriculture usage. These wells are varied in the drilling technique and depth. Some wells are about 5-10 m. depth, and the others are more than 30 meters.

The rock layer types in this region belong to Al-Fat'ha Formation, which is known to have repeated cycles. Each cycle consists of gypsum, marl, limestone, and halite [1]. The land in this area comprised of a 0-5m layer of soil. This may contain in some places a high amount of secondary gypsum and halite, as well as the rock fragments of gypsum and carbonates due to weathering in *situ* of the Fat'ha Formation layers.

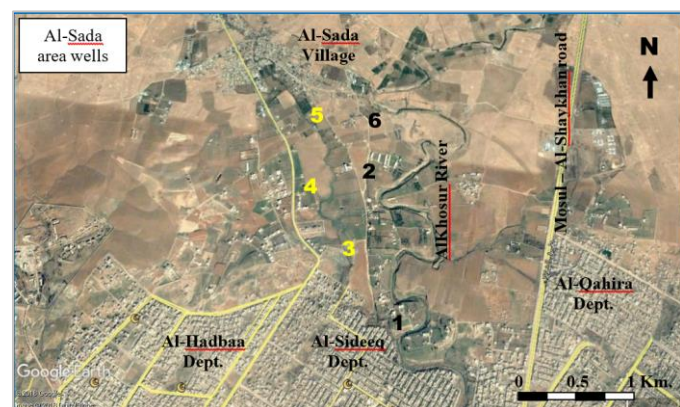


Figure 1: Location map of wells in Al-Sada area.

Groundwater is found almost everywhere beneath the earth's surface not in a single widespread aquifer but in thousands of local aquifer systems and compartments that have similar characters [2]. Knowledge of the occurrence, replenishment, and recovery of groundwater has special significance in arid and semi-arid regions due to discrepancy in monsoonal rainfall, insufficient surface waters, and over-drafting of groundwater resources, [3]. The chemical alteration of rainwater depends on several factors such as soil–water interaction, dissolution of mineral species, and anthropogenic activities [4].

The concentrations of dissolved ions in groundwater samples are generally governed by lithology, nature of geochemical reactions, and solubility of interaction rocks, [5,6].

The groundwater quality is affected by dissolving gypsum. Groundwater takes different passages in the gypsiferous rocks, in the form of channels, fractures, joints, veins, and veinlets. These channels are assumed to be fractures where gypsum had been dissolved. Groundwater is moving in different levels, dissolving gypsum rocks as the main part of the Al-Fat'ha Formation, as well as the fragments of gypsum scattered within the topsoil. It varies among the locations depending upon several factors controlling the groundwater quality like, rocks type, type and amount of the soluble minerals, area of contact between rock and water (porosity), medium temperature, fluid pressure, and flow velocity [2,7]. Calcium carbonate assumed to be the main component of limestone and marl, as well as clay minerals mainly illite, chlorite, and the limited ratio of montmorillonite [8]. These minerals found within Al-Fat'ha Formation are affecting the nature of groundwater quality, due to the dissolving of calcium carbonate [9,10]. High sulfate concentration is known to reduce the activity of aerobic microorganisms, (one of the main producing source of CO_2). Carbonic acid (CO_2 in water) is indirectly responsible for producing bicarbonate by carbonate dissolving, [11].

The present work aims to clarify the impact of aquifer type rocks and the effect of soil and weathered fragments on the chemical nature and quality of the groundwater in Al-Sada wells.

2. Results and Discussions

The chemical composition of groundwater results from the geochemical processes occurring as water reacts with the geologic materials, which it flows. [5].

Dissolving of carbonate, sulfate, and chloride minerals within the aquifer is in general, were a major source of groundwater salinity. The solution of the aquifer matrix is most pronounced with more soluble lithologies, such as carbonate and evaporate [12,13].

2.1. Potential of hydrogen (pH)

All well water show a slight variation in pH values, due to the probable activity of dissolving actions of rocks by groundwater and rock fragments in the upper layer of soils by rainwater precipitation, which are infiltrated to the soil and upper parts of rock layers. Rainwater depends on the carbon dioxide evolving, as well as the other bio-activities by plant roots and microorganisms and dissolving of salt

* Corresponding Author

Dams and Water Resources Researches Center, University of Mosul, Mosul, Iraq.

E-mail address: kotaybatawfiq@gmail.com (Kotayba T. Al-Youzbakey).

1685-4732 / 1685-4740 © 2020 UQU All rights reserved.

compounds on the soil surface are influence on the pH of infiltrated water.

All pH values are around pH=7 (Table 1). This declares that the effect of groundwater activity for dissolving is more than the rainwater precipitations.

2.2. Electrical conductivity (EC)

Electrical conductivity reflected the water content of cations and anions. Table (1) shows that the EC values divided into two groups, the first one includes the shallow wells (1, 2 and 6) indicate that there is variance in EC for each well due to the effect of rainwater and the chemical and biochemical activities to dissolved the rock fragments in the upper part of the soil. While the 2nd group which includes the deep wells (3, 4, and 5) have closed values of EC for each well due to the effect of groundwater in rock layers mainly.

2.3. Total Hardness (TH)

Hardness components are affected by the type of rock beds that represent the reservoir or water pass through them[14]. The gypsum/anhydrite bedrocks are the main sources of both Ca^{2+} and SO_4^{2-} , as well as limestone beds (Ca^{2+} and CO_3^{2-}) within Fat'ha Formation are the main constituents of permanent hardness. In addition to the dissolving actions on soil surface compounds (calcareous soil, rock fragments, and secondary salts).

As mention above, TH values are closed for each well in deep kinds, while they varied in shallow wells group.

Table 1: Physical parameters for the water of Al-Sada area wells.

Parameters	Sampling Date	Shallow Wells No.			Deep Wells No.		
		1	2	6	3	4	5
pH units	Nov. 2013	6.9	6.8	7.2	7.1	6.9	6.8
	Jan. 2014	7.0	6.8	7.6	7.0	7.1	7.0
	Mar. 2014	7.4	7.1		7.4	7.5	7.2
EC $\mu\text{S}/\text{cm}$	Nov. 2013	3140	5510	990	2720	2550	3310
	Jan. 2014	7740	3530	1340	2570	3280	3680
	Mar. 2014	9400	2130		3270	4150	3800
TH mg/l	Nov. 2013	2200	1600	600	1740	2640	2500
	Jan. 2014	1420	1460	880	1680	2000	2300
	Mar. 2014	1500	900		1760	2260	2480
TDS mg/l	Nov. 2013	4100	5740	980	3360	3650	4380
	Jan. 2014	7030	3480	1350	3050	3630	4200
	Mar. 2014	8130	1630		3100	3010	4030

2.4. Total dissolved solids (TDS)

Total dissolved solids represent all unstable minerals under weathering conditions (e.g. gypsum/anhydrite, calcite, dolomite, and secondary minerals) by groundwater and infiltrated water with aquifer and topsoil, respectively.

All TDS values are different for each shallow well according to the role of the infiltration rainwater, mainly, and its variance effect on soil compounds from location to another. While in the deep water wells all the TDS values almost are similar in each well.

In addition to, the variety of TDS and other physical parameters among shallow and deep wells according to the location, topography, soil type, and water infiltration quantities.

2.5. Calcium and Magnesium (Ca^{2+} & Mg^{2+})

Evaporite and Carbonate rocks found within Al-Fat'ha Formation are mainly composed of many minerals which represent the main sources of calcium and magnesium: gypsum ($\text{CaSO}_4 \cdot 2\text{H}_2\text{O}$), anhydrite (CaSO_4) calcite (CaCO_3), dolomite ($\text{Ca Mg}(\text{CO}_3)_2$) and gypsiferous and calcareous cementing materials in bedrocks. As well as, from the weathered rock fragments, some type of clay minerals and secondary minerals like halite and secondary gypsum. All these minerals have the ability to effected by weathering conditions, and dissolved in water, with a pH less than 8 [15, 16]. The figure shows a positive relationship between calcium and sulfates which indicates that the main source of calcium comes from the dissolution of gypsum/anhydrite (Figure 2). In turn Figure (3) show a random relationship between calcium and carbonate, which represents a secondary effect of dissolving carbonate. The most calcium concentrations in deep well water seem to be around 400 mg/l which are ranged between 264 – 577 mg/l. these closed values are due to the effect of groundwater activities. In the shallow well water, calcium concentrations are different, and in general are less than the above values of deep wells.

The same conditions affect the magnesium concentrations in both shallow and deep wells. Magnesium in wells water has come from the dissolving of marl mainly (Figure 4), as well as dolomite and some kinds of clay minerals found within carbonate rocks. Magnesium in deep wells is around 250 mg/l, while in the shallow wells ranged (23 to 148) mg/l.

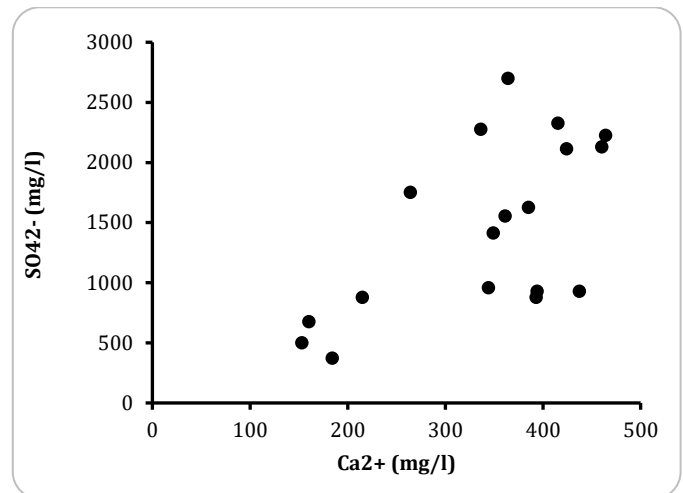


Figure 2: The semi linear relationship between calcium and sulfates in wells water.

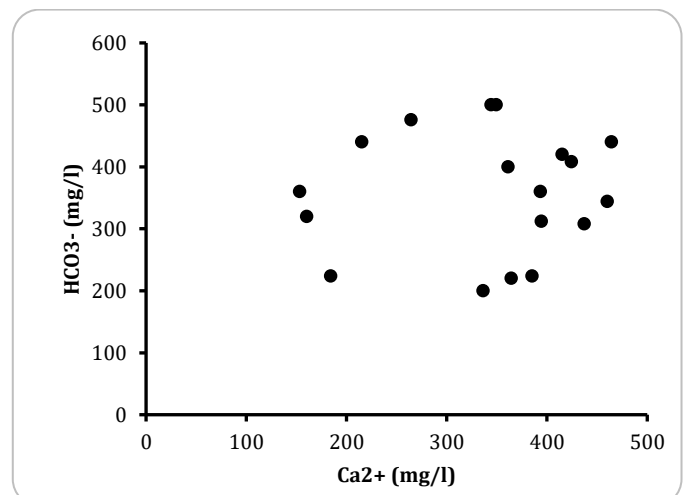


Figure 3: The random relationship between calcium and bicarbonates in wells water.

2.6. Sodium and Potassium (Na^+ & K^+)

Sodium and potassium (alkalies cations) are found in halide minerals as halite within Fat'ha Formation layers and as secondary minerals especially at the upper part of the soil. Due to the high solubility of alkalies, most of the secondary minerals are dissolved by the rain precipitation and leaching by surface water to other places of the soil surface. Figure (5) declares that there is a clear relationship

between sodium and chloride which reflects the effect of dissolving halite within Fat'ha Formation and the secondary halite in the upper part of the soil.

In otherwise, potassium may come from some kind of clay minerals, a well as the dissolving of fertilizer compounds. Table (2) and Figure (6) show that there is a random relationship between potassium and nitrate anions, which indicates that the chemical fertilizers (N.P.K.) were not used in the area [9].

In general, sodium founds in high concentrations in all wells. Sodium ranged (60-342) mg/l in deep wells, while it ranged (14-1940) mg/l in shallow wells. This may indicate that the low varieties in the first group due to the dissolving of halite which founds in the rocks of Fat'ha Formation, while the wide-ranged in second group reflect the effect of rain and surface water on dissolving the secondary halite in the upper part of the soil, and it is related to the weather conditions through the year [10].

Potassium found in the well water samples in very low concentrations which were ranged (0.5 – 14) mg/l, this low

concentration reflects that potassium comes from clay minerals within marl in Fat'ha Formation or from the secondary halides.

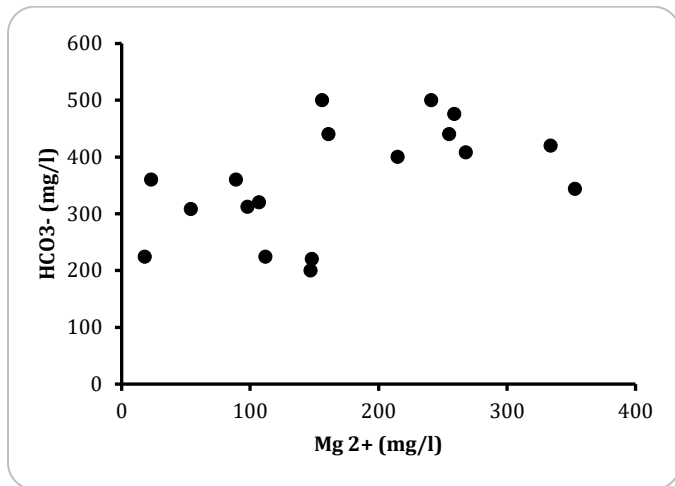


Figure 4: The random relationship between magnesium and bicarbonates in wells water.

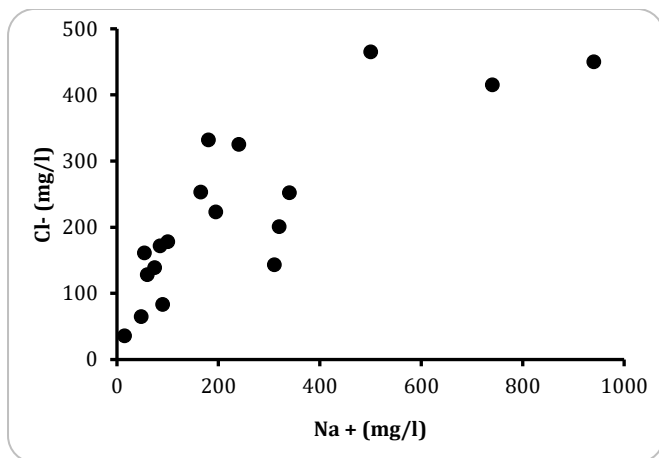


Figure 5: The relationship between sodium and chloride in wells water.

2.7. Alkalinity (HCO₃⁻):

The alkalinity represents the bicarbonate, which is a product from the solubility of limestone and carbonate cementing material in marl beds within Fat'ha Formation.

In general, alkalinity concentrations in deep wells water (344-511) mg/l were more than shallow wells water (200-360) mg/l. The values of alkalinity in the first group are due to the solubility of limestone layers that alternated with gypsum/anhydrite layers within Fat'ha Formation, which depend on the groundwater activity. In turn, the limestone rock fragments within the upper part of the soil as well as, the subsurface limestone beds were the main sources of alkalinity in shallow wells water, which depend on the infiltration of surface water and rainfall activity.

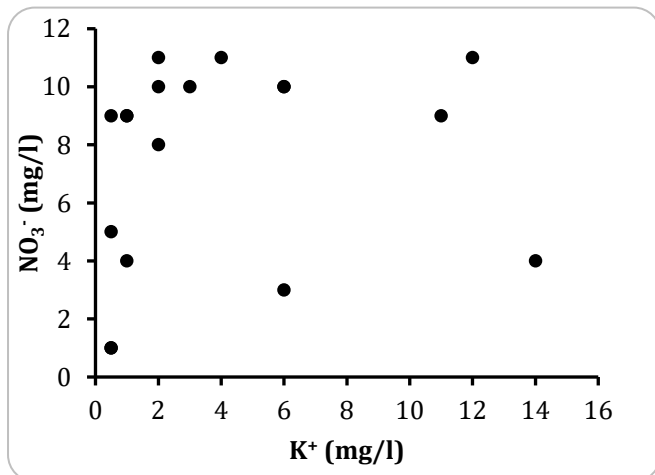


Figure 6: The relationship between potassium and nitrate in wells water.

Table 2: The chemical composition (mg/l) of the studied well's water.

Cations & Anions	Sampling date	Shallow Wells No.			Deep Wells No.			
		1	2	6	3	4	5	
Cations	Ca ²⁺	Nov/2013	737	393	120	344	577	449
		Jan/2014	304	385	160	264	415	464
		Mar/2014	336	184		361	424	360
	Mg ²⁺	Nov/2013	54	23	39	156	161	241
		Jan/2014	148	112	107	299	354	255
		Mar/2014	147	98		215	268	353
	Na ⁺	Nov/2013	180	240	48	103	195	165
		Jan/2014	1940	499	90	310	321	342
		Mar/2014	1704	14		60	85	74
	K ⁺	Nov/2013	2	2	0.5	0.5	0.5	4
		Jan/2014	6	6	6	1	1	12
		Mar/2014	14	3		1	2	11
Anions	HCO ₃ ⁻	Nov/2013	308	360	360	500	440	511
		Jan/2014	220	224	320	476	420	440
		Mar/2014	200	312		401	408	344
	SO ₄ ²⁻	Nov/2013	928	878	500	957	876	1014
		Jan/2014	2700	1625	675	1750	2325	2425
		Mar/2014	3375	929		2253	2314	2728
	Cl ⁻	Nov/2013	332	1018	65	178	223	253
		Jan/2014	1470	465	83	143	201	252
		Mar/2014	1415	161		168	172	239
	NO ₃ ⁻	Nov/2013	10	11	1	5	9	11
		Jan/2014	10	10	3	4	9	11
		Mar/2014	4	10		9	8	9

2.8. Sulfate (SO₄²⁻):

Sulfate compound occurrence in water resources in high concentration will affect directly and/or indirectly on the bicarbonate concentration because the sulfur compound inhibits the aerobic microorganism activity to produce carbon dioxide, Hence the carbon dioxide pressure affected on this equilibrium [17]. The equilibrium state between the soluble minerals like carbonate and gypsum control the concentrations of bicarbonates and sulfates in groundwater [15].

Sulfate anions are assumed to have the highest concentrations in these water resources due to the high solubility of gypsum. So there is no difference in sulfate concentrations among wells in all sampling dates. Table (2) shows that there is an increase in sulfate concentrations toward the rainfall months. Figure (7) declare the relationship between sulfate and sodium, which reflect the occurrence of Sodium as halide minerals (halite) within Fat'ha Formation layers.

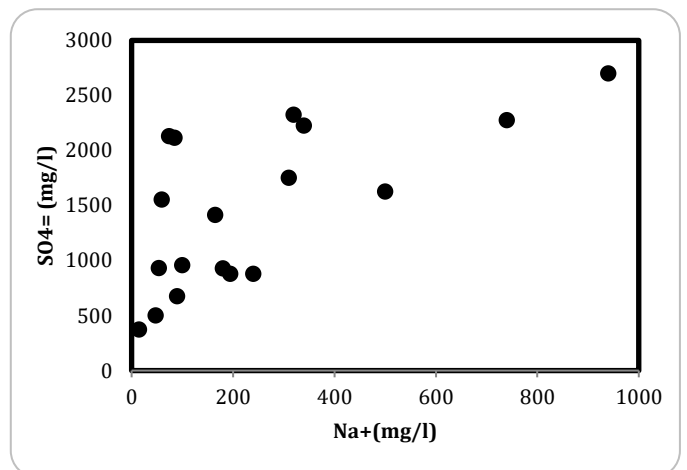


Figure 7: The relationship between sodium and sulfate in wells water.

2.9. Chloride (Cl⁻)

It is the most dissolving anion in water. It is easily washed from the topsoil by dissolving of secondary salts of halides like halite mainly, by precipitation and surface water runoff. Because of that, its occurrence is limited in soil, due to its infiltration to the groundwater system. Animal urine and solid waste are also the sources for chloride.

Table (2) shows that the concentrations of chloride in deep wells water are ranged from (143-253) mg/l, these values are around 203 mg/l which is mean that chlorides product from the dissolving of halite beds within Fat'ha Formation, and its solubility depending on the groundwater activity. In shallow boreholes water, the concentrations of chloride are in a wide range, they are (332 – 1470) mg/l in well 1,

(161 – 1018) mg/l in well 2, and (65 & 83) mg/l in well 3. These ranges reflect the effect of surface water and rainfall activities on the soil surface, which contain different amounts of secondary halite.

2.10. Nitrate (NO_3^-)

This anion is derived from fertilizer, plant decaying, and animal waste. These assume to be the main sources of nitrogen compounds found in soil which directly and/or indirectly ended to the watercourse [18]. As well as, the effect of the atmospheric spark which is the natural source of nitrogen compounds. Nitrogen fixation bacteria found in some plant roots are also responsible for their concentration in the water resources [19].

All water wells sample reflect the low concentration of nitrate anion which were ranged (1-11) mg/l. These low values may be due to the low activity of nitrogen fixation bacteria, and there is no effect of fertilization activities in the area as mention above (Figure 6).

3. Classification and assessment of water quality

Groundwater quality depends on the quality of recharged water, atmospheric precipitation, inland surface water, and on sub-surface geochemical processes [3]. It is important to assess the quality of groundwater in any basin and/or urban area that influences the suitability of water for domestic, irrigation, and industrial needs. Important hydrogeologic factors such as rainfall, mineral weathering, topographic relief, and biological activity in a given basin are important for controlling recharge and hydrogeochemical reactions responsible for chemical constituents contaminating the groundwater [4,6,16].

Table (3) shows the concentration of cations and anions (*epm/l*) of the water of the well. Depending on the electrical conductivity values Wells No. 3,4 and 5 are classified as high salinity and wells No. 1 and 2 as a very high salinity all these wells their waters are unfair for irrigation, only well No.6 is moderate and safe only with permeable soil and moderate leaching, (Richard, 1954) in [20].

The U.S. – Salinity Lab. Classify water depending on their contents of total dissolved solids and electrical conductivity into for classes *C1-C4*, (U.S. – salinity lab. in [21]). According to the T.D.S & E.C. values, the type of water for all wells is classified as *C4* which means that the well waters are used for plants to bear very high salinity water in well porosity soil with continuous washing actions. Except well No. 6 its water quality classified as *C3* which is used for plants to bear salinity with continuous washing.

Table 3: The cations and anions concentrations (*epm/l*) of the water of the studied well.

Sampl. date	Ions	Well No.					
		No.1	No.2	No.3	No.4	No.5	No.6
Nov. 2013	Ca ²⁺	21.85	19.65	17.20	10.75	17.45	7.65
	Mg ²⁺	4.44	1.89	12.84	13.25	19.84	7.33
	Na ⁺	7.83	10.43	4.35	8.48	7.17	2.09
	K ⁺	0.05	0.05	0.01	0.01	0.10	0.01
	Σcations	34.17	32.03	34.40	32.49	44.56	17.07
	HCO ₃ ⁻	5.05	5.90	8.20	7.21	8.20	5.90
	SO ₄ ²⁻	19.33	18.29	19.94	18.29	29.46	10.42
	Cl ⁻	9.35	9.15	5.01	6.28	7.13	1.83
	NO ₃ ⁻	0.16	0.18	0.08	0.15	0.18	0.02
	Σanions	33.90	33.53	33.23	31.93	44.96	18.17
Jan. 2014	Ca ²⁺	18.20	19.25	13.20	20.75	23.20	8.00
	Mg ²⁺	12.18	9.22	21.32	27.49	20.99	8.81
	Na ⁺	40.87	21.74	13.48	13.91	14.78	3.91
	K ⁺	0.15	0.15	0.03	0.03	0.31	0.15
	Σcations	71.40	50.36	48.02	62.18	59.28	20.87
	HCO ₃ ⁻	3.61	3.67	7.80	6.89	7.21	5.25
	SO ₄ ²⁻	56.25	33.85	36.46	48.44	46.35	14.06
	Cl ⁻	12.68	13.10	4.03	5.66	7.10	2.34
	NO ₃ ⁻	0.16	0.16	0.06	0.15	0.18	0.05
	Σanions	72.69	50.79	48.35	61.13	60.84	21.69
Mar. 2014	Ca ²⁺	32.17	2.35	2.61	3.70	3.22	
	Mg ²⁺	12.10	8.07	17.70	22.06	29.05	
	Na ⁺	32.17	2.35	2.61	3.70	3.22	
	K ⁺	0.36	0.08	0.03	0.05	0.28	
	Σcations	61.43	30.19	38.38	47.00	55.55	
	HCO ₃ ⁻	3.28	5.11	6.56	6.69	5.64	
	SO ₄ ²⁻	47.40	19.35	32.35	44.04	44.33	
	Cl ⁻	11.69	4.54	3.61	4.85	3.92	
NO ₃ ⁻	0.06	0.16	0.15	0.13	0.15		
Σanions	62.43	29.17	42.66	55.70	54.03		

The RSC values for all wells are below the 1.25 epm/l (Willcox, 1955 classification of irrigation water in [21]). which indicate that there are no hazardous effects of bicarbonate on the quality of water for agricultural purpose due to the high concentration of sulfates (Ca-sulfate) in well waters, [6].

Taylor (1972) in [21] classified irrigation water into 4 classes; little, moderate, medium, and severe according to their content of chlorides. Wells No. (1 & 2) are classified as class 4 (severe) which could be used for plant bear high chloride contents, these wells are affected by surface water and rainfall activities on dissolving secondary halite in topsoil. Wells No. (3, 4 & 5) are classified as class 3 (medium) which could be used for plant bearing chloride contents. These wells are deep and reflect its content of chlorides within layers of Fat'ha Formation.

U.S. – salinity laboratory classified the irrigation water according to the sharing effect of electrical conductivity (*C*) and sodium adsorption ratio (*S*) into 16 orders as (*C-S*). all well water belongs to the order (*C4-S1*) except well No. (6) is belong order (*C3-S1*). All well waters could be used for plants bearing high salinity with continuous washing processes.

4. Materials and Methods

Six wells were selected in the Al-Sada area (1, 2, 3, 4, 5, and 6) for water quality evaluation. Water samples collected during 17/11/2013, 27/1/2014, and 30/3/2014. water duplicate samples had been collected in clean dry polyethylene bottles for chemical analyses according to standard methods [22]. Some water quality analyses (pH, EC, TH, TDS, Ca²⁺, Mg²⁺, Na⁺, K⁺, HCO₃⁻, SO₄²⁻, Cl⁻ and NO₃⁻) were tested in the laboratory of geochemistry in Dams and Water Resources Researches Center – Mosul University. The turbidity test did not repeat because of the very low turbidity values for all wells water in the first run. The instruments used are pH meter type (PHILIPS, PW 9421), EC - meter type (OGAWA, TOA, CM-205), total hardness, calcium and bicarbonate measured by titration with ethylene diamine tetraacetic acid (EDTA), magnesium was calculated from total hardness and calcium contents. Dry the water sample at 110 ° C to calculate the TDS using an oven. Flame-photometer type (OGAWA, ANA-10KL), used for sodium and potassium determinations. Sulfates were estimated using the colorimetric technique. chloride were analyzed by volumetric methods. Spectrophotometer type (OGAWA, OSK 7724), for nitrate determination. As well as, electronic balance type (Mettler H54 AR) were used.

Ions were converted from milligram per liter to milliequivalent per liter, and anions balanced against cations as a control check of the reliability of the analyses results, (Table 3).

SAR can indicate the degree to which irrigation water tends to enter into cation-exchange reactions in the soil. Sodium replacing adsorbed calcium and magnesium is a hazard as it causes damage to the soil structure and becomes compact and impervious [5].

$$SAR = Na \div \sqrt{(Ca + Mg)/2} \quad (\text{all concentrations are in } epm)$$

Residual sodium carbonate (RSC) has been calculated to determine the hazardous effect of carbonate and bicarbonate on the quality of water for agricultural purposes and has been determined by the Equation: [5]

$$RSC = (CO_3 + HCO_3) - (Ca + Mg) \quad (\text{all concentrations are in } epm)$$

5. Conclusion

Low porosity of gypsiferous marl retarded the channeling of water passage through the rocks. This phenomenon shows the differences between positions and sources of water, depth, quantity, and ion concentrations. It reflects its properties, characteristics, and uses.

Precipitation mainly through storms is collecting water in the wades running off the topsoil. Water quality in these wades is extremely affected by soil types and salinity. Sodium and chloride are the most probable ions due to their high dissolving ability, in addition to calcium, magnesium, and other elements.

Due to the chemical properties of all wells water, they are classified saline to high saline water. Moreover, the irrigation activities need experience in selecting plants that bear salinity, well leaching works, and permeable soils.

References

- [1] S. Q. Al-Naqib, T. A. Aghwan. Sedimentological Study of the Clastic Units of the Lower Fars Formation. *Iraqi Geol. J.*, **1993**, 26, 108–121, 1993.
- [2] K. E. Leizou, J. O. Nduka, A. W. Verla. Evaluation of Water Quality Index of the Brass River, Bayelsa State, South-South, Nigeria. *Int. J. Res. - Granthaalayah*, **2017**, 5, 277–287. doi: [10.5281/zenodo.894650](https://doi.org/10.5281/zenodo.894650).
- [3] M. Vasanthavigar, *et al.*, Application of water quality index for groundwater quality assessment: Thirumanimuttar sub-basin, Tamilnadu, India. *Environ. Monit. Assess.*, **2010**, 171, 595–609. doi: [10.1007/s10661-009-1302-1](https://doi.org/10.1007/s10661-009-1302-1).
- [4] J. Raju, U. K. Shukla, P. Ram. Hydrogeochemistry for the assessment of groundwater quality in Varanasi: A fast-urbanizing center in Uttar Pradesh, India. *Environ. Monit. Assess.*, **2011**, 173, 279–300, doi: [10.1007/s10661-010-1387-6](https://doi.org/10.1007/s10661-010-1387-6).
- [5] N. Aghazadeh A. A. Mogaddam. Assessment of Groundwater Quality and its Suitability for Drinking and Agricultural Uses in the Oshnavieh Area, Northwest of Iran. *J. Environ. Prot. (Irvine., Calif.)*, **2010**, 01, 30–40. doi: [10.4236/jep.2010.11005](https://doi.org/10.4236/jep.2010.11005).
- [6] B. B. Kapoor, F. Inam, S. S. Deo. Assessment of Physico-Chemical Quality of Ground Water in Some Rural Areas Receiving Industrial Wastewater Discharges in Nagpur District, Maharashtra State, India. Title. *TIJST*, 2016, 4, 149–155.
- [7] J. A. Toth. A Conceptual model of the groundwater regime and the hydrogeologic environment. *J. Hydrol.*, **1970**, 164–167.
- [8] Mustafa, A. M., “Sedimentological studies of the Lower Fars Formation in Sinjar basin, Iraq,” Mosul, 1980.
- [9] K. T. Al-Youzbakey, Y. F. Eclimes. Hydrological and Hydrogeochemical Study for Alqoush Plain (Northern Iraq) to Protect Region from the Drought,” in *The 9th Periodical Scientific Conference for Dams and Water Resources Research Center*, 28-29 Nov. **2018**, 2018, 165–176.
- [10] K. T. Al-Youzbakey, A. M. Sulaiman, D. A. Ismaeel. The Evaluation of Chemical Characterization for Selected Wells Water in Mosul – Bahshiqah – Shalalat Area, Ninivah Governorate, Northern Iraq,” in *The 9th Periodical Scientific Conference for Dams and Water Resources Research Center*, 28-29 Nov. **2018**, 2018, 201–216.
- [11] C. N. Sawyer. P. L. McCarty. *Chemistry for Environmental Engineering*, 3rd editio. McGraw-Hill Book Company, **1978**.
- [12] Wagner, W., *Groundwater in Arab Middle East*. Berlin: Springer-Verlag, 2011.
- [13] R. Brassington. *Field hydrogeology*, 4th ed. Hoboken, USA: John Wiley & Sons Ltd, **2017**.
- [14] D. K. Todd. *Ground Water Hydrology*, 2nd Editio. New York: John Wiley & Sons, **1980**.
- [15] F. H. Chappelle. Geochemistry of Groundwater. *TREATISE on GEOCHEMISTRY*, First edit., H. D. Holland and K. K. Turekian, Eds. Elsevier Pregamon, **2004**, 425–449.
- [16] R. Gupta, A. K. Misra. Groundwater quality analysis of quaternary aquifers in Jhajjar District, Haryana, India: Focus on groundwater fluoride and health implications. *Alexandria Eng. J.*, **2018**, 57, 375–381. doi: [10.1016/j.aej.2016.08.031](https://doi.org/10.1016/j.aej.2016.08.031).
- [17] F. M. Phillips, M. C. Castro. Groundwater Dating and Residence-time Measurements,” in *TREATISE on GEOCHEMISTRY*, First edit., H. D. Holland and K. K. Turekian, Eds. Elsevier Pregamon, **2004**, 451–497.
- [18] W. H. Organization, Guidelines for drinking water quality, health criteria and other supporting information Alexandria, Egypt, **1989**.
- [19] D. Deming. *Introduction to Hydrogeology*. McGraw-Hill Company, **2002**.
- [20] G. I. Obiefuna, A. Sheriff. Assessment of Shallow Ground Water Quality of Pindiga Gombe Area, Yola Area, NE, Nigeria for Irrigation and Domestic Purposes. *Res. J. Environ. Earth Sci.*, **2011**, 3, 131–141.
- [21] S. A. Abawi, M. S. Hassan. *The Practice Engineering for Environment. Water Analysis*. Dar Al-Hekma for Publishing, University of Mosul, **1990**.
- [22] J. Brandi, L. Wilson-Wilde. *Standard Methods*. **2013**.

and utilizing a renewable resource and industrial waste, CNSL, for an advanced pharmaceutical application.

The aim of research work is to enrich/modify tCNSL with bio-synthesized CuO [Cu-tCNSL] by "Green Chemistry" protocol, to elucidate the structure of CNSL and Cu-tCNSL by FTIR and ^1H NMR, to study their antibacterial behavior against Gram-negative and Gram-positive bacteria and to explore the possibility of formulating CNSL, and Cu-tCNSL into ointments.

2. Results and discussion

The synthesis was carried out through the chemical reaction between -OH group of CNSL and Cu-Ac, by one-pot, one-step *in-situ* reaction, without any solvent, surfactant, crosslinker, catalyst, or any other external agents. CNSL serves as the matrix, diluent, reaction medium, providing functional sites for reaction to occur. The overall strategy suggests utilization of an agricultural by-product by simple method, in very short reaction time, i.e., 15 minutes. The overall approach follows the principles of "Green Chemistry".

The reaction was also accomplished at higher temperatures (60°C and 80°C). It was found that the samples obtained in this way were very viscous and were cured/dried over time; and thus could not be formulated in ointments or properly dissolved in xylene to study their antibacterial behavior. As a result of drying/curing, the samples had a limited pot life, so they could not be kept for future use. To overcome this problem, we repeated the reaction at 30°C. The reaction took place in similar manner. The samples obtained at this temperature were sufficiently viscous, showed free-flowing tendency, and were ideal for ointment formulation. They did not dry/cure and so could be easily secured for future use. The introduction of CuO in tCNSL was confirmed by FTIR and ^1H NMR spectral analyses as discussed in proceeding sections and antibacterial activity was also investigated. The ointments could be formulated well from tCNSL, bees wax [BW], white soft paraffin [WP] and Cu-tCNSL (Figure 2). Homogeneity tests were conducted on the formulated ointments, tCNSLO and Cu-tCNSLO, and no separation of contents was observed (Figure 3). The antibacterial study revealed that Cu-tCNSL showed good antibacterial activity.



Figure 2a: Cu-tCNSL



Figure 2b: Preparation of BW and WP mixture

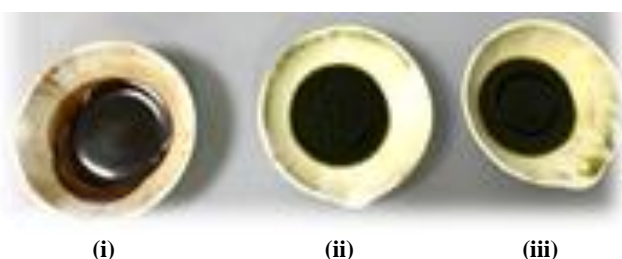


Figure 2c: Preparation of Cu-tCNSLO ointments from (i) 5T, (ii) 10T and (iii) 15T

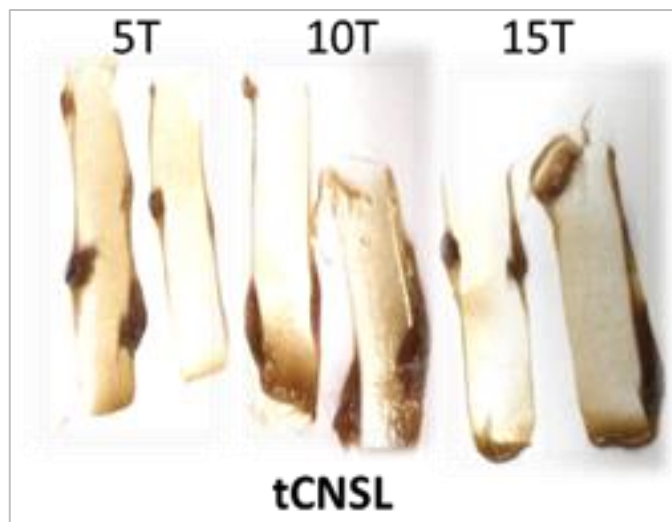


Figure 3: Homogeneity test of the prepared ointments

2.1. FTIR spectral analysis

The absorption bands observed in FTIR spectra of tCNSL and Cu-tCNSL are given below:

tCNSL(cm^{-1}): 3400-3300 (-OH, intermolecular hydrogen bonded), 3080 (Ar C=C-H), 3010 (C=C-H), 2926(asymm CH_2/CH_3) and 2854 (symm CH_2/CH_3), 1600-1500 (Ar C=C and C=C), 1486 (C-H bending), 1350 (O-H bending), 1268 and 1155 (phenolic C-O), 1074 (phenolic C-OH), 997(ArC=C), 912 and 876 (=C-H), 780 and 694(-C=C-H, out of plane bending).

Cu-tCNSL(cm^{-1}): Changes were observed in absorption bands of phenolic -OH, C=C str and C-OH, along with the presence of an additional band at 648 cm^{-1} (Cu-O).

As mentioned above, Cu-tCNSL showed the presence of absorption bands in FTIR typical to those present in FTIR spectrum of tCNSL. However, in FTIR spectrum of Cu-tCNSL, the -OH band was suppressed, indicating that during chemical reaction with Cu-Ac, -OH of CNSL was consumed. There is an additional band at 648 cm^{-1} (Cu-O), supporting the presence of CuO, formed due to chemical reaction between phenolic -OH and CuAc.

2.2. ^1H NMR spectral analysis

^1H NMR spectra of tCNSL and Cu-tCNSL were given in Figures 4 and 5. ^1H NMR spectrum of tCNSL showed the presence of methyl, methylene protons, unsaturation and phenolic hydroxyl. These peaks were also present in ^1H NMR spectrum of pure Cardanol [11]. Thus, Figure 4 confirms that tCNSL used in this research has Cardanol. The unmarked peak in the spectrum at 3.9ppm indicated the presence of (non hydrogen bonded) hydroxyls. In ^1H NMR spectrum of Cu-tCNSL, peak for -OH disappears confirming that the chemical reaction between Cu-Ac and tCNSL occurs at phenolic -OH, which was also observed in FTIR spectra discussed above.

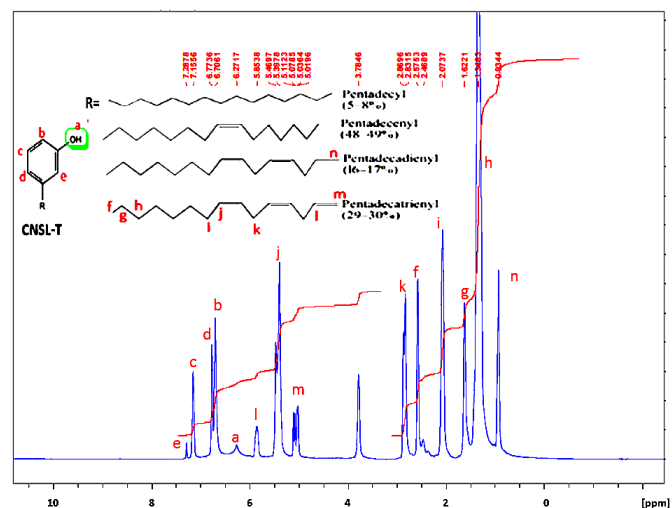


Figure 4: ^1H NMR spectrum of tCNSL

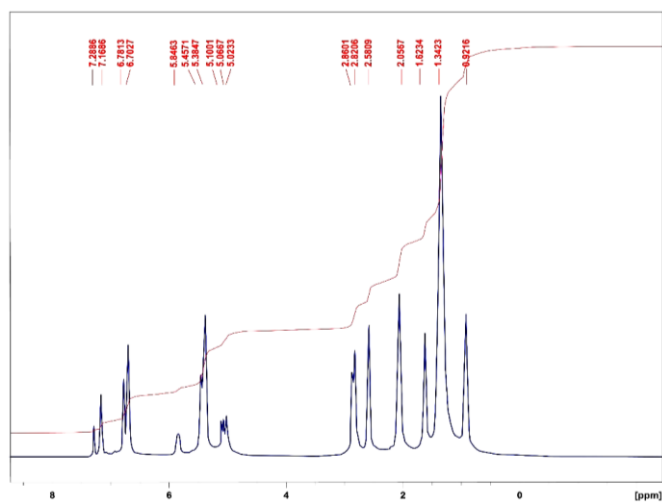


Figure 5: ^1H NMR spectrum of Cu-tCNSL

2.3. TEM image analysis

Transmission electron micrograph of Cu-tCNSL (Figure 6) showed the presence of nanosized CuO which occurred as nanosized spheres with well-defined boundaries, embedded in tCNSL matrix.

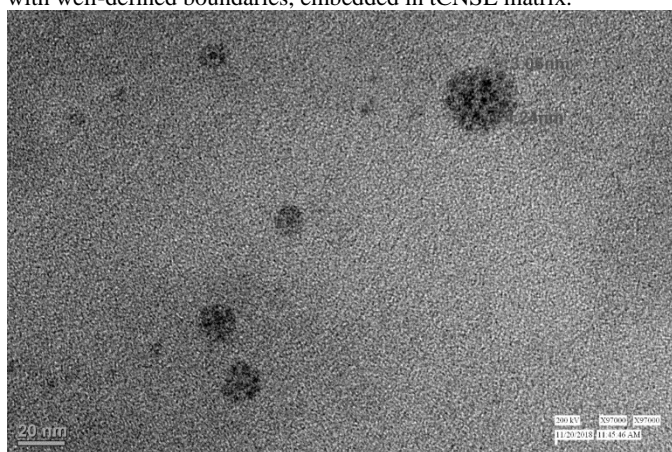
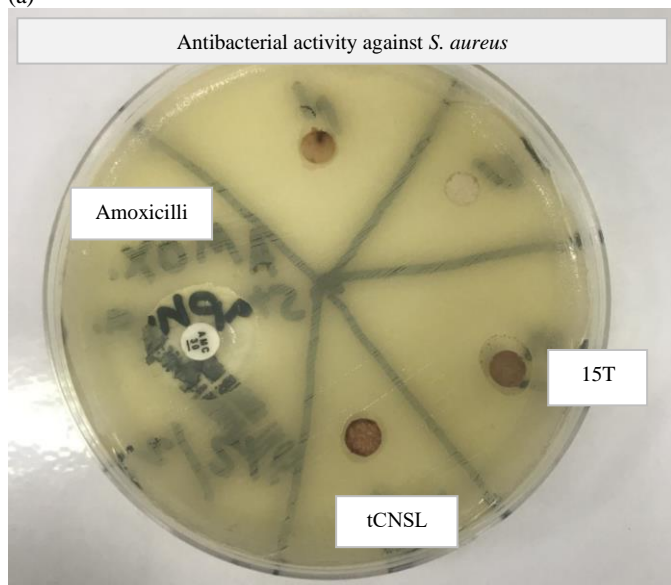


Figure 6: Transmission electron micrograph of Cu-tCNSL

2.4. Antibacterial activity

Antibacterial behavior of test samples was observed as zone of inhibition of bacterial growth. In addition, all samples dissolved well in xylene and antibacterial investigation was carried out for all samples. The concentration of test samples for antibacterial activity was taken as $150\mu\text{g/mL}$, in xylene. It was observed that sample 15T showed good antibacterial activity (Figure 7) against *Staphylococcus aureus*, while with the Gram-negative *Pseudomonas aeruginosa*, all the product samples showed no antibacterial activity.

(a)



(b)

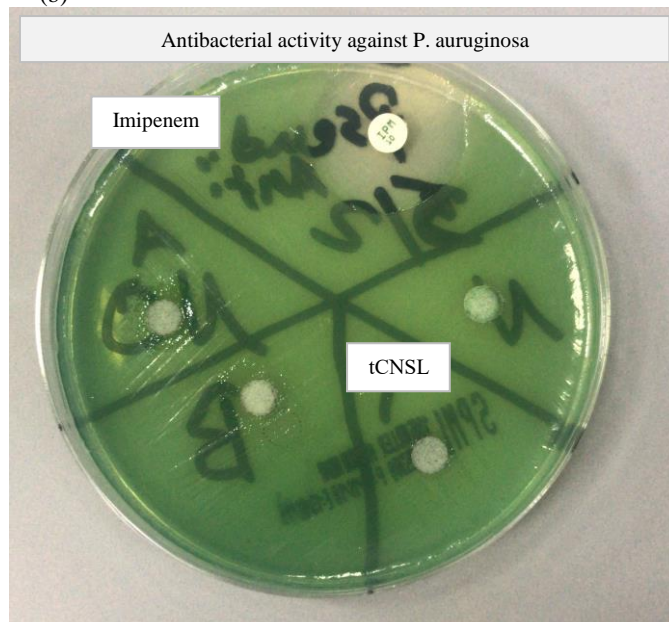


Figure 7: Antibacterial activity of tCNSL and 15T against (a) *S. aureus* (showing small inhibition zone with 15T) and (b) *P. aeruginosa* (showing no inhibition zone for all test except the positive control Imipenem) at $150\mu\text{g/mL}$, in xylene

Table 1: Antibacterial activity of the samples at different concentrations against *S. aureus* (A-250 $\mu\text{g/mL}$, B-325 $\mu\text{g/mL}$ and C-500 $\mu\text{g/mL}$, in xylene)

Cu-tCNSL			
A	15%	20%	25%
	9 mm	7 mm	8 mm
B	15%	20%	25%
	8 mm	8 mm	7 mm
C	15%	20%	25%
	7 mm	8 mm	No inhibition zone

The samples were further prepared in three concentrations: A-250 $\mu\text{g/mL}$, B-325 $\mu\text{g/mL}$ and C-500 $\mu\text{g/mL}$, in xylene. In *Staphylococcus aureus*, Cu-tCNSL (15%) and tCNSL showed antibacterial activity, at $150\mu\text{g/mL}$, in xylene (Figure 7) and also at A-250 $\mu\text{g/mL}$, B-325 $\mu\text{g/mL}$ and C-500 $\mu\text{g/mL}$, in xylene (Table 1). Good antibacterial activity was expected at higher concentration (above 250 $\mu\text{g/mL}$ of these materials, however, at higher loading of CuAc (20 and 25 %, Table 1) and at higher concentrations (325 $\mu\text{g/mL}$ and C-500 $\mu\text{g/mL}$, in xylene), the antibacterial activity deteriorated (Table 1). Good results were obtained at A-250 $\mu\text{g/mL}$ concentration and 15% loading of Cu-Ac (Table 1). The research work still needs more investigation, in terms of optimization of reaction conditions and the concentration of Cu-Ac.

3. Materials and Methods

tCNSL was procured from Golden Cashew Product Pvt. Ltd., Pondicherry, India.

Cu (CH_3COO) $_2\cdot\text{H}_2\text{O}$ (Cu-Ac), molecular mass- 199.7 g/mol, bees wax [BW], white soft paraffin [WP] were used as received.

3.1. Preparation of Cu-tCNSL

tCNSL was placed in a flask, and calculated amount of finely powdered CuAc was added, in small portions, with continuous stirring at $30\pm 5^\circ\text{C}$. After complete addition of CuAc, stirring was continued until the end of the reaction, to obtain Cu-tCNSL (Figure 2). The percent composition of Cu-tCNSL is given in Table 2, coded as 5 T, 10T, 15T, 20T and 25T.

Table 2: Percent composition of Cu-tCNSL

Cu-tCNSL	CuAc
5T	5%
10T	10%
15T	15%
20T	20%
25T	25%

3.2. Preparation of BW and WP mixture

Calculated amount of BW was taken in a clean mortar and placed on a hot water bath to dissolve beeswax. Next, required amount of WP was added to the mortar containing molten beeswax, and both were mixed thoroughly with pestle to obtain a homogenous mixture of BW and WP (Figure 2b).

3.3. Preparation of ointment

tCNSL and Cu-tCNSL were added to the homogenous mixture of BW and WP, in separate mortars, and again with a pestle mixed thoroughly for homogenization. Homogenization test was conducted to confirm homogenous mixing of contents. The prepared ointments were named as tCNSLO, and Cu-tCNSLO respectively (Figure 2c).

3.4. Sample photos

The photographs of samples were taken by Sony XZ phone camera.

3.5. FTIR

The spectra were taken on Tensor 37, Bruker Germany (by Opus 6.5 software).

3.6. ¹H NMR

The spectra were recorded on Bruker Germany spectrometer.

3.7. TEM

The image was taken on TECNAI G2 30S-TWIN instrument.

3.8. Homogenization test

This test was conducted to confirm the formation of homogenous mixture of ointment. 3.9. Antibacterial activity

Two bacterial isolates used in this experiment, *Staphylococcus aureus* and *Pseudomonas aeruginosa*, were sub-cultured on blood agar and incubated for 18 h at 37°C. From single colonies formed for these bacterial growths, two-three colonies were inoculated into Nutrient broth media and incubated for 18 h at 37°C to make a suspension for each bacterium. These suspensions were standardized at 600 nm optical density equal to 0.1 to make assure the inoculum prepared have same number of cells to prepare for antibacterial activity test. The disc diffusion method was adopted according to the CLSI for antimicrobial susceptibility (CLSI, 2010) each bacterial suspension applied by a cotton swab was then spread on Muller-Hinton agar media evenly to be prepared for the application of the discs contain antibacterial. The discs prepared by impregnating each disc (6mm diameter, 0.9mm thick) of filter paper into the solution prepared for each sample. We estimated that each disc contains 20µl of the sample solution. Four prepared filter paper discs were impregnated into the different chemical preparation then by using sterile forceps these discs were applied onto the surface of the prepared media. One disc (Amoxicillin for *S. aureus* and Imipenem for *P. aeruginosa*) was added in each plate as a standard positive control. Two plates were prepared with the discs for each bacterial species. The plates were incubated for 24 h at 37°C. All prepared samples were diluted in xylene.

4. Conclusions

Our results revealed that 3-4 nm sized spherical CuO particles were embedded in CNSL matrix by solvent free approach. The possibility to formulate ointments from tCNSL and Cu-tCNSL, in different % loading of copper acetate, was investigated, and homogenous ointments were obtained. This research demonstrates that we can prepare ointment from Cu-tCNSL, which showed antibacterial activity to kill Gram-positive bacteria. In this study we found that we can benefit from an agricultural waste material by its chemical conversion into a valuable pharmaceutical product, thus adding significant value to an otherwise waste material. Because CNSL is a natural product, it is cheap and safe and does not have any side effects.

Our recommendations and future plans are to carry out skin irritation tests and study the antifungal behavior of the samples. The research work has not been previously carried out and extensive studies are required to be done so that we can optimize the reaction conditions and concentration of copper, to find the best composition.

NOTE: Authors claim there is no conflict of interest

Author Contributions: All authors contributed to the study conception, design, material preparation, data collection and analysis. Drs Eram Sharmin, Najla Obaid and Mariam Mojally read and approved the final manuscript.

Funding: This research received no external funding

Acknowledgments: Dr Fahmina Zafar is thankful to the Department of Science & Technology, New Delhi, India for project under the Women Scientists' Scheme (WOS) for Research in Basic/Applied Sciences (Ref. No. SR/WOS-A/CS-97/2016).

Authors are thankful to Dr. Hanan Al-Harbi (Department of Pharmaceutics, College of Pharmacy, UQU) for her guidance during this research work and also to Dr. Mohammad Abdel Wahab (Department of Pharmaceutics, College of Pharmacy, UQU) for carrying out spectroscopic analysis of the samples.

Authors thank with appreciation Mr. Mohammad Younus Nomani (BFA Applied Arts, Faculty of Fine Arts, Jamia Millia Islamia, New Delhi, India) for improvement in artwork quality.

Conflicts of Interest: The authors declare no conflict of interest.

References

- [1] S. Khan, S. Masood, K. Siddiqui, M. Alam, F. Zafar, Q.M. Rizwanul Haque, N. Nishat. Utilization of renewable waste material for the sustainable development of thermally stable and biologically active aliphatic amine modified Cardanol (phenolic lipid) - Formaldehyde free standing films. *J. Cleaner Prod.* **2018**, *196*, 1644-1656. doi: <https://doi.org/10.1016/j.jclepro.2018.06.081>
- [2] F. França, N. Ricardo, F. Rodrigues, J. Souza, J. Feitosa. Comparison between physico-chemical properties of the technical Cashew Nut Shell Liquid (CNSL) and those natural extracted from solvent and pressing. *Polímeros*, **2011**, *21*, 156-160. doi: [10.1590/S0104-14282011005000028](https://doi.org/10.1590/S0104-14282011005000028).
- [3] F. Zafar, S. Khan, A. Ghosal, M. Azam, E. Sharmin, Q.M. Rizwanul Haq, N. Nishat. Clean synthesis and characterization of green nanostructured polymeric thin films from endogenous Mg (II) ions coordinated methylolated-Cashew nutshell liquid. *J. Cleaner Prod.* **2019**, *238*, 117716. doi: <https://doi.org/10.1016/j.jclepro.2019.117716>.
- [4] V.S. Balachandran, S.R. Jadhav, P.K. Vemula, G. John. Recent advances in cardanol chemistry in a nutshell: from a nut to nanomaterials. *Chem. Soc. Rev.*, **2013**, *42*, 427-438. <https://doi.org/10.1039/C2CS35344J>
- [5] S. Kanehashi, R. Masuda, K. Yokoyama, T. Kanamoto, H. Nakashima, T. Miyakoshi. Development of a cashew nut shell liquid (CNSL)-based polymer for antibacterial activity. *J. Appl. Polym. Sci.*, **2015**, *132*, 42725. doi: [10.1002/app.42725](https://doi.org/10.1002/app.42725)
- [6] D. Lomonaco, G.M. Pinheiro Santiago, Y.S. Ferreira, Â.M. Campos Arriaga, S.E. Mazzetto, G. Mele, G. Vasapollo. Study of technical CNSL and its main components as new green larvicides. *Green Chem.* **2009**, *11*, 31-33. doi: [10.1039/B811504D](https://doi.org/10.1039/B811504D).
- [7] Y. Shi, P.C.J. Kamer, D.J. Cole-Hamilton. Synthesis of pharmaceutical drugs from cardanol derived from cashew nut shell liquid. *Green Chem.* **2019**, *21*, 1043-1053. doi: [10.1039/C8GC03823F](https://doi.org/10.1039/C8GC03823F).
- [8] G. John, S. Nagarajan, P.K. Vemula, J.R. Silverman, C.K.S. Pillai. Natural monomers: A mine for functional and sustainable materials - Occurrence, chemical modification and polymerization. *Prog. Polym. Sci.* **2019**, *92*, 158-209. doi: <https://doi.org/10.1016/j.progpolymsci.2019.02.008>.
- [9] C. Voiron, S. Caillol, N.V. Sadavarte, B.V. Tawade, B. Boutevin, P.P. Wadgaonkar. Functionalization of cardanol: towards biobased polymers and additives. *Polym. Chem.* **2014**, *5*, 3142-3162. doi: [10.1039/C3PY01194A](https://doi.org/10.1039/C3PY01194A).
- [10] J. Mgaya, G.B. Shombe, S.C. Masikane, S. Mlowe, E.B. Mubofu, N. Revaprasadu. Cashew nut shell: a potential bio-resource for the production of bio-sourced chemicals, materials and fuels. *Green Chem.* **2019**, *21*, 1186-1201. doi: [10.1039/C8GC02972E](https://doi.org/10.1039/C8GC02972E).
- [11] F. Zafar, M. Azam, E. Sharmin, H. Zafar, Q.M. Rizwanul Haq, N. Nishat. Nanostructured coordination complexes/polymers derived from cardanol: "one-pot, two-step" solventless synthesis and characterization. *RSC Adv.*, **2016**, *6*, 6607-6622. doi: [10.1039/C5RA20171C](https://doi.org/10.1039/C5RA20171C).

- [12] T. de J. A. de S. Andrade, B.Q. Araújo, A.M.de G. L. Citó, J. da Silva, J. Saffi, M.F. Richter, A. de B. F. Ferraz. Antioxidant properties and chemical composition of technical Cashew Nut Shell Liquid (tCNSL). *Food Chem.*, **2011**, *126*, 1044-1048. doi: <https://doi.org/10.1016/j.foodchem.2010.11.122>
- [13] A. Kozubek, J.H.P. Tyman. Resorcinolic Lipids, the Natural Non-isoprenoid Phenolic Amphiphiles and Their Biological Activity. *Chem. Rev.*, **1999**, *99*, 1-26. doi: [10.1021/cr970464o](https://doi.org/10.1021/cr970464o).
- [14] M. Ahamed, H.A. Alhadlaq, M.A.M. Khan, P. Karuppiyah, N.A. Al-Dhabi. Synthesis, characterization, and antimicrobial activity of copper oxide nanoparticles. *J. Nanomater.*, **2014**, *2014*,4. doi: [10.1155/2014/637858](https://doi.org/10.1155/2014/637858).
- [15] E. Sharmin, F. Zafar, D. Akram, S. Ahmad. Plant oil polyol nanocomposite for antibacterial polyurethane coating. *Prog. Org. Coat.*, **2013**, *76*, 541-547. doi: <http://dx.doi.org/10.1016/j.porgcoat.2012.10.027>.



Checklist of Flora and Floristic Study of Wadi Al-Hamar Region in Libya

Naser O. I. Omar^a, Mohamed A. Alaib^b, Naser G. El-Mghrbi^c and Abdul Hamid K. Alzerbi^{d*}.

^a Department of Botany, Faculty of Arts and Sciences, University of Benghazi- Alabear Brach, Libya.

^b Department of Botany, Faculty of Sciences, University of Benghazi, Benghazi, Libya.

^c Department of Botany, Faculty of Sciences, University of Ajdabiya, Ajdabiya, Libya.

^d Department of Botany, Faculty of Arts and Sciences, University of Benghazi, Tocra, Libya.

ARTICLE INFO

Article History:

Submission date: 08/03/2020

Accepted date: 23/06/2020

Keywords:

Floristic, Raunkiaer life forms, Wadi Al-Hamar, Libya.

ABSTRACT

The piece of work has been designed to study the present-day vegetation and document the flora of wild plants of the Wadi Al-Hamar region north Middle Libya. A survey of plant species of the Wadi was conducted between October 2017 to May 2018, with two trips per month at least. The plant specimens were collected in flowering or in fruiting stage. Data inventory has been documented in the form of family, Botanical name, vernacular name, life form, and habit. The study revealed the presence of 112 species within 93 genera of vascular plants belonging to 31 families, of which 13 species are belonging to monocotyledons and 99 belonging to dicotyledons. The family Asteraceae was the richest (21 species) followed by Fabaceae (19 species), then Poaceae and Brassicaceae (8 and 7 species respectively). In this study, two endemic species have been collected. The most dominant life form was therophytes having 72 species (64.28%) followed by chamaephyte having 16 species (14.28%), Hemicryptophytes 9 species (8.03%), Geophytes 8 species (7.14%), Phanerophytes 6 species (5.35%) and Parasites 1 species (0.89%). Finally, most of the species were herbs (87.5%).

1. Introduction

Libya is a huge arid desert with an area of about 1,760,000 square kilometers and covers the majority of North Africa. It is bordered by the Mediterranean Sea, Egypt, Sudan, Chad, Niger, Algeria, and Tunisia. It lies between 18° and 33°N and 9° and 25°E. Consisting mainly of desert and the Mediterranean coast. In Libya, about 94 to 96 % of the land is desert and it is one of the driest countries in the world [1]. Floristic studies gain increasing importance in recent years in response to the need for developing and under-developing countries to assess their plant wealth. Many floristic diversity studies have been conducted in different parts of the world. Thus, floristic studies are undertaken by many researchers worldwide at different levels [2].

A various floristic study has been conducted on the Flora of Libya, e. g. Lemaire in [3], reported some observations on Sylphium which was one of the most important extinct plant species in Cyrenaica. Della-Cella [4] had conducted the first taxonomic study on Flora of Libya and collected about 260 species from the coastal belt of Libya. Viviani [5] published Flora Libycae specimen and reported 1200 plant samples [6]. Rohlf [7] provided the most comprehensive information on the vegetation of Tripolitania, Fezzan, Ghadames, Kufra, Aoujila, and Cirenaica as well as a list of vernacular names of plants. Durand and Barratte [8] had published Florae Libycae Prodrum and listed 1026 species. Pampanini [9] had published two books namely, Plantae Tripolitanae and Prodrumo Della Flora Cirenaica, respectively. Keith [10] published A Preliminary Check List of the Flora of Libya, provided their local names and uses. Boulos [11] published a bibliography about the flora and vegetation of Libya. The University of Tripoli and the Arab Development Institute adopted the flora of Libya projects and have published between 1976 to 1989. through last three decades, Numerous researchers have worked on floristic composition and ecological studies on regional or local floras of certain parts of the country; examples include the studies of Asker [12] on Wadi Al-Asrah, Al-Hamed [6] on Wadi Al-Agar, Al-Habony [13] on Tobruk province, Alaib and Ihsaen [14].

Moreover, floristic studies are not only important to know the variety of plants present in an area, but also their socio-economical significants. They provide shelter, food, medicine and everything for the human being and other species of that area [15]. The specific goals

of the study were to analysis the vegetation, prepare preliminary list of the species of flowering plants, life-form and the diversity in the Wadi Al-Hamar.

2. Study Area

The study area is located about 90 Km east of Sitre City in the middle of northern Libya, bordered to the north by the Mediterranean Sea and from the south side at approximately 31° 01' to 30° 59' N latitude and 17° 28' E longitudes. The area rises to about 11 m above sea level. Al-Wadi Al-Ahmar is one of the main and important valleys in the northern middle part of Libya (Figure 1). Where meet several valleys from the south, which originated from floodwaters in the rainy years, resulting in water drifts in the form of deep grooves that all gather together and take a downward slope towards the north, forming the delta of the valley ending in moving dunes.



Figure 1: Map of the study area

3. Soil

The soil in the study area is deep. The soil depth is more than 150 cm. Besides the soil is characterized by light texture, it is between sand and loamy sand. Therefore, it's characterized by high surface filtration with low water holding capacity. Electrical conductivity (EC) of the soil in the study area is about 1.2 mmhos/cm, which is very good in terms of, salts content. The coastal area of the Delta is characterized by sand dunes (Clay 2.69, Silt 2.21, Sand 95). The pH value is 9, the

* Corresponding Author

Department of Botany, Faculty of Arts and Sciences, University of Benghazi, Tocra, Libya.

E-mail address: abdulhamid.alzerbi@uob.edu.ly (Abdul Hamid K. Alzerbi).

1685-4732 / 1685-4740 © 2020 UQU All rights reserved.

salt content is 2662 ppm and the calcium carbonate is 73% and the organic matter is 0.32%. The soil of central area of the valley mixed from sandy to loamy sand (Silt 4.64, Sand 89, Clay 5.36), pH8.59, salinity 480 ppm, calcium carbonate ratio 4.67%, organic matter 0.24%, whereas the southern interior areas at the beginning of the composition of the valley, which are characterized by the dark red soil pH 8.27.

4. Climate

The climate of the study area is subtropical semi-arid to arid [16]. It is chiefly characterized by its aridity and by its wide variation in temperatures. The temperatures are high and the rainfall is low. As a result, there can be an abrupt transition from one kind of weather to another, in summer it is extremely hot. The heat of summer is often aggravated by Ghibli winds. There is a hot dry season from May to October and a cold and rainy season from November to April.

5. Materials and methods

The study area was regularly visited from October 2017 to May 2018. The plant specimens were collected in flowering or in fruiting condition.

For drying, the presser containing the specimens was placed in the sun. After that, the specimens were examined individually, rearranged, transferred to a fresh sheet and again tightly bonded in the presser. The specimens were changed to dry sheet every 24 or 48 hours until they were completely dry.

Table 1: List of species recorded in the study area with their families, Vernacular name, life form and Growth form (Th. = Therophytes, Ch. = Chaemophytes, H. = Hemi-cryptophytes, Ph. = Phanerophytes, G. = Geophytes, and P. = Parasites) Dicotyledons.

Species.	Vernacular name	Family	Life form	Growth form
<i>Emex spinosus</i> (L.) Campd	Dors el-azouz and el-henzab	Polygonaceae	Th.	Herb
<i>Polygonum equisetiforme</i> Sibth. And Sm.	Gurdab	Polygonaceae	H.	Subshrub
<i>Rumex pictus</i> Forssk.	Hommada	Polygonaceae	Th.	Herb
<i>Mesembryanthemum crystallinum</i> L.	Ghassoul	Aizoaceae	Th.	Herb
<i>Silene cerastioides</i> L.		Caryophyllaceae	Th.	Herb
<i>Vaccaria pyramidata</i> Medik.	Ful el Arab	Caryophyllaceae	Th.	Herb
<i>Paronychia arabica</i> (Linn.) Dc.	Tifun	Illecebraceae	H.	Herb
<i>Atriplex halimus</i> L.	Kataff	Chenopodiaceae	Ph.	Subshrub
<i>Bassia muricata</i> (L.) Aschers.	Chouleta, Ghabbir	Chenopodiaceae	Th.	Herb
<i>Beta vulgaris</i> L.	Seleg	Chenopodiaceae	Th.	Herb
<i>Chenopodium murale</i> L.	Effena	Chenopodiaceae	Th.	Herb
<i>Halocnemum strobilaceum</i> (Pall.) M.Bieb.	Hdidat, Rehsal, Shenin	Chenopodiaceae	Ch.	Subshrub
<i>Salsola kali</i> L.		Chenopodiaceae	Th.	Subshrub
<i>Suaeda vera</i> Forssk ex J.F.Gmel	Souida, Essabata	Chenopodiaceae	Ch.	Subshrub
<i>Amaranthus viridis</i> L.	Buzinzir	Amaranthaceae	Th.	Herb
<i>Adonis dentata</i> Delile	Zeghalil	Ranunculaceae	Th.	Herb
<i>Glaucium corniculatum</i> (L.) Rud.	Gurn- aljadian	Papaveraceae	Th.	Herb
<i>Papaver hybridum</i> L.	Bugraun, Garaun	Papaveraceae	Th.	Herb
<i>Hypecoum geslinii</i> Coss.et kral		Hypecoaceae	Th.	subshrub
<i>Brassica tournefortii</i> Gouan	Shultam	Brassicaceae	Th.	Herb
<i>Diploaxis muralis</i> (L.) Dc. ssp. Muralis		Brassicaceae	Th.	Herb
<i>Enarthrocarpus clavatus</i> Del.ex Goder.	Shultam	Brassicaceae	Th.	Herb
<i>Hussonia pinnata</i> (Viv.) Jafri		Brassicaceae	Th.	Herb
<i>Lobularia libyca</i> (Viv.) Meisner		Brassicaceae	Th.	Herb
<i>Matthiola longipetala</i> (Vent.) Dc. Ssp. Longipetala		Brassicaceae	Th.	Herb
<i>Sisymbrium irio</i> L.		Brassicaceae	Th.	Herb
<i>Reseda alba</i> L.spp. decursiva (Forsk.) Maire	m"sawiyah, Fattolet El Holi	Resedaceae	Th.	Herb
<i>Argyrolobium uniflorum</i> (Dence.) Jaub. & Sapach	Ergah, Kherta	Fabaceae	Ch.	Herb
<i>Astragalus asterias</i> Stev. ex Ledeb		Fabaceae	Th.	Herb
<i>Astragalus boeticus</i> L.	Grambushia	Fabaceae	Th.	Herb
<i>Astragalus cabrinus</i> L.	Shaewit Erraie	Fabaceae	H.	Herb
<i>Astragalus peregrinus</i> Vahl		Fabaceae	Th.	Herb
<i>Hippocrepis multisiliquosa</i> L.		Fabaceae	Th.	Herb
<i>Lathyrus clymenum</i> L.		Fabaceae	Th.	Herb
<i>Lotus cytisoides</i> L.		Fabaceae	Ch.	Herb
<i>Lotus halophilus</i> Boiss & Spruner.	Nafel, Gurn al – Ghazzal	Fabaceae	Th.	Herb
<i>Medicago disciformis</i> Dc.		Fabaceae	Th.	Herb
<i>Medicago littoralis</i> Rohde ex Lois	Nafal	Fabaceae	Th.	Herb
<i>Medicago sativa</i> L.	Gadb, safsafa,	Fabaceae	Th.	Herb
<i>Medicago minima</i> (L.) Bart.	Nafal	Fabaceae	Th.	Herb
<i>Melilotus indicus</i> (L.) All		Fabaceae	Th.	Herb
<i>Ononis serrata</i> Forsk.		Fabaceae	Th.	Herb
<i>Retama raetam</i> (Forsk.) webb.		Fabaceae	Ph.	subshrub
<i>Trigonella maritima</i> Delile ex Poirret	Kherta, Garat	Fabaceae	Th.	Herb
<i>Vicia monantha</i> Retz.		Fabaceae	Th.	Herb
<i>Vicia sativa</i> L.	Jilban.	Fabaceae	Th.	Herb
<i>Vicia villosa</i> Roth	Jelbana Hmam	Fabaceae	Th.	Herb

When specimens were completely dry they were mounted on herbarium sheet with stander size (27 x 42 cm) with the aid of adhesives. On the lower right-hand corner of the herbarium sheet, a label was glued and all information from the field notebook was transferred to it. First, the family of the plant was determined by the use of an artificial key to the families. The genus and species were identified by the utilization of available taxonomic literature [17-19,10,20,21].

After drying, specimens were flooded with poisoning solution (Mercuric chloride 15 gm, Ammonium chloride 35 gm, in 1000 ml ethanol 96%) to protect them from fungi and pests [22]. Or placed in an oven at 60° C for 4-6 hours, which is enough to kill eggs of insects [23]. All plant species studied, were classified according to their growth habits, and Raunkiaer's life forms system [24] was used. The percentage composition of each of these life form categories was calculated.

6. Results and Discussion

6.1. Enumeration of species

Taxa collected from the study area are enumerated here. For the arrangement of families, Engler's syllabus der Pflanzen families, 12th edition [25] were used. The circumscription of the families is the same as in flora of Libya. The genera and species in each family are arranged alphabetically (Table 1 and Table 2).

Species.	Vernacular name	Family	Life form	Growth form
<i>Oxalis pes-caprae</i> L.	Hummdha	Oxalidaceae	Th.	Herb
<i>Erodium cicutarium</i> (L.) L' Herit	Dahmiyet el-ghazl.	Geraniaceae	Th.	Herb
<i>Euphorbia terracina</i> L.	Lebbena	Euphorbiaceae	H.	Herb
<i>Malva parviflora</i> L. var. <i>parviflora</i>	Khobaiz	Malvaceae	Th.	Herb
<i>Malva sylvestris</i> L.	Khobaiz	Malvaceae	H.	Herb
<i>Thymelaea hirsuta</i> (L.) Endl.	Metnan	Thymelaeaceae	Ph.	Subshrub
<i>Helianthemum lippii</i> var. <i>sessiliflorum</i> (Desf.) Murb.	Lerga.	Cistaceae	Ch.	Herb
<i>Nitraria retusa</i> (Forsk.) Asch		Zygophyllaceae	Ph.	Shrub
<i>Daucus syrticus</i> Murb		Apiaceae	Th.	Herb
<i>Pituranthos tortuosus</i> (Desf.) Benth.	Gazzah.	Apiaceae	Ch.	Subshrub
<i>Pseudorlaya pumila</i> (L.) Gramde		Apiaceae	Th.	Herb
<i>Anagallis arvensis</i> var. <i>caerulea</i> (L.) Gouan	Ain Algatuu	Primulaceae	Th.	Herb
<i>Convolvulus althaeoides</i> L.	Ullak	Convolvulaceae	G.	Herb
<i>Convolvulus arvensis</i> L.	Ullak	Convolvulaceae	G.	Herb
<i>Convolvulus supinus</i> Coss. et Kral	Ullak	Convolvulaceae	Th.	Herb
<i>Echium angustifolium</i> Mill.	Henna alagrab, abat elgula	Boraginaceae	Ch.	Subshrub
<i>Echium horridum</i> Batt		Boraginaceae	Ch.	Subshrub
<i>Gastrocotyle hispida</i> (Forsk) Bunge		Boraginaceae	Th.	Herb
<i>Heliotropium ramosissimum</i> (Lehm.) De.	Tahaunna, tahenna	Boraginaceae	Ch.	Herb
<i>Ajuga iva</i> (L.) Shreber	Shandgura	Lamiaceae	Th.	Herb
<i>Salvia lanigera</i> Poir.	Sag en naga	Lamiaceae	Ch.	Herb
<i>Teucrium davaeanum</i> Coss.		Lamiaceae	Ch.	Herb
<i>Lycium europeum</i> L.	Awesaj	Solanaceae	Ph.	Shrub
<i>Solanum nigrum</i> L. var. <i>Nigrum</i>	Anab ed. Deeb	Solanaceae	H.	Herb
<i>Nicotiana glauca</i> R.C. Graham	Akkuzemusa.	Solanaceae	Ph.	Shrub
<i>Haplophyllum tuberculatum</i> (Forsk) Juss.	Affia	Rutaceae	Ch.	Herb
<i>Kickxia aegyptiaca</i> (L.) Nabelek ssp. <i>Aegyptiaca</i>	Amekchin	Scrophulariaceae	Ch.	Herb
<i>Linaria tarhunensis</i> Pamp.		Scrophulariaceae	Th.	Herb
<i>Linaria tenuis</i> (Viv.) Spreng.		Scrophulariaceae	Th.	Herb
<i>Orobanche schultzii</i> Mutel.		Orobanchaceae	P.	Herb
<i>Plantago albicans</i> L.	Aenm.	Plantaginaceae	H.	Herb
<i>Anacyclus monanthos</i> (L.) Thell.	Tagrefta, Serat elkabesh.	Asteraceae	Th.	Herb
<i>Artemisia momosperma</i> Delile	Tguft	Asteraceae	Ch.	Herb
<i>Anthemis secundiramea</i> Biv.		Asteraceae	Th.	Herb
<i>Calendula tripterocarpa</i> Rupr.		Asteraceae	Th.	Herb
<i>Carduus getulus</i> Pomel		Asteraceae	Th.	Herb
<i>Centurea alexandrina</i> Delile	Mrrier.	Asteraceae	Th.	Herb
<i>Centurea dimorpha</i> Viv.	Bla 'ala	Asteraceae	Th.	Herb
<i>Chrysanthemum coronarium</i> L.	Gahwan	Asteraceae	Th.	Herb
<i>Conyza aegyptiaca</i> (L.) Dryander		Asteraceae	Th.	Herb
<i>Conyza bonariensis</i> (L.) Comq.	Ashbet Zamora	Asteraceae	Th.	Herb
<i>Crepis senecioides</i> Delile		Asteraceae	Th.	Herb
<i>Echinops galalensis</i> Schweinf	Shembet Elgatoos	Asteraceae	H.	Herb
<i>Hypochaeris achyrophorus</i> L.		Asteraceae	Th.	Herb
<i>Launaea resedifolia</i> (L.) O. Kuntze	Adeeda.	Asteraceae	Th.	Herb
<i>Onopordum arenarium</i> (Desf.) Pomel	Libid	Asteraceae	H.	Herb
<i>Reichardia tingitana</i> (L.) Roth.	Sahani.	Asteraceae	Th.	Herb
<i>Rhantterium suaveolens</i> Desf.		Asteraceae	Ch.	Herb
<i>Rhaponticum acaule</i> (L.) DC.		Asteraceae	Ch.	Herb
<i>Senecio gallicus</i> Chiaux	Daraita, Mourare.	Asteraceae	Th.	Herb
<i>Senecio vulgaris</i> L.	Kraa Eddjaja	Asteraceae	Th.	Herb
<i>Sonchus oleraceus</i> L.	Tefaf.	Asteraceae	Th.	Herb

Table 2: List of species recorded in the study area with their families, Vernacular name, life form and Growth form (Th. = Therophytes and G. = Geophytes) Monocotyledons

<i>Asphodelus fistulosus</i> L.	Lehiat ettaes	Liliaceae	G.	Herb
<i>Muscari comosum</i> (L.) Mill.	Keltout , Katout	Liliaceae	G.	Herb
<i>Scilla Preuviana</i> L.	Possaila	Liliaceae	G.	Herb
<i>Allium subhirsutum</i> L.	Ghazul.	Alliaceae	G.	Herb
<i>Allium nigrum</i> L.		Alliaceae	G.	Herb
<i>Avena barbata</i> Pott ex Link		Poaceae	Th.	Herb
<i>Bromus rigidus</i> Roth.		Poaceae	Th.	Herb
<i>Cutandia dichotoma</i> (Forsk.) Trabut	Zewahn , bu 'rukba	Poaceae	Th.	Herb
<i>Cynodon dactylon</i> (L.) Pers.	Najem, Najjeel	Poaceae	G.	Herb
<i>Hordeum murinum</i> L. ssp. <i>Leporinum</i> (link.) Arcang.		Poaceae	Th.	Herb
<i>Lolium rigidum</i> Gaud.	Bomanjor.	Poaceae	Th.	Herb
<i>Phalaris minor</i> Retz.	Zewan	Poaceae	Th.	Herb
<i>Stipa capensis</i> Thunb.	Behma	Poaceae	Th.	Herb

At the end of the survey there was a total of 112 species of flowering plants, 93 representing genera belong to 31 families that have been collected and identified, of which 99 taxa belonging to 81 genera that belong to Dicotyledons which distributes in 28 families; whereas 13 taxa belonging to 12 genera and 3 families are belonging to monocotyledons (Table 3). The ratio of Dicotyledons to Monocotyledons is roughly 8: 1.

Table 3: Different taxonomic groups present in the study area.

Plant group	No. of families	No. of Genera	No. Species
Dicotyledons	28	81	99
Monocotyledons	3	12	13
Total	31	92	112

From floristic analysis were carried out which showed the most highly represented families were Asteraceae and Fabaceae being the richest with 21 and 19 species respectively. The next largest family was Poaceae with 8 species. Brassicaceae and Chenopodiaceae with 7 species followed by Boraginaceae represented by 4 species (Figure 2). Seven families namely, Convolvulaceae, Polygonaceae, Lamiaceae, Solanaceae, Liliaceae, Apiaceae and Scrophulariaceae, were represented by 3 species each. The families which include 2 species were Alliaceae and Caryophyllaceae, whereas the rest families were represented by only a single species occupying different habitats. A comparison of families in the largest number of species recorded in this study is similar to the studies in different regions of Libya, example studies of Asker [12], Al-Hamedy [6], Al-Habony [13], Alaib and Ihsaen [14] (Table 3).

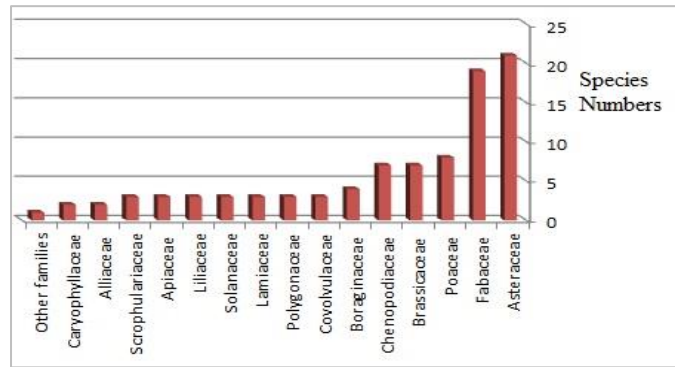


Figure 2: Floristic richness-Diversity-of the study area

According to the number of species in each genus in the study area, *Astragalus* and *Medicago* were the only two genera represented by four species each. Two genera, *Vicia* and *Convolvulus* have three species each. Six genera namely, *Lotus*, *Malva*, *Echium*, *Linaria*, *Centurea*, *Conyza* and *Allium* were represented by two species each in the study area.

In this study, two species considered as endemic species to Libya. These species namely, *Linaria tarhunensis* and *Teucrium davaenum*.

Plant life forms were categorized as Therophytes with 72 species (64.28%), Chamaephytes with 16 species (14.28%), Hemicryptophytes with 9 species (8.03%), Geophytes with 8 species (7.14%), Phanerophytes with 6 species (5.35%), Parasites with 1 species (0.89%) (Figure 3). Therophytes and Chamaephytes were dominated in Wadi Al Hamar. These findings were in agreement with previous studies on different regions of Libya which have been recorded by many researchers such as Al-Habony [13], Ihsaen [26], Mahklouf and Al Sghair [27], who reported that the dominance of these two life forms may be due to hot dry climate, topography variations and biotic influence.

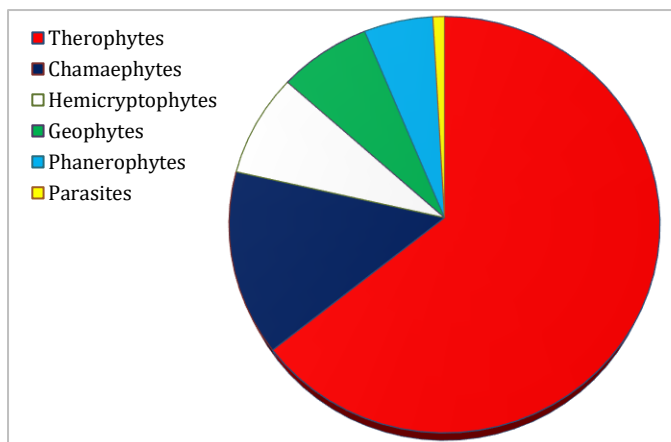


Figure 3: Biological spectrum of plant species in the flora of Libya.

The study showed that the growth habits of species were distributed as herbs 98 species (87.5%) and subshrubs to shrubs 14 species (12.5%). The dominance of herbs over the other growth habits can be attributed to the short life cycle that enables them to resist the instability of the ecosystem [28].



Malva parviflora



Malva sylvestris



Orobanche schultzei



Atriplex halimus



Paronychia arabica



Phalaris minor



Anagallis arvensis



Oxalis pes-caprae



Asphodelus fistulosus



Convolvulus althaeoides



Papaver hybridum



Reichardia tingitana

*Sonchus oleraceus**Centurea dimorpha**Anthemis secundiramea**Chrysanthemum coronarium**Astragalus cabrinus**Melilotus indicus*

7. Conclusion

The findings of this study clearly show that the flora is poor floristically which may be attributed to its topography, edaphic factors, and climatic conditions.

Reference

- [1] L.R. Holdridge, Determination of world plant formations from simple climatic data. *Science*. 1974, 105, 367-368. DOI: 10.1126/science.105.2727.367
- [2] G. P. Ravindra, A. D. Kshirsagar. Floristic Study of Shirur Region Pune, Maharashtra, India. *Int. Res. J. Biological Sci.*, 2013, 2(5), 78-82.
- [3] Lemair, Les antiquites de la cyrenaique ou il est aussi question du "seltion" que M. Bonnet areconnu etra le Phlomis floccosa. France, 1703.
- [4] P. Della-Cella, Viaggio da Tripoli di Barberia alle frontier occidental del. 1, Egitto. 222 P., 2plates and 1map Geneva, 1819.
- [5] D. Viviani, Flora Libycae Specimen Sive Plantarum Eneumaratio. *Gnaue*, 1824. I-XII. 1-68.27 tables.
- [6] R. Al-Hamedi, Floristic and Ecological Study of Wadi Al-Agar. *M.Sc. Thesis*. Benghazi University, Libya, 1999.
- [7] G. Rohlfs, Reise nach Kurta and beschrei Bung der Oase, Miltg Africa-ges. *Deutsch land*, 1881, 2, 17-39.
- [8] E. Durand, G. Barratte, Avec la collaboration de Ascherson P, Muschler, B.W. and Apercn Geolg R. Sur la tripdilaira par meunier Florae Libcae prodromus, on catalogue Raiaonne des plantes de Tripoli, 1910.
- [9] Pampanini. Prodromo della flora Cirenaica forli *Tipgrafia Valbonesi*, 1930-1931 69-81.
- [10] H. G. Keith, A Preliminary Check-list of Libyan Flora. *The Government of the Libyan Arab Republic, Ministry of Agriculture and Agrarian Reform*, Tripoli, Libya 2, 1965.
- [11] L. Boulos, Our present knowledge on the flora and vegetation of Libya, *Webbia*, 1972, 26, 366-400.
- [12] A. M. Asker, Vegetation and Flora of Wadi Al-Asrha. *M.Sc. Thesis*, Benghazi University, Libya, 1998.
- [13] M. E. Al-Habony, Vegetation and Flora of a Sector Along the Mediterranean Coast of Libya from Tobruk to Egyptian Border. *M.Sc. Thesis*. Benghazi University, Libya, 1999.
- [14] M. A. Alaib, N. O. Ihsaen, Weed Flora of Great Man-Made River agriculture Project (Sirte). *Journal of Agriculture and Environment for International Development*. 2008, 102(3).
- [15] H. S. Shehata, T. M. Galal. Factors affecting the distribution and associated species of *Malva parviflora* in the Nile Delta, Egypt. *Weed Biol. Manag*, 2014, 15, 42-52. <https://doi.org/10.1111/wbm.12063>
- [16] I. El-Maghrabi, Geological map of Libya sheet Qasr Sirte. Industrial Research center, Tripoli, 1977.
- [17] F. B. Erteb, A key to the families of the flora of Libya. Tripoli intl Scientific Bookshop Tripoli- Libya and Intl. pub. & Dist. House Cairo- Egypt, 1994.
- [18] S. I. Ali, S. M. H. Jafri, Flora of Libya, Vols. 1-24 Department of Botany, University of Tripoli, Tripoli 1976-1977.
- [19] A. El-Gadi, Flora of Libya. Vols. 145-147. Department of Botany, Al-faateh Univ., Tripoli, 1988-1989.
- [20] S. M. H. Jafri, A.A. El-Gadi, Flora of Libya. 25-144 Department of Botany, Tripoli University, Tripoli, 1977-1986.
- [21] V. Tackholm, Students flora of Egypt. 2nd ed. Cairo University, Cairo, 1974.
- [22] G. F. El-Sahar, Introduction to Plant Taxonomy. Dar Mediterranean Sea Publishing, 1987.
- [23] A. E. Radford, W.C. Dickson, J. R. Massey. Vascular plant systematic. The president and Fellows of Harvard University, 1974.
- [24] C. Raunkiaer, The life forms of plants and statistical plant geography, Clarendon Press, Oxford, 1934.
- [25] H. A. Melchoir, Engler's syllabus der Pflanzenfamilien, 12th Ed., part II, Borntraeger, Berlin, 1964.
- [26] N. O. Ihsaen, Weed Flora of Great Man-Made River agriculture Project (Sirte). *M.Sc. Thesis*. Sirte University, Libya 2005.
- [27] M. H. Mahklouf, F. G. Al Sghair. Biodiversity and Floristic Study of Al-Hdaba Treatment Plant Tripoli-Libya. *American Journal of Life Science Researches* 2016, 4(3), 101-103. <http://dx.doi.org/10.21859/ajlsr-040307>
- [28] N. H. Gomaa, Composition and diversity of weed communities in Al-Jouf province, northern Saudi Arabia. *Saudi J. Biol. Sci.* 2012, 19, 369-376. doi: 10.1016/j.sjbs.2012.05.002



Radiative atomic and collisional data for Ar VI allowed and forbidden lines

Haykel Elabidi

Common First Year Deanship, Physics Department, Umm Al-Qura University, Makkah, Saudi Arabia.^bLaboratory of Molecular Spectroscopy and Dynamics, Sciences Faculty of Bizerte, Carthage University, Tunisia.

ARTICLE INFO

Article History:

Submission date: 17/11/2019

Accepted date: 16/11/2020

Keywords:

Atomic data, forbidden transitions, electron scattering, effective collision strengths.

ABSTRACT

Energy levels, lifetimes, oscillator strengths, radiative decay rates, line strengths, electron-impact collision strengths and effective collision strengths are presented for aluminium-like Ar VI. New radiative data for forbidden lines are presented for the first time. We used the following 12 configurations in our work: $3s^2 3p$, $3s 3p^2$, $3s^2 3d$, $3p^3$, $3s 3p 3d$, $3s^2 4s$, $3s^2 4p$, $3p^2 3d$, $3s^2 4d$, $3s 3p 4s$, $3s 3p 4p$ and $3s 3p 4d$ yielding to 121 fine structure levels. The calculations have been carried out using the AUTOSTRUCTURE code. It included the one-body and the two-body (fine and non-fine structure) interactions of the Breit–Pauli Hamiltonian. No results for forbidden transitions have been found in the literature. For the collisional problem, the distorted wave approximation has been assumed. Collision strengths have been calculated at six electron energies: 10, 50, 100, 200, 400 and 800 Ry. Convergence of collision strengths with total angular momentum has been studied at each electron energy. For some lines, we make use also of the codes SUPERSTRUCTURE/DISTORTED WAVE/JAJOM to compare with the AUTOSTRUCTURE results. Effective collision strengths have been calculated for a wide range of temperatures up to 3.6×10^5 K, and are compared to those from the Breit–Pauli R-matrix method.

1. Introduction

Radiative atomic and collisional data have an important role in modelling of astrophysical plasmas and in tokamaks. In the case of non-local thermodynamic equilibrium (NLTE) plasmas, it is important to know all the excitation/ de-excitation processes that contribute to the intensity of the lines. Consequently, electron collision strengths are required for calculating level populations and spectral line intensities. These parameters can provide diagnostics of temperature, density, and abundance of elements in a plasma. Argon ions are important in astrophysics and in fusion [1,2]. The Ar VI absorption lines have been identified in the spectrum of a hydrogen-rich star LS V +46°21 [3]. These authors identified the Ar VI transition at 1303.87 Å as an isolated line in the HST/STIS (Space Telescope Imaging Spectrograph aboard the Hubble Space Telescope) spectrum of that star. It was the first time that Ar VI has been detected in the photosphere of any star. Excitation data for argon ions are also required to analyse data collected by spectrographs onboard other satellites, such as Chandra or XMM-Newton to be used as plasma diagnostics of stellar temperature and density.

The first results for the spectrum of Ar VI in the vacuum ultraviolet were published by Phillips and Parker [4]. A list of many theoretical and experimental works dedicated to the Ar VI ion before 1992 was reported in [5]. Recently, a new analysis of the Ar VI spectrum in the vacuum ultraviolet region was reported by Rainerie *et al.* [6], where adjusted and new energy levels and new classified lines were obtained. Calculations of energy levels, oscillator strengths and lifetimes have been performed by Gupta and Msezane [7] using only ten configurations. Newer calculations that provide oscillator strengths and transitions probabilities for Ar VI were presented in Froese Fischer *et al.* [8], where the authors used the multiconfiguration Hartree-Fock (MCHF) and the multiconfiguration Dirac-Hartree-Fock (MCDHF) methods. Electron-impact excitation calculations have been done for the argon isonuclear sequence using the first-order many-body perturbation theory [9] and using the Breit-Pauli R-matrix method [2]. The results of [2] have been provided as effective collision strengths. Some preliminary results for Ar VI have been presented in [10] (only for some transitions and without effective collision strengths). Here, we report a complete set of radiative atomic data

(including for the first time forbidden transitions) and distorted wave collisional data: collision strengths and effective collision strengths for Ar VI.

We report in this work 121 Ar VI energy levels and compare them to the values compiled by the National Institute of Standards and Technology (NIST) [11] and to the newer existing theoretical results of Froese Fischer [8], where the MCHF method has been used. The radiative data (line strengths, absorption oscillator strengths and radiative decay rates) for electric dipole (E1) transitions involving the 121 levels have been compared to the MCHF results of [8]. Line strengths and radiative decay rates for electric quadrupole (E2) and octopole (E3) and magnetic dipole (M1) and quadrupole (M2) transitions have been calculated, since they are also required for plasma modelling. No data for forbidden lines have been found in the literature to perform comparisons. Additionally, theoretical lifetimes are listed for all the 121 obtained levels. Electron-impact excitation collision strengths at six electron energies 10, 50, 100, 200, 400 and 800 Ry have also been presented. The structure and collision calculations have been carried out using the AUTOSTRUCTURE code (AS) of Badnell [12,13]. We study the convergence of collision strengths with the total angular momentum, and we illustrate this for some transitions. In several cases, we perform scattering calculations using the University College London (UCL) codes: SUPERSTRUCTURE (SST) [14], DISTORTED WAVE (DW) [15] and JAJOM [16,17] and compare with the AS results. We present also effective collision strengths for large temperature range suitable for plasma modelling.

2. Description of the numerical method

2.1. Structure

The atomic structure has been calculated using the AS code of Badnell [12,13], by constructing target wavefunctions using radial wavefunctions calculated in a scaled Thomas–Fermi–Dirac–Amaldi statistical model potential. The scaling parameters λ_{nl} (depending on n and l) are determined by minimizing the sum of the energies of all the target terms, computed in LS coupling, i.e. neglecting all relativistic effects. In this code, besides the one-body and the two-body fine structure interactions, the two-body non-fine structure operators of the Breit–Pauli Hamiltonian, namely contact spin–spin,

* Corresponding Author

Common First Year Deanship, Physics Department, Umm Al-Qura University, Makkah, Saudi Arabia.

E-mail address: haelabidi@uqu.edu.sa (Haykel Elabidi).

1685-4732 / 1685-4740 © 2020 UQU All rights reserved.

two-body Darwin and orbit-orbit are incorporated. More details of these interactions and how they are incorporated can be found in [12-14], here, we present only a brief description of the theory.

The non-relativistic case is described by the Hamiltonian:

$$H_{nr} = \sum_{i=1}^N h_i + \sum_{j>i}^{N+1} \frac{2}{r_{ij}}, \text{ and } h_i = -\nabla_i^2 - \frac{ZZ}{r_i}, \quad (1)$$

where N is the number of electrons, Z is the nuclear charge, the energy is expressed in Ry and lengths are given in units of the Bohr radius $a_0 = \hbar^2/me^2 = 0.529 \text{ \AA}$. The problem of N body with $N > 1$ cannot be solved rigorously. The approximate solutions satisfy the variational principle:

$$\delta\{f|H - E|f'\} = 0. \quad (2)$$

f and f' are the trial functions ($f = C\alpha SL$) where C is a given configuration and α is a degeneracy parameter used when more than one term with the same SL correspond to a specific configuration C . With the Hamiltonian given by equation (1), the total spin \mathbf{S} and the total angular momentum \mathbf{L} are separately conserved and so the correspondent quantum numbers S and L are "good" quantum numbers for the system. The approximate functions $|fM_S M_L\rangle$ for the N -electrons system are developed in terms of Slater states $|u\rangle$ (defined as the product of the N one-electron functions):

$$|f\rangle = \sum_u |u\rangle\langle u|f\rangle, \text{ where } |u\rangle = \prod_{q=1}^N |n_q l_q \mu_q m_q\rangle, \quad (3)$$

where $n_q l_q \mu_q m_q$ are the quantum numbers of the q^{th} electron. The system obeys the exclusion principle of Pauli and thus the product in equation (3) has to be antisymmetric. The summation over the states u in (3) includes those states satisfying $M_S = \sum_{q=1}^N \mu_q$ and $M_L = \sum_{q=1}^N m_q$. The non relativistic part is treated in LS coupling. The relativistic interactions are introduced through the N -electrons Breit-Pauli Hamiltonian [18]: $H_{BP} = H_{nr} + H_{rc}$, where H_{nr} is given by (1) and:

$$H_{rc} = \sum_{i=1}^N \left\{ \underbrace{f_i(mass)}_{\text{mass-variation}} + \underbrace{f_i(d)}_{\text{Darwin}} + \underbrace{f_i(so)}_{\text{spin-orbit}} \right\} + \sum_{i>j} \left\{ \underbrace{g_{ij}(so + so')}_{\text{spin-other-orbit}} + \underbrace{g_{ij}(ss')}_{\text{spin-spin}} + \underbrace{g_{ij}(css')}_{\text{contact-spin-spin}} + \underbrace{g_{ij}(d)}_{\text{Darwin}} + \underbrace{g_{ij}(oo')}_{\text{orbit-orbit}} \right\}. \quad (4)$$

The first sum describes the one-body terms, and the second one describes two-body terms. The three last terms in the second sum represent the two-body non-fine structure interactions which are ignored in SST [14], but incorporated in AS [13]. The expressions of all the terms in equation (4) are given explicitly in [14]. With the introduction of the relativistic corrections through the Hamiltonian H_{BP} , the operators \mathbf{L}_z and \mathbf{S}_z (projections of \mathbf{L} and \mathbf{S}) no longer commute with H_{BP} and consequently, M_L and M_S are not "good" quantum numbers. Consequently, we introduce the total angular momentum $\mathbf{J} = \mathbf{S} + \mathbf{L}$ and its projection J_z , where the corresponding quantum numbers J and M_J (with S and L) are now conserved, and the state in this intermediate coupling will be defined by $|\Delta SLJM_J\rangle$, where Δ is a linear combination of the states $|C\alpha SLJM_J\rangle$.

The radiative data are obtained by evaluating the momentum operator \mathbf{P} corresponding to the type of the transition between the upper (u) and lower (l) states of the transition:

$$\langle u|\mathbf{P}|l\rangle. \quad (5)$$

Depending on the type of the transition, the operator \mathbf{P} is the electric momentum $\mathbf{P}^{E\lambda}$ for dipole ($\lambda=1$), quadrupole ($\lambda=2$) and octopole ($\lambda=3$) transitions and magnetic momentum $\mathbf{P}^{M\lambda}$ for dipole ($\lambda=1$) and quadrupole ($\lambda=2$) transitions. All the radiative quantities can be deduced from the line strength $S(u, l) = S(l, u)$ defined by:

$$S^{E\lambda}(u, l) = |\langle u|\mathbf{P}^{E\lambda}|l\rangle|^2 \text{ and } S^{M\lambda}(u, l) = |\langle u|\mathbf{P}^{M\lambda}|l\rangle|^2. \quad (6)$$

For the electric dipole transitions, the absorption oscillator strength (dimensionless) is expressed in terms of the line strength (in atomic unit, 1 a.u. = $6.460 \times 10^{-36} \text{ cm}^2 \cdot \text{esu}^2$):

$$f_{lu} = \frac{303.75}{g_l \lambda_{ul}} S^{E1}, \quad g_l f_{lu} = -g_u f_{ul} = g f \quad (7)$$

g_u and g_l are the statistical weights of the upper and lower levels and λ_{ul} is the transition wavelength in \AA . We give here the expressions of the radiative decay rates (in s^{-1}) for each type of transition in terms of the line strength (π is the parity of the system):

- For the electric dipole (E1) transitions ($\Delta J = 0, \pm 1$ and $\Delta\pi \neq 0$):

$$A_{ul}^{E1} = \frac{2.0261 \times 10^{18}}{g_u \lambda_{ul}^3} S^{E1} \quad (8)$$

- For the electric quadrupole (E2) transitions ($\Delta J = 0, \pm 1, \pm 2$ and $\Delta\pi = 0$):

$$A_{ul}^{E2} = \frac{1.1199 \times 10^{18}}{g_u \lambda_{ul}^5} S^{E2} \quad (9)$$

- For the electric octopole (E3) transitions ($\Delta J = \pm 2, \pm 3$ and $\Delta\pi \neq 0$):

$$A_{ul}^{E3} = \frac{3.1435 \times 10^{17}}{g_u \lambda_{ul}^7} S^{E3} \quad (10)$$

- For the magnetic dipole (M1) transitions ($\Delta J = 0, \pm 1, \pm 2$ and $\Delta\pi = 0$):

$$A_{ul}^{M1} = \frac{2.6974 \times 10^{13}}{g_u \lambda_{ul}^3} S^{M1} \quad (11)$$

- For the magnetic quadrupole (M2) transitions ($\Delta J = 0, \pm 1, \pm 2$ and $\Delta\pi \neq 0$):

$$A_{ul}^{M2} = \frac{1.4910 \times 10^{13}}{g_u \lambda_{ul}^5} S^{M2} \quad (12)$$

The quantities defined by equations (6–12) are evaluated in the code AS.

2.2. Electron scattering theory

Dimensionless collision strength Ω is related to the cross section σ by the following relationship:

$$\Omega(E) = \frac{k_i^2 g_i}{\pi a_0^2} \sigma(E), \quad (13)$$

where k_i is the incident electron energy in Ry, g_i is the statistical weight of the initial level and a_0 is the Bohr radius in cm. Both collision strength and cross section describe the intrinsic probability of collisional excitation and de-excitation in an atomic transition at a particular electron energy, but collision strength is preferred because it is symmetric and dimensionless.

Recently, the Breit-Pauli Distorted Wave (BPDW) approach for electron-impact excitation of atomic ions has been implemented in the AS code [13], which we use it for the scattering problem in the present paper. In AS, the hole system is described by an antisymmetric wavefunction Ψ consisting in a wavefunction ψ for the N -electrons emitter and a scattered free electron wavefunction ϕ :

$$\Psi = \mathcal{A}\psi\phi. \quad (14)$$

Equation (14) does not couple the emitter states and this represents the assumption of the distorted wave approach. The partial collision strengths are evaluated in the code AS using the corresponding transition matrix T [13]:

$$\Omega_{\alpha\beta, \alpha'\beta'} = g_\beta |T_{\alpha\beta, \alpha'\beta'}|^2 \quad (15)$$

α labels the emitter state and β labels all the other quantum numbers defining the scattering. g_β is the statistical weight of the hole system (scattered electron+emitter), it is equal to $(2J+1)$ in our case. The transition matrices are evaluated between levels in the coupled representation which are obtained from those in the uncoupled representation through the following relation [19]:

$$|\Gamma_i S_i L_i J_i K S\rangle = \sum_{SL} (-1)^{-J_i - 2S_i - J - l - s} [L J_i K S]^{\frac{1}{2}} \begin{Bmatrix} L & l & L_i \\ U_i & S_i & K \end{Bmatrix} \begin{Bmatrix} L & J & S \\ s & S_i & K \end{Bmatrix} |\Gamma_i L_i L S_i S\rangle$$

where capital letters refer to the total system quantum numbers, those with indices refer to the emitter quantum numbers and l and s are for the colliding electron. Terms in braces are the 6-j symbols [20] and $[a, b, \dots] = (2a+1)(2b+1)\dots$. We note that the distorted wave approximation (DW) is adequate for moderately and highly charged ions and the agreement between the DW and more sophisticated methods (close coupling for example) is good. Collision strengths are calculated at the same set of final scattered energies for all transitions: zero gives all threshold transitions, for example. It is known that collision strengths converge slowly with angular momentum for allowed transitions, consequently, for large l values, a 'top-up' for dipole transitions making use of the sum rule of Burgess and Shorey [21] is used. For higher multipoles, a geometric series in energy in combination with the degenerate energy limit [22] is used to take into account large l contributions to collision strengths.

As it is mentioned before, in some cases we show a comparison between the results of the AS code and the UCL ones SST/DW/JAJOM. In SST [14], the scaling parameters λ_l depend only on l and the two-body non-fine structure operators of the Breit-Pauli Hamiltonian are omitted. SST supplies also the so called Term Coupling Coefficients (TCC) which will be used in compiling fine structure collision strengths in a next step. The DW code [15]

calculates collision strengths in LS coupling schema, and then fine structure collision strengths for low partial waves l of the incoming electron (in our case l up to 25) are obtained by the JAJOM code [16]. This code uses the reactance matrix elements in LS coupling together with the TCC obtained from the structure calculations to obtain collision strengths in intermediate coupling. For large values of l , the above method becomes cumbersome and inaccurate but the contributions of these values of l to collision strengths cannot be neglected. For $l \geq 26$, we have adopted two different procedures: for allowed transitions, the contribution has been taken into account using the JAJOM-CBe program (Dubau, unpublished results) based upon the Coulomb-Bethe formulation of Burgess and Sheorey [19] and adapted to JAJOM. For forbidden transitions, the contribution has been estimated by the SERIE-GEOM program (Dubau, unpublished results) assuming a geometric series behaviour for high partial wave collision strengths [23,24].

3. Results and Discussions

3.1. Energy levels and lifetimes

We have used in our work 12 configurations: $3s^2 3p$, $3s3p^2$, $3s^2 3d$, $3p^3$, $3s3p3d$, $3s^2 4s$, $3s^2 4p$, $3p^2 3d$, $3s^2 4d$, $3s3p4s$, $3s3p4p$ and $3s3p4d$ yielding to 121 fine structure levels. The scaling parameters (λ_{nl}) from the code AS used in our calculations are presented in the following Table:

nl	1s	2s	2p	3s	3p	3d	4s	4p	4d
λ_{nl}	2.16164	1.12732	1.04711	1.12692	1.08290	1.09618	1.11797	1.06717	1.08986

We presented in Table 1 our 121 fine structure levels. For the available 60 lowest levels, we compared with the results of Froese Fischer *et al.* [8] and with those from NIST [11]. Calculated lifetimes for the 121 levels and fine structure splitting were also provided. We recalled that the lifetime τ for a level j is defined as follow:

$$\tau_j = \frac{1}{\sum_i A_{ji}} \quad (16)$$

where A_{ji} is the radiative decay rate (Eq. 8) from the level j to all the possible lower levels (here levels corresponding to electric dipole transitions E1).

Our level energies showed a good agreement with the MCHF results [8] and NIST [11] ones. The averaged difference didn't exceed 3 %, except for the levels 35 and 36, and from 39 to 42 ($3s3p3d^2 P^o$, $^2D^o$ and $^2F^o$), the difference is about 5 %. We will see later that this difference has an influence on the agreement of radiative data. In three cases (marked in **bold** in Table 1), high differences have been found in the term splitting between our results and those from the MCHF formalism [8]. These three cases were recapitulated in Table 2. We noted that for these cases also, our energies and the MCHF ones agree well (about 2 %). We remarked also that the disagreement in the splitting existed also for the results of NIST [11].

Table 1: Our energy levels (E) in cm^{-1} for Ar VI compared to the MCHF [8] and to those from the NIST database [11], and their lifetimes τ . Levels marked by (*) are inverted regrading to the MCHF ones. $aE \pm b$ means $a \times 10^{\pm b}$.

i	Conf.	Level	E	Split	MCHF	NIST	τ (s)
1	$3s^2 3p$	$^2P^o_{1/2}$	0		0	0	
2	$3s^2 3p$	$^2P^o_{3/2}$	2193	2193	2047.39	2207.88	
3	$3s3p^2$	$^4P^o_{1/2}$	98527		98746.57	100157.5	2.49162E-06
4	$3s3p^2$	$^4P^o_{3/2}$	99318	791	99486.49	100957.6	1.06021E-05
5	$3s3p^2$	$^4P^o_{5/2}$	100550	2023	100619.02	102191.6	4.46445E-06
6	$3s3p^2$	$^2D_{3/2}$	132837		131753.79	132462.7	2.68797E-09
7	$3s3p^2$	$^2D_{5/2}$	132941	104	131850.54	132574.7	2.83518E-09
8	$3s3p^2$	$^2S_{1/2}$	182207		170176.45	169803.9	1.52380E-10
9	$3s3p^2$	$^2P_{1/2}$	186817		184439.40	182182.1	6.92884E-11
10	$3s3p^2$	$^2P_{3/2}$	187971	1154	185742.72	183577.3	6.59349E-11
11	$3s^2 3d$	$^2D_{3/2}$	226446		220303.14	218595.9	5.02145E-11
12	$3s^2 3d$	$^2D_{5/2}$	226570	124	220425.89	218655.8	5.13475E-11
13	$3p^3$	$^2D^o_{3/2}$	259969		260240.43	260068.7	1.60535E-09
14	$3p^3$	$^2D^o_{5/2}$	260172	203	260438.99	260272.9	1.58868E-09
15	$3p^3$	$^4S^o_{3/2}$	276426		271519.72	270511.8	7.00082E-11
16	$3s3p3d$	$^4F^o_{3/2}$	290227		289823.12	–	2.35284E-07
17	$3s3p3d$	$^4F^o_{5/2}$	290666	439	290245.49	–	1.86730E-07
18	$3s3p3d$	$^4F^o_{7/2}$	291293	1066	290847.72	–	2.10417E-07
19	$3s3p3d$	$^4F^o_{9/2}$	292119	1892	–	–	–
20	$3p^3$	$^2P^o_{3/2}$	302062		294030.80	294086.0	1.81863E-10
21	$3p^3$	$^2P^o_{1/2}$	302227	165	294908.42	294101.3	1.79490E-10
22	$3s3p3d$	$^4P^o_{5/2}$	317702		316397.02	316351.	7.79352E-11
23	$3s3p3d$	$^4P^o_{3/2}$	318264	562	316939.22	316974.	7.67369E-11
24	$3s3p3d$	$^4P^o_{1/2}$	318668	966	317346.50	317459.	7.66836E-11
25	$3s3p3d$	$^4D^o_{1/2}$	322184		319648.31	319273.	4.89429E-11
26	$3s3p3d$	$^4D^o_{3/2}$	322409	225	319881.51	319539.	4.93415E-11
27	$3s3p3d$	$^4D^o_{5/2}$	322676	492	320128.54	319771.	4.95428E-11
28	$3s3p3d$	$^4D^o_{7/2}$	322908	724	320314.56	319905.	4.94792E-11
29	$3s3p3d$	$^2D^o_{5/2}$	340542		329993.40	328960.4	5.56251E-11
30	$3s3p3d$	$^2D^o_{3/2}$	340608	66	330027.48	328992.	5.55703E-11

Table 1: Continued.

<i>i</i>	Conf.	Level	<i>E</i>	Split	MCHF	NIST	τ (s)
31	3s ² 4s	² S _{1/2}	351315		342005.10	342302.	5.13580E-11
32	3s3p3d	² F _{5/2} ^o	354312		344753.74	344309.8	1.08695E-10
33	3s3p3d	² F _{7/2} ^o	356046	1734	346387.33	346076.	1.06337E-10
34	3s3p3d	² P _{3/2} ^o	388109		376940.45	375657.8	4.35879E-11
35	3s3p3d	² P _{1/2} ^o	388405	296	377374.76	–	4.46216E-11
36	3s3p3d	² F _{5/2} ^o	398287		378377.68	376421.	4.01109E-11
37	3s3p3d	² F _{3/2} ^o	398760	473	378802.50	376905.	3.97745E-11
38	3s ² 4p	² P _{1/2} ^o	400653		389461.60	–	1.18727E-10
39	3s ² 4p	² P _{3/2} ^o	401062	409	389633.73	–	1.16972E-10
40	3s3p3d	² D _{3/2} ^o	418963 *		398713.63	395494.	2.50441E-11
41	3s3p3d	² D _{5/2} ^o	419532 *	569	399043.44	395807.	2.43203E-11
42	3s3p3d	² P _{1/2} ^o	419881 *		396100.64	–	2.89757E-11
43	3s3p3d	² P _{3/2} ^o	420223 *	342	396568.11	–	2.84833E-11
44	3p ² 3d	⁴ F _{3/2}	448677		–	–	1.43142E-10
45	3p ² 3d	⁴ F _{5/2}	449117	440	–	–	1.42676E-10
46	3p ² 3d	⁴ F _{7/2}	449743	1066	–	–	1.42015E-10
47	3p ² 3d	⁴ F _{9/2}	450558	1881	–	–	1.41173E-10
48	3s3p4s	⁴ P _{1/2} ^o	455089		453718.27	454096.	7.63457E-11
49	3s3p4s	⁴ P _{3/2} ^o	455807	718	454441.10	454874.	7.64552E-11
50	3s3p4s	⁴ P _{5/2} ^o	457074	1985	455734.06	456280.	7.67432E-11
51	3p ² 3d	⁴ D _{1/2}	457611		–	–	1.27696E-10
52	3p ² 3d	⁴ D _{3/2}	457777	166	–	–	1.27602E-10
53	3p ² 3d	⁴ D _{5/2}	457888	277	–	–	1.44789E-10
54	3p ² 3d	⁴ D _{7/2}	458058	447	–	–	1.45251E-10
55	3p ² 3d	² F _{5/2}	459061		–	–	2.62343E-10
56	3p ² 3d	² F _{7/2}	460472	1411	–	–	2.57006E-10
57	3p ² 3d	² P _{3/2}	462127		–	–	7.41930E-11
58	3p ² 3d	² P _{1/2}	463691	1564	–	–	7.31090E-11
59	3s ² 4d	² D _{3/2}	465362		–	454751.	2.36279E-10
60	3s ² 4d	² D _{5/2}	465420	58	–	454807.	2.30475E-10

Table 1: Continued.

<i>i</i>	Conf.	Level	<i>E</i>	τ (s)	<i>i</i>	Conf.	Level	<i>E</i>	τ (s)
61	3s3p4s	² P _{1/2} ^o	472094	6.06111E-11	92	3p ² 3d	² D _{5/2}	560675	2.70723E-11
62	3s3p4s	² P _{3/2} ^o	473486	5.94949E-11	93	3p ² 3d	² D _{3/2}	561606	2.70336E-11
63	3p ² 3d	² G _{7/2}	483923	4.49121E-10	94	3s3p4d	⁴ D _{3/2}	568023	1.80540E-10
64	3p ² 3d	² G _{9/2}	484086	4.53471E-10	95	3s3p4d	⁴ D _{1/2}	568045	1.71875E-10
65	3p ² 3d	⁴ P _{5/2}	489801	2.82277E-11	96	3s3p4d	⁴ D _{5/2}	568135	1.82025E-10
66	3p ² 3d	⁴ P _{3/2}	490368	2.80070E-11	97	3s3p4d	⁴ D _{7/2}	568531	1.78977E-10
67	3p ² 3d	⁴ P _{1/2}	490671	2.79000E-11	98	3s3p4d	⁴ F _{3/2}	569174	3.86712E-10
68	3p ² 3d	² D _{5/2}	499460	3.82183E-11	99	3s3p4d	⁴ F _{5/2}	569727	3.89187E-10
69	3p ² 3d	² D _{3/2}	499571	3.80270E-11	100	3s3p4d	² D _{3/2}	570181	3.89371E-10
70	3s3p4p	⁴ D _{1/2}	500380	2.41899E-10	101	3s3p4d	² D _{5/2}	570442	3.75059E-10
71	3s3p4p	⁴ D _{3/2}	500920	2.44565E-10	102	3s3p4d	⁴ F _{7/2}	570567	3.90887E-10
72	3s3p4p	⁴ D _{5/2}	501794	2.47776E-10	103	3s3p4d	⁴ F _{9/2}	571148	4.61991E-10
73	3s3p4p	⁴ D _{7/2}	502954	2.46570E-10	104	3s3p4d	⁴ P _{5/2}	574207	2.36460E-10
74	3s3p4p	² P _{1/2}	503633	1.42575E-10	105	3s3p4d	⁴ P _{3/2}	574719	2.40067E-10
75	3s3p4p	² P _{3/2}	503960	1.42132E-10	106	3s3p4d	⁴ P _{1/2}	575032	2.42982E-10
76	3s3p4p	⁴ S _{3/2}	508141	2.41812E-10	107	3s3p4d	² F _{5/2}	577336	2.26096E-10
77	3s3p4p	⁴ P _{1/2}	509018	1.84588E-10	108	3s3p4p	² P _{1/2}	578471	5.40903E-11
78	3s3p4p	⁴ P _{3/2}	509736	1.92658E-10	109	3s3p4d	² F _{7/2}	578473	2.24880E-10
79	3s3p4p	⁴ P _{5/2}	510261	1.85721E-10	110	3s3p4p	² P _{3/2}	578956	5.39334E-11
80	3p ² 3d	² D _{3/2}	512284	7.30063E-11	111	3s3p4p	² D _{3/2}	580817	5.22153E-11
81	3s3p4p	² D _{5/2}	513909	7.34621E-11	112	3s3p4p	² D _{5/2}	581163	5.23804E-11
82	3p ² 3d	² S _{1/2}	518616	4.70268E-11	113	3s3p4d	² P _{3/2}	581968	1.85910E-10
83	3s3p4p	² D _{3/2}	522641	1.66337E-10	114	3s3p4d	² P _{1/2}	582723	1.82666E-10
84	3p ² 3d	² D _{5/2}	523977	1.63683E-10	115	3s3p4p	² S _{1/2}	591134	5.69581E-11
85	3s3p4p	² S _{1/2}	531376	1.03863E-10	116	3s3p4d	² D _{3/2}	638746	5.47023E-11
86	3s3p4s	² P _{1/2} ^o	532709	3.47490E-11	117	3s3p4d	² D _{5/2}	638822	5.44126E-11
87	3s3p4s	² P _{3/2} ^o	532853	3.50560E-11	118	3s3p4d	² F _{5/2}	642340	1.02040E-10
88	3p ² 3d	² F _{5/2}	541730	2.59138E-11	119	3s3p4d	² F _{7/2}	642351	1.01992E-10
89	3p ² 3d	² F _{7/2}	541825	2.58749E-11	120	3s3p4d	² P _{1/2}	649049	4.80934E-11
90	3p ² 3d	² P _{1/2}	545089	3.54412E-11	121	3s3p4d	² P _{3/2}	649139	4.77992E-11
91	3p ² 3d	² P _{3/2}	545837	3.54137E-11					

Table 2: Splitting (Split) between our levels. MCHF stands for the results of [8] and NIST for those of [11].

Index	Conf.	Level	<i>E</i>	MCHF	NIST	Split	Split (MCHF)	Split (NIST)
20	3p ³	² P _{3/2} ^o	302062	294030.80	294086.0			
21	3p ³	² P _{1/2} ^o	302227	294908.42	294101.3	165	877.62	15.3
29	3s3p3d	² D _{5/2} ^o	340542	329993.40	328960.4			
30	3s3p3d	² D _{3/2} ^o	340608	330027.48	328992.	66	34.08	31.6
34	3s3p3d	² P _{3/2} ^o	388109	376940.45	375657.8			
35	3s3p3d	² P _{1/2} ^o	388405	377374.76	–	296	434.31	–

3.2. Radiative data

We presented in Table 3 our line strengths (*S*), oscillator strengths in absorption (*f_{ik}*) and radiative decay rates (*A_{ki}*) for electric dipole (E1) transitions from the lowest 12 levels to the lowest 43 ones (belonging to the first seven configurations 3s²3p, 3s3p², 3s²3d, 3p³, 3s3p3d, 3s²4s and 3s²4p). Our results for electric dipole transitions were compared to the MCHF ones [8], since they were the only provided in this reference. We excluded from our tables transitions that were not provided in [8] or those for which the radiative decay rates are less than 10⁴ s⁻¹. Differences between the two results were ranging from 2 % to 50 % with an averaged difference of about 25 %. Almost all the transitions presenting a huge difference involved levels from 35 to 42 (3s3p3d ²P^o, ²D^o and ²F^o). As we mentioned in the precedent subsection, the energies of these levels presented the most important disagreement (≈ 5 %) between our values and those of [8]. This could be one of the origins of the difference in the radiative data.

Radiative atomic data for forbidden transitions (E2, M1) were presented in Table 4 and those for forbidden transitions (E3, M2) were presented in Table 5. To the best of our knowledge, there were no radiative data for Ar VI forbidden transitions. These parameters are the first to be published, and may be of high interest in plasma modelling. Transitions for which the type was designed as E2/M1 was a mix of electric quadrupole and magnetic dipole transitions. The presented values of line strengths (*S*) and radiative decay rates (*A_{ki}*) correspond to the most probable process: *A_{ki}* = max(*A_{ki}*^{E2}, *A_{ki}*^{M1}). In the database NIST [11], only the results of one forbidden transition 3s²3p ²P_{1/2}^o – 3s²3p ²P_{3/2}^o (1 – 2) has been found. The results of this transition were presented in the Table below, and the agreement between them and our values is good.

<i>i – k</i>	<i>S</i>	<i>S^{NIST}</i>	<i>A_{ki}</i>	<i>A_{ki}^{NIST}</i>
1 – 2	1.333E+00	1.3E+00	9.484E–02	9.7E–02

Table 3: Our line strengths (*S*), oscillator strengths in absorption (*f_{ik}*) and radiative decay rates (*A_{ki}*) for electric dipole E1 transitions compared to MCHF ones [8]. aE±b means a×10^{±b}. *i* and *k* label the levels in Table 1.

Trans. <i>i – k</i>	<i>S</i>		<i>f_{ik}</i>		<i>A_{ki}</i> (s ⁻¹)	
	Present	MCHF	Present	MCHF	Present	MCHF
1 – 3	2.603E–04	2.966E–04	4.000E–05	4.449E–05	2.522E+05	2.894E+05
1 – 4	8.752E–06	1.211E–05	1.320E–06	1.829E–06	4.343E+03	6.038E+03
1 – 6	2.763E–01	3.560E–01	5.575E–02	7.124E–02	3.281E+08	4.125E+08
1 – 8	7.839E–01	4.536E–01	2.169E–01	1.172E–01	4.804E+09	2.265E+09
1 – 9	1.093E+00	1.448E+00	3.103E–01	4.055E–01	7.223E+09	9.201E+09
1 – 10	7.879E–01	7.941E–01	2.249E–01	2.240E–01	2.650E+09	2.578E+09
1 – 11	2.807E+00	2.800E+00	9.653E–01	9.367E–01	1.651E+10	1.516E+10
1 – 31	1.463E–01	1.606E–01	7.808E–02	8.343E–02	6.428E+09	6.510E+09
2 – 3	1.647E–04	2.225E–04	3.895E–05	1.634E–05	1.491E+05	2.039E+05
2 – 4	1.939E–04	1.796E–04	1.430E–05	1.329E–05	8.998E+04	8.414E+04
2 – 5	6.971E–04	7.448E–04	5.207E–05	5.575E–05	2.240E+05	2.409E+05
2 – 6	3.891E–02	5.313E–02	3.860E–03	5.233E–03	4.395E+07	5.872E+07
2 – 7	4.673E–01	6.051E–01	4.640E–02	5.965E–02	3.527E+08	4.469E+08
2 – 8	2.975E–01	5.597E–01	4.068E–02	7.146E–02	1.758E+09	2.695E+09
2 – 9	1.131E+00	8.896E–01	1.585E–01	1.232E–01	7.210E+09	5.468E+09
2 – 10	3.854E+00	3.897E+00	5.437E–01	5.436E–01	1.252E+10	1.224E+10
2 – 11	5.964E–01	5.943E–01	1.016E–01	9.849E–02	3.407E+09	3.130E+09
2 – 12	5.105E+00	5.096E+00	8.699E–01	8.450E–01	1.948E+10	1.792E+10
3 – 13	5.932E–05	–	1.455E–05	–	1.264E+05	–
3 – 15	8.534E–01	8.532E–01	2.306E–01	2.239E–01	2.434E+09	2.229E+09
3 – 16	2.355E–04	2.327E–04	6.856E–05	6.752E–05	8.403E+05	8.222E+05
3 – 20	1.447E–03	–	4.472E–04	–	6.179E+06	–
3 – 21	7.996E–06	–	2.474E–06	–	6.847E+04	–
3 – 23	1.402E+00	1.338E+00	4.679E–01	4.434E–01	7.536E+09	7.041E+09
3 – 24	3.283E–01	3.465E–01	1.098E–01	1.150E–01	3.549E+09	3.666E+09
3 – 25	1.385E+00	1.254E+00	4.704E–01	4.208E–01	1.569E+10	1.370E+10
3 – 26	1.117E+00	9.434E–01	3.799E–01	3.169E–01	6.351E+09	5.168E+09
4 – 15	1.705E+00	1.705E+00	2.293E–01	2.227E–01	4.798E+09	4.396E+09
4 – 16	3.193E–04	3.031E–04	4.629E–05	4.381E–05	1.125E+06	1.059E+06
4 – 17	1.255E–03	1.216E–03	1.823E–04	1.761E–04	2.969E+06	2.850E+06
4 – 20	2.894E–03	–	4.455E–04	–	1.222E+07	–
4 – 21	9.949E–05	–	1.533E–05	–	8.420E+05	–
4 – 22	1.748E+00	1.699E+00	2.899E–01	2.798E–01	6.148E+09	5.855E+09
4 – 23	1.179E–01	4.937E–02	1.960E–02	8.153E–03	6.268E+08	2.571E+08
4 – 24	8.877E–01	6.924E–01	1.479E–01	1.145E–01	9.491E+09	7.253E+09
4 – 25	4.224E–01	4.462E–01	7.149E–02	7.460E–02	4.737E+09	4.824E+09
4 – 26	2.139E+00	2.054E+00	3.623E–01	3.437E–01	1.203E+10	1.114E+10
4 – 27	3.151E+00	2.823E+00	5.345E–01	4.730E–01	1.186E+10	1.024E+10

Table 3: Continued.

Trans. <i>i - k</i>	<i>S</i>		<i>f_{ik}</i>		<i>A_{ki} (s⁻¹)</i>	
	Present	MCHF	Present	MCHF	Present	MCHF
5 - 13	1.313E-04	-	1.060E-05	-	2.695E+05	-
5 - 14	4.644E-04	-	3.753E-05	-	6.378E+05	-
5 - 15	2.559E+00	2.557E+00	2.278E-01	2.212E-01	7.051E+09	6.464E+09
5 - 16	2.855E-05	3.195E-05	2.742E-06	3.061E-06	9.870E+04	1.096E+05
5 - 17	5.581E-04	5.498E-04	5.371E-05	5.278E-05	1.295E+06	1.266E+06
5 - 18	2.620E-03	2.562E-03	2.530E-04	2.467E-04	4.605E+06	4.467E+06
5 - 20	1.249E-03	-	1.274E-04	-	5.176E+06	-
5 - 22	1.932E+00	-	2.124E-01	-	6.681E+09	-
5 - 23	9.307E-01	-	1.026E-01	-	4.865E+09	-
5 - 26	3.405E-01	3.712E-01	3.824E-02	4.120E-02	1.883E+09	1.982E+09
5 - 27	2.247E+00	2.249E+00	2.527E-01	2.499E-01	8.318E+09	8.032E+09
5 - 28	7.256E+00	6.868E+00	8.168E-01	7.639E-01	2.020E+10	1.844E+10
6 - 13	4.400E-01	5.371E-01	4.248E-02	5.240E-02	4.579E+08	5.770E+08
6 - 14	5.464E-02	7.125E-02	5.283E-03	6.963E-03	3.809E+07	5.128E+07
6 - 15	6.793E-05	-	7.408E-06	-	1.019E+05	-
6 - 16	9.437E-04	1.120E-03	1.128E-04	1.344E-04	1.864E+06	2.240E+06
6 - 20	1.885E-01	1.771E-01	2.422E-02	2.182E-02	4.627E+08	3.834E+08
6 - 21	1.006E+00	9.206E-01	1.294E-01	1.141E-01	4.954E+09	4.051E+09
6 - 29	4.325E-01	4.032E-01	6.822E-02	6.070E-02	1.309E+09	1.061E+09
6 - 30	3.501E+00	3.265E+00	5.523E-01	4.916E-01	1.590E+10	1.289E+10
6 - 32	2.248E+00	1.897E+00	3.781E-01	3.068E-01	8.247E+09	6.190E+09
6 - 34	4.429E-03	6.093E-03	8.586E-04	1.134E-03	3.732E+07	4.549E+07
6 - 35	2.448E-02	3.519E-02	4.750E-03	6.563E-03	4.139E+08	5.282E+08
6 - 37	1.910E+00	1.897E+00	3.857E-01	3.068E-01	1.213E+10	6.190E+09
6 - 38	1.025E-01	9.226E-02	2.084E-02	1.806E-02	1.994E+09	1.600E+09
6 - 39	2.165E-02	1.973E-02	4.410E-03	3.863E-03	2.116E+08	1.714E+08
6 - 40	4.053E-03	-	8.807E-04	-	4.809E+07	-
7 - 13	7.465E-02	9.116E-02	4.801E-03	5.925E-03	7.751E+07	9.773E+07
7 - 14	7.309E-01	8.895E-01	4.708E-02	5.791E-02	5.083E+08	6.387E+08
7 - 15	2.838E-04	-	2.062E-05	-	4.247E+05	-
7 - 16	1.571E-04	2.873E-04	1.251E-05	2.298E-05	3.097E+05	5.738E+05
7 - 17	7.995E-04	1.013E-03	6.384E-05	8.122E-05	1.059E+06	1.359E+06
7 - 18	1.090E-04	1.407E-04	8.741E-06	1.132E-05	1.097E+05	1.432E+05
7 - 20	1.789E+00	1.624E+00	1.532E-01	1.334E-01	4.384E+09	3.510E+09
7 - 22	1.235E-03	-	1.155E-04	-	2.630E+06	-
7 - 23	5.866E-04	-	5.504E-05	-	1.891E+06	-
7 - 26	4.776E-04	-	4.581E-05	-	1.645E+06	-
7 - 28	4.345E-03	-	4.179E-04	-	7.544E+06	-
7 - 29	5.393E+00	5.029E+00	5.668E-01	5.044E-01	1.629E+10	1.321E+10
7 - 30	3.679E-01	3.439E-01	3.867E-02	3.450E-02	1.669E+09	1.356E+09

Table 3: Continued.

Trans. <i>i - k</i>	<i>S</i>		<i>f_{ik}</i>		<i>A_{ki} (s⁻¹)</i>	
	Present	MCHF	Present	MCHF	Present	MCHF
7 - 32	2.020E-01	1.730E-01	2.264E-02	1.865E-02	7.401E+08	5.639E+08
7 - 33	3.261E+00	2.721E+00	3.684E-01	2.955E-01	9.173E+09	6.805E+09
7 - 34	3.665E-02	5.253E-02	4.735E-03	6.518E-03	3.085E+08	3.917E+08
7 - 36	2.721E+00	2.721E+00	3.656E-01	2.955E-01	1.288E+10	6.805E+09
7 - 37	1.294E-01	1.730E-01	1.742E-02	1.865E-02	8.210E+08	5.639E+08
7 - 39	1.950E-01	1.754E-01	2.647E-02	2.289E-02	1.904E+09	1.522E+09
7 - 40	2.165E-04	-	3.135E-05	-	2.566E+06	-
7 - 41	3.561E-03	-	5.166E-04	-	2.830E+07	-
7 - 43	1.195E-04	-	1.737E-05	-	1.435E+06	-
8 - 13	3.172E-02	5.700E-03	3.747E-03	7.797E-04	7.556E+06	2.109E+06
8 - 20	2.109E-01	2.942E-01	3.840E-02	5.534E-02	1.840E+08	2.831E+08
8 - 21	2.133E-02	1.026E-01	3.888E-03	1.944E-02	3.736E+07	2.017E+08
8 - 34	3.995E+00	3.236E+00	1.249E+00	1.016E+00	1.766E+10	1.449E+10
8 - 35	1.380E+00	1.437E+00	4.321E-01	4.523E-01	1.225E+10	1.295E+10
8 - 38	1.399E-01	1.579E-02	4.643E-02	5.258E-03	1.478E+09	1.687E+08
8 - 39	4.486E-01	3.713E-02	1.491E-01	1.238E-02	2.382E+09	1.988E+08
8 - 40	1.025E-01	1.823E-02	3.686E-02	6.327E-03	6.892E+08	1.102E+08
8 - 42	3.475E-01	2.890E-01	1.254E-01	9.915E-02	4.726E+09	3.376E+09
8 - 43	2.250E-01	4.538E-01	8.133E-02	1.560E-01	1.537E+09	2.667E+09
9 - 13	3.387E-01	4.665E-01	3.763E-02	5.371E-02	6.715E+07	1.029E+08
9 - 16	1.216E-05	2.806E-05	1.910E-06	4.492E-06	6.813E+03	1.664E+04
9 - 20	3.869E-02	1.169E-01	6.772E-03	1.945E-02	3.000E+07	7.793E+07
9 - 21	2.753E-01	3.616E-01	4.825E-02	6.068E-02	4.287E+08	4.939E+08
9 - 30	1.463E-01	1.787E-01	3.416E-02	3.951E-02	2.695E+08	2.793E+08
9 - 34	6.492E-03	-	1.985E-03	-	2.682E+07	-
9 - 35	7.887E-01	4.705E-01	2.415E-01	1.379E-01	6.546E+09	3.423E+09
9 - 38	2.013E-01	4.945E-01	6.537E-02	1.540E-01	1.994E+09	4.318E+09
9 - 39	1.051E-02	3.357E-01	3.420E-03	1.046E-01	5.236E+07	1.469E+09
9 - 40	4.612E+00	4.028E+00	1.626E+00	1.311E+00	2.923E+10	2.007E+10
9 - 42	7.632E-01	4.631E-01	2.701E-01	1.489E-01	9.788E+09	4.449E+09
9 - 43	1.835E-03	4.839E-01	6.506E-04	1.559E-01	1.182E+07	2.340E+09
10 - 13	6.180E-02	7.363E-02	3.379E-03	4.166E-03	1.168E+07	1.542E+07
10 - 14	6.431E-01	8.104E-01	3.526E-02	4.597E-02	8.173E+07	1.140E+08
10 - 15	1.545E-03	-	1.038E-04	-	5.417E+05	-
10 - 20	5.490E-01	8.244E-01	4.757E-02	6.779E-02	4.130E+08	5.303E+08
10 - 21	9.868E-02	1.537E-01	8.562E-03	1.274E-02	1.491E+08	2.026E+08
10 - 29	2.586E-01	2.922E-01	2.996E-02	3.201E-02	3.101E+08	2.962E+08
10 - 30	3.864E-02	4.242E-02	4.478E-03	4.647E-03	6.959E+07	6.454E+07
10 - 34	7.649E-01	9.668E-01	1.162E-01	1.548E-01	3.106E+09	4.589E+09

Table 3: Continued.

Trans. <i>i - k</i>	<i>S</i>		<i>f_{ik}</i>		<i>A_{ki} (s⁻¹)</i>	
	Present	MCHF	Present	MCHF	Present	MCHF
10 - 35	1.392E-01	2.657E-01	2.119E-02	4.245E-02	1.135E+09	2.506E+09
10 - 37	9.221E-04	-	1.476E-04	-	2.916E+06	-
10 - 38	6.045E-02	2.547E-01	9.763E-03	3.940E-02	5.891E+08	2.182E+09
10 - 39	2.619E-01	1.129E+00	4.237E-02	1.748E-01	1.283E+09	4.846E+09
10 - 40	6.570E-02	1.210E+00	1.152E-02	1.957E-01	4.102E+08	5.920E+09
10 - 41	7.702E+00	7.981E+00	1.354E+00	1.293E+00	3.229E+10	2.615E+10
10 - 42	5.183E-01	2.657E-01	9.129E-02	4.245E-02	6.550E+09	2.506E+09
10 - 43	3.243E+00	9.668E-01	5.719E-01	1.548E-01	2.058E+10	4.589E+09
11 - 1	2.843E-02	5.225E-02	7.236E-04	1.585E-03	5.424E+05	1.686E+06
11 - 14	2.770E-03	-	7.093E-05	-	3.588E+04	-
11 - 16	2.838E-05	8.551E-05	1.375E-06	4.515E-06	3.730E+03	1.455E+04
11 - 17	3.214E-04	3.760E-04	1.567E-05	1.997E-05	2.875E+04	4.345E+04
11 - 30	5.691E-02	-	4.934E-03	-	4.289E+07	-
11 - 32	2.707E-01	-	2.628E-02	-	1.911E+08	-
11 - 34	1.056E-01	5.443E-02	1.296E-02	7.286E-03	2.260E+08	1.510E+08
11 - 35	4.736E-01	6.892E-01	5.825E-02	9.201E-02	2.038E+09	3.793E+09
11 - 37	6.606E+00	4.281E+00	8.645E-01	5.153E-01	1.141E+10	5.756E+09
11 - 38	3.703E-01	1.423E+00	4.898E-02	1.827E-01	1.983E+09	6.976E+09
11 - 39	7.093E-02	2.462E-01	9.406E-03	3.166E-02	1.913E+08	6.056E+08
11 - 40	1.258E+00	2.387E+00	1.840E-01	3.234E-01	4.548E+09	6.867E+09
11 - 41	2.004E-01	2.104E-01	2.938E-02	2.855E-02	4.871E+08	4.057E+08
11 - 42	1.832E+00	6.892E-01	2.691E-01	9.201E-02	1.343E+10	3.793E+09
11 - 43	1.335E+00	5.443E-02	1.965E-01	7.286E-03	4.922E+09	1.510E+08
12 - 13	3.410E-03	-	5.766E-05	-	6.436E+04	-
12 - 14	4.413E-02	8.176E-02	7.508E-04	1.656E-03	5.654E+05	1.769E+06
12 - 18	5.494E-04	5.910E-04	1.800E-05	2.107E-05	3.773E+04	5.227E+04
12 - 20	6.310E-03	-	2.411E-04	-	1.375E+06	-
12 - 22	3.935E-04	-	1.815E-05	-	1.006E+05	-
12 - 23	6.650E-05	-	3.087E-06	-	2.597E+04	-
12 - 26	2.150E-04	-	1.043E-05	-	9.588E+04	-
12 - 28	3.100E-04	-	1.512E-05	-	7.020E+04	-
12 - 29	8.624E-02	1.853E-01	4.976E-03	1.028E-02	4.311E+07	8.230E+07
12 - 30	4.785E-03	-	2.763E-04	-	3.595E+06	-
12 - 32	2.819E-02	5.099E-02	1.823E-03	3.209E-03	1.984E+07	3.309E+07
12 - 33	4.012E-01	7.623E-01	2.630E-02	4.861E-02	2.205E+08	3.858E+08
12 - 34	7.263E-01	2.557E-01	5.940E-02	2.026E-02	1.551E+09	4.966E+08
12 - 36	9.393E+00	6.064E+00	8.166E-01	4.849E-01	1.205E+10	6.052E+09
12 - 37	4.477E-01	2.829E-01	3.903E-02	2.268E-02	7.719E+08	3.795E+08
12 - 39	7.890E-01	2.903E+00	6.969E-02	2.487E-01	2.123E+09	7.123E+09
12 - 40	1.386E+00	-	1.350E-01	-	4.999E+09	-

Table 4: Our line strengths *S*(a.u) and radiative decay rates *A_{ki}* (s⁻¹) for electric quadrupole (E2) and magnetic dipole (M1) transitions *i - j* where 1 ≤ *i* ≤ 31 and *j* up to the level 43.

<i>i - k</i>	<i>S^{E2}</i>	<i>S^{M1}</i>	<i>A_{ki}^{E2}</i>	<i>A_{ki}^{M1}</i>	<i>i - k</i>	<i>S^{E2}</i>	<i>S^{M1}</i>	<i>A_{ki}^{E2}</i>	<i>A_{ki}^{M1}</i>
1 - 2	2.585E+00	1.333E+00	3.673E-06	9.484E-02	2 - 13	1.492E+00	2.518E-06	4.754E+04	2.909E-01
1 - 13	1.668E+00	8.392E-07	5.546E+04	9.943E-02	2 - 14	3.654E+00	1.314E-06	7.793E+04	1.014E-01
1 - 14	1.077E+00	0.000E+00	2.397E+04	0.000E+00	2 - 15	2.561E-03	4.652E-06	1.112E+02	6.470E-01
1 - 15	1.528E-03	1.017E-06	6.906E+01	1.449E-01	2 - 16	1.508E-05	8.888E-09	8.371E-01	1.432E-03
1 - 16	5.109E-05	2.319E-08	2.945E+00	3.822E-03	2 - 17	6.119E-05	9.015E-09	2.282E+00	9.728E-04
1 - 17	5.141E-07	0.000E+00	1.991E-02	0.000E+00	2 - 18	3.353E-05	0.000E+00	9.479E-01	0.000E+00
1 - 20	1.032E+00	1.408E-06	7.270E+04	2.617E-01	2 - 20	1.240E+00	3.093E-10	8.416E+04	5.624E-05
1 - 22	3.125E-05	0.000E+00	1.888E+00	0.000E+00	2 - 21	1.120E+00	1.632E-06	1.525E+05	5.946E-01
1 - 23	2.209E-06	5.349E-09	2.020E-01	1.163E-03	2 - 22	1.037E-04	4.216E-07	6.049E+00	5.953E-02
1 - 24	0.000E+00	8.745E-08	0.000E+00	3.817E-02	2 - 23	1.814E-05	1.470E-07	1.602E+00	3.130E-02
1 - 25	0.000E+00	2.212E-07	0.000E+00	9.976E-02	2 - 24	2.962E-06	6.675E-08	5.266E-01	2.853E-02
1 - 26	2.298E-06	5.227E-07	2.241E-01	1.181E-01	2 - 25	2.831E-05	8.577E-08	5.319E+00	3.790E-02
1 - 27	2.705E-07	0.000E+00	1.766E-02	0.000E+00	2 - 26	2.645E-05	1.100E-07	2.493E+00	2.436E-02
1 - 29	2.050E-01	0.000E+00	1.752E+04	0.000E+00	2 - 27	6.689E-06	6.500E-07	4.221E-01	9.619E-02
1 - 30	2.663E-01	4.821E-07	3.418E+04	1.285E-01	2 - 28	3.541E-06	0.000E+00	1.682E-01	0.000E+00
1 - 32	6.143E+00	0.000E+00	6.403E+05	0.000E+00	2 - 29	5.122E-01	3.389E-07	4.240E+04	5.901E-02
1 - 34	1.906E+00	7.710E-07	4.699E+05	3.040E-01	2 - 30	2.137E-01	9.542E-07	2.655E+04	2.494E-01
1 - 35	0.000E+00	7.191E-10	0.000E+00	5.683E-04	2 - 32	1.787E+00	5.450E-10	1.805E+05	1.070E-04
1 - 37	1.829E-02	0.000E+00	3.441E+03	0.000E+00	2 - 33	1.057E+01	0.000E+00	8.210E+05	0.000E+00
1 - 38	0.000E+00	1.741E-08	1.512E-02	0.000E+00	2 - 34	1.767E+00	1.511E-08	4.234E+05	5.857E-03
1 - 39	3.246E-01	8.278E-06	9.430E+04	3.601E+00	2 - 35	1.869E+00	1.225E-06	8.994E+05	9.515E-01
1 - 40	1.609E+00	1.825E-07	5.815E+05	9.048E-02	2 - 36	3.799E-02	0.000E+00	5.185E+03	0.000E+00
1 - 41	7.106E-01	0.000E+00	1.724E+05	0.000E+00	2 - 37	9.852E-03	7.096E-09	1.804E+03	1.990E-03
1 - 42	0.000E+00	1.649E-10	0.000E+00	1.646E-04	2 - 38	3.564-01	1.019E-05	2.005E+05	8.692E+00
1 - 43	1.145E-01	9.979E-07	4.201E+04	4.993E-01	2 - 39	3.993E-01	2.587E-07	1.129E+05	1.107E-01

Table 4: Continued.

$i - k$	S^{E2}	S^{M1}	A_{ki}^{E2}	A_{ki}^{M1}	$i - k$	S^{E2}	S^{M1}	A_{ki}^{E2}	A_{ki}^{M1}
3 - 4	3.370E-01	3.330E+00	2.927E-09	1.113E-02	5 - 12	5.525E-04	9.534E-05	3.278E-01	8.578E-01
3 - 5	3.026E+00	0.000E+00	1.914E-06	0.000E+00	5 - 31	4.835E-04	0.000E+00	2.685E+01	0.000E+00
3 - 6	8.486E-04	4.399E-04	1.211E-01	1.198E-01	6 - 7	2.367E+00	2.398E+00	5.472E-13	1.226E-05
3 - 7	2.573E-05	0.000E+00	2.318E-05	0.000E+00	6 - 8	3.026E+00	2.169E-05	4.969E+01	3.521E-02
3 - 8	0.000E+00	3.644E-04	0.000E+00	2.800E+00	6 - 9	5.455E-01	3.400E-04	1.400E+01	7.212E-01
3 - 9	0.000E+00	3.019E-05	0.000E+00	2.869E-01	6 - 10	1.072E-01	1.121E-03	1.529E+00	1.266E+00
3 - 10	9.137E-05	4.323E-05	1.464E-02	2.086E-01	6 - 11	3.836E-02	1.137E-07	7.720E+00	6.291E-04
3 - 11	6.926E-04	6.106E-06	6.642E-01	8.619E-02	6 - 12	1.604E-02	9.463E-07	2.167E+00	3.504E-03
3 - 12	8.085E-04	0.000E+00	5.194E-01	0.000E+00	6 - 31	6.160E-01	3.677E-11	1.717E+04	5.172E-06
3 - 31	0.000E+00	1.442E-08	0.000E+00	3.143E-03	7 - 8	5.154E+00	0.000E+00	8.376E+01	0.000E+00
4 - 5	4.224E+00	3.597E+00	2.235E-07	3.022E-02	7 - 9	1.648E-01	0.000E+00	4.189E+00	0.000E+00
4 - 6	1.882E-04	1.742E-03	2.229E-04	4.424E-01	7 - 10	1.505E-01	6.573E-04	2.127E+00	7.387E-01
4 - 7	5.811E-03	1.524E-03	4.661E-03	2.604E-01	7 - 11	1.529E-02	1.361E-06	3.061E+00	7.503E-03
4 - 8	3.750E-05	1.341E-03	8.217E-03	1.030E+01	7 - 12	6.369E-02	5.043E-10	8.554E+00	1.861E-06
4 - 9	3.021E-04	8.854E-05	8.677E-02	8.000E-01	7 - 31	9.296E-01	0.000E+00	2.585E+04	0.000E+00
4 - 10	2.020E-04	1.006E-04	3.098E-02	4.727-01	8 - 9	0.000E+00	1.777E-01	0.000E+00	2.347E-01
4 - 11	1.618E-05	2.447E-05	1.540E-02	3.390E-01	8 - 10	1.331E-01	9.586E-02	2.371E-05	1.238E-01
4 - 12	8.630E-05	1.736E-05	5.375E-02	1.608E-01	8 - 11	1.467E+00	8.497E-06	6.960E+00	4.961E-03
4 - 31	4.616E-05	6.703E-08	2.627E+00	1.447E-02	8 - 12	2.287E+00	0.000E+00	7.336E+00	0.000E+00
5 - 6	5.072E-03	6.231E-04	4.983E-03	1.414E-01	8 - 31	0.000E+00	2.853E-08	1.861E-03	0.000E+00
5 - 7	2.110E-02	7.652E-03	1.404E-02	1.169E+00	9 - 10	1.928E+00	1.237E+00	1.104E-07	1.281E-02
5 - 8	1.191E-03	0.000E+00	2.422E-01	0.000E+00	9 - 11	1.596E-01	1.068E-04	4.368E-01	4.481E-02
5 - 9	9.077E-05	0.000E+00	2.428E-02	0.000E+00	9 - 12	1.434E-01	0.000E+00	2.658E-01	0.000E+00
5 - 10	3.448E-07	1.237E-04	4.929E-05	5.573E-01	9 - 31	0.000E+00	4.087E-07	0.000E+00	2.454E-02
5 - 11	1.377E-04	6.689E-06	1.220E-01	9.001E-02	10 - 11	3.105E-04	3.778E-04	7.330E-04	1.451E-01

Table 5: Same as in Table 4 but for electric octopole (E3) and magnetic quadrupole (M2) transitions.

$i - k$	S^{E3}	S^{M2}	A_{ki}^{E3}	A_{ki}^{M2}	$i - k$	S^{E3}	S^{M2}	A_{ki}^{E3}	A_{ki}^{M2}
1 - 5	1.677E-03	1.764E+01	9.130E-08	4.505E-02	9-41	5.010E+00	7.689E+00	9.704E-02	1.304E+00
1 - 7	2.699E+00	4.108E+01	1.038E-03	4.238E-01	10-18	5.505E-04	1.801E-03	2.720E-08	3.953E-06
3 - 12	7.918E+00	2.368E+00	1.272E-01	3.513E-01	10-19	7.422E-04	0.000E+00	3.102E-08	0.000E+00
3 - 14	2.896E-05	4.409E+00	4.376E-08	1.209E-01	10-28	1.034E-07	2.378E+01	3.312E-11	1.982E-01
8 - 14	1.618E-01	1.606E+00	1.485E-06	1.150E-03	10-33	1.516E+01	1.087E+01	2.258E-02	2.716E-01
8 - 17	1.128E-03	1.862E-04	1.043E-07	6.943E-07	10-36	3.227E+00	2.576E+00	2.308E-02	1.976E-01
8 - 18	1.903E-03	0.000E+00	1.375E-07	0.000E+00	11-18	4.198E-05	5.797E+00	7.957E-11	1.239E-03
8 - 22	1.479E-04	2.090E+01	6.498E-08	2.371E-01	11-19	4.657E-05	0.000E+00	7.715E-11	0.000E+00
8 - 27	2.052E-04	4.079E-04	1.161E-07	5.543E-06	11-28	1.742E-04	5.291E+00	5.321E-09	8.235E-03
8 - 28	5.409E-04	0.000E+00	2.321E-07	0.000E+00	11-33	2.466E-01	4.702E+01	5.952E-05	3.204E-01
8 - 29	1.570E-02	1.922E+01	2.053E-05	4.752E-01	11-36	5.125E-01	6.286E+00	8.913E-04	1.755E-01
8 - 32	5.248E+00	3.179E-01	1.230E-02	1.193E-02	12-19	3.245E-04	1.739E+01	5.306E-10	3.138E-03
8 - 33	1.544E+00	0.000E+00	2.911E-03	0.000E+00	12-21	2.222E-01	3.940E-01	4.957E-06	7.280E-04
8 - 36	1.179E+01	0.000E+00	1.019E-01	0.000E+00	12-24	1.794E-04	8.882E-01	1.585E-08	4.387E-03
8 - 37	5.841E+00	1.115E-01	6.836E-02	1.320E-02	12-25	5.327E-04	2.155E+00	6.119E-06	1.284E-02
8 - 41	3.266E-01	7.346E-01	7.258E-03	1.374E-01	12-35	1.264E+01	6.741E+00	5.776E-02	5.579E-01
9 - 14	2.032E+00	2.564E+00	1.217E-05	1.353E-03	12-38	2.113E+01	8.320E+00	1.610E-01	9.916E-01
9 - 17	1.575E-05	1.330E-02	1.075E-09	3.992E-05	12-42	1.188E-01	5.000E-01	1.884E-03	1.006E-01
9 - 18	1.146E-04	0.000E+00	6.121E-09	0.000E+00	14-31	3.212E-07	5.163E-03	2.639E-11	2.421E-05
9 - 22	1.378E-03	6.108E+00	4.752E-07	5.830E-02	17-31	3.054E-05	4.402E-06	1.449E-10	2.693E-09
9 - 27	2.244E-04	8.276E+00	1.005E-07	9.519E-02	18-31	5.687E-05	0.000E+00	2.510E-10	0.000E+00
9 - 28	3.417E-05	0.000E+00	1.161E-08	0.000E+00	22-31	1.073E-07	2.982E-02	8.183E-15	9.539E-07
9 - 29	2.893E-01	1.973E+01	3.075E-04	4.209E-01	27-31	1.038E-05	7.715E-04	2.580E-13	1.108E-08
9 - 32	4.332E+00	5.336E+00	8.397E-03	1.748E-01	28-31	6.932E-05	0.000E+00	1.627E-12	0.000E+00
9 - 33	7.135E+00	0.000E+00	1.115E-02	0.000E+00	29-31	3.271E-05	4.397E-02	8.664E-16	4.757E-09
9 - 36	1.467E-02	0.000E+00	1.090E-04	0.000E+00	31-36	5.087E-01	0.000E+00	1.009E-07	0.000E+00
9 - 37	3.634E+00	1.559E+00	3.658E-02	1.656E-01	31-41	3.574E-02	1.552E-02	1.288E-10	5.697E-06

3.3. Collision strengths

We presented in Table 6 our collision strengths calculated using the code AS [13]. We selected the transitions from the ten lowest levels to the 21 other ones: Ω_{ik} with $i = 1 - 5$ and $k = 2 - 21$. Levels are belonging to the first five configurations $3s^2 3p$, $3s3p^2$, $3s^2 3d$, $3p^3$ and four levels ($^4F_{3/2-9/2}^o$) from the configuration $3s3p3d$. Collision strengths are provided at six electron energies 10, 50, 100, 200, 400 and 800 Ry. For illustration, we present in Figure 1 collision strengths for 4 transitions as a function of electron energy calculated using the AS code and using the UCL codes SST/DW/JAJOM. We remark that for M1 and E2 transitions $1 - 2$ ($3s^2 3p^2 P_{1/2}^o - 3s^2 3p^2 P_{3/2}^o$) and

$2 - 30$ ($3s^2 3p^2 P_{3/2}^o - 3s3p3d^2 D_{3/2}^o$) displayed in panels (a) and (b) of Figure 1, the collision strengths from AS converge well to the infinite energy Born limits. This is not true for the electric dipole transitions $1 - 6$ ($3s^2 3p^2 P_{1/2}^o - 3s3p^2 D_{3/2}^o$) and $1 - 11$ ($3s^2 3p^2 P_{1/2}^o - 3s^2 3d^2 D_{3/2}^o$) displayed in panels c and d of Figure 1, where we found that the corresponding collision strengths do not converge to the Born limit as the UCL results. We remark also that the collision strengths from AS of some transitions have the same behaviour as those from UCL but they are not in good agreement with them such as the transition $3s^2 3p^2 P_{3/2}^o - 3s3p3d^2 D_{3/2}^o$ (2-30). There are no other collisional results provided as collision strengths Ω to compare with.

Table 6: Excitation collision strengths (Ω_{ik}) for transitions from the lowest s levels to the other 21 ones (levels from configurations $3s^2 3p$, $3s3p^2$, $3s^2 3d$, $3p^3$, and some from $3s3p3d$). BORN refers to the infinite energy Born limits. $aE \pm b$ means $a \times 10^{\pm b}$.

$i - k$	10 Ry	50 Ry	100 Ry	200 Ry	400 Ry	800 Ry	BORN
1-2	6.080E-01	5.859E-01	5.827E-01	5.668E-01	4.853E-01	3.298E-01	5.63E-01
1-3	1.575E-02	2.673E-03	2.238E-03	2.446E-03	2.718E-03	3.037E-03	3.47E-04
1-4	2.094E-02	1.301E-03	2.127E-04	9.799E-05	9.536E-05	1.032E-04	1.17E-05
1-5	1.294E-02	7.891E-04	1.131E-04	3.675E-05	2.605E-05	1.717E-05	2.94E-05
1-6	1.130E+00	1.692E+00	2.054E+00	2.377E+00	2.677E+00	3.012E+00	3.68E-01
1-7	6.397E-02	4.056E-02	4.205E-02	4.278E-02	3.743E-02	2.603E-02	4.62E-02
1-8	2.615E+00	3.957E+00	4.990E+00	5.931E+00	6.819E+00	7.822E+00	1.05E+00
1-9	3.626E+00	5.486E+00	6.929E+00	8.243E+00	9.473E+00	1.085E+01	1.46E+00
1-10	2.597E+00	3.919E+00	4.953E+00	5.899E+00	6.788E+00	7.793E+00	1.05E+00
1-11	7.916E+00	1.210E+01	1.571E+01	1.911E+01	2.240E+01	2.616E+01	3.74E+00
1-12	7.883E-02	9.918E-02	1.074E-01	1.092E-01	9.440E-02	6.510E-02	1.19E-01
1-13	2.340E-01	3.251E-01	3.494E-01	3.508E-01	3.019E-01	2.061E-01	3.58E-01
1-14	1.516E-01	2.103E-01	2.259E-01	2.264E-01	1.943E-01	1.328E-01	2.31E-01
1-15	3.374E-04	3.204E-04	3.312E-04	3.307E-04	2.862E-04	1.957E-04	3.36E-04
1-16	1.236E-02	8.545E-04	1.563E-04	3.401E-05	1.297E-05	7.121E-06	1.16E-05
1-17	1.430E-02	9.782E-04	1.680E-04	2.628E-05	3.604E-06	4.441E-07	1.39E-07
1-18	1.094E-02	7.507E-04	1.290E-04	2.029E-05	2.827E-06	3.456E-07	8.40E-08
1-19	9.892E-05	1.355E-05	1.800E-06	1.932E-07	7.954E-08	1.588E-08	0.00E+00
1-20	1.398E-01	2.013E-01	2.181E-01	2.198E-01	1.898E-01	1.296E-01	2.24E-01
1-21	6.022E-04	5.193E-04	5.174E-04	5.121E-04	4.983E-04	4.145E-04	5.07E-04

Table 6: Continued.

$i - k$	10 Ry	50 Ry	100 Ry	200 Ry	400 Ry	800 Ry	BORN
2-3	9.593E-03	1.669E-03	1.414E-03	1.548E-03	1.722E-03	1.927E-03	2.20E-04
2-4	2.676E-02	2.902E-03	1.791E-03	1.855E-03	2.046E-03	2.276E-03	2.59E-04
2-5	6.036E-02	8.281E-03	6.163E-03	6.610E-03	7.319E-03	8.154E-03	9.29E-04
2-6	2.409E-01	2.901E-01	3.413E-01	3.836E-01	4.154E-01	4.486E-01	5.19E-02
2-7	1.976E+00	2.909E+00	3.520E+00	4.062E+00	4.563E+00	5.122E+00	6.23E-01
2-8	9.920E-01	1.496E+00	1.886E+00	2.243E+00	2.583E+00	2.970E+00	3.97E-01
2-9	3.755E+00	5.680E+00	7.169E+00	8.525E+00	9.801E+00	1.124E+01	1.51E+00
2-10	1.276E+01	1.932E+01	2.440E+01	2.903E+01	3.337E+01	3.827E+01	5.14E+00
2-11	1.797E+00	2.710E+00	3.483E+00	4.195E+00	4.864E+00	5.629E+00	7.95E-01
2-21	1.522E-01	2.183E-01	2.367E-01	2.389E-01	2.068E-01	1.413E-01	2.44E-01
3-4	1.421E-01	8.135E-02	7.733E-02	7.458E-02	6.388E-02	4.346E-02	7.39E-02
3-5	6.764E-01	6.889E-01	6.877E-01	6.695E-01	5.741E-01	3.911E-01	6.64E-01
3-6	1.770E-02	1.388E-03	4.289E-04	2.346E-04	1.751E-04	1.158E-04	1.93E-04
3-7	1.116E-02	7.111E-04	1.407E-04	3.072E-05	9.323E-06	4.192E-06	5.66E-06
3-8	2.170E-03	2.652E-04	5.758E-05	9.419E-06	3.718E-06	2.462E-06	2.96E-06
3-9	3.942E-04	9.442E-05	2.282E-05	2.972E-06	5.865E-07	1.537E-07	9.07E-09
3-10	3.167E-03	2.370E-04	6.171E-05	2.624E-05	1.708E-05	1.085E-05	1.90E-05
3-11	2.914E-03	3.364E-04	1.801E-04	1.453E-04	1.184E-04	7.954E-05	1.41E-04
3-12	2.165E-03	2.864E-04	1.846E-04	1.605E-04	1.316E-04	8.855E-05	1.60E-04
3-13	3.029E-02	1.944E-03	5.684E-04	4.793E-04	5.361E-04	6.109E-04	7.91E-05
3-14	6.388E-03	3.680E-04	5.265E-05	5.968E-06	8.717E-07	2.770E-07	4.06E-07
3-15	2.923E+00	4.406E+00	5.529E+00	6.549E+00	7.504E+00	8.580E+00	1.14E+00
3-16	5.474E-03	1.427E-03	1.473E-03	1.709E-03	1.979E-03	2.296E-03	3.14E-04
3-17	4.694E-02	6.604E-02	7.172E-02	7.328E-02	6.390E-02	4.433E-02	7.94E-02
3-18	8.060E-02	1.202E-01	1.309E-01	1.337E-01	1.165E-01	8.074E-02	1.45E-01
3-19	3.554E-03	2.144E-04	3.747E-05	4.987E-06	4.657E-07	2.994E-08	0.00E+00
3-20	8.016E-03	7.082E-03	8.774E-03	1.049E-02	1.213E-02	1.399E-02	1.93E-03
3-21	5.634E-03	3.830E-04	9.136E-05	6.450E-05	7.054E-05	7.921E-05	1.07E-05

Table 6: Continued.

$i - k$	10 Ry	50 Ry	100 Ry	200 Ry	400 Ry	800 Ry	BORN
4-5	1.017E+00	9.680E-01	9.621E-01	9.356E-01	8.012E-01	5.454E-01	9.27E-01
4-6	2.751E-02	1.874E-03	3.912E-04	9.733E-05	3.922E-05	2.108E-05	3.53E-05
4-7	3.171E-02	3.300E-03	1.704E-03	1.363E-03	1.124E-03	7.596E-04	1.29E-03
4-8	4.027E-03	4.902E-04	1.090E-04	2.143E-05	1.024E-05	6.271E-06	9.41E-06
4-9	2.017E-03	2.913E-04	1.145E-04	7.044E-05	5.526E-05	3.685E-05	6.43E-05
4-10	5.740E-03	5.029E-04	1.366E-04	5.731E-05	3.820E-05	2.456E-05	4.26E-05
4-11	4.644E-03	3.276E-04	6.661E-05	1.443E-05	4.721E-06	2.194E-06	3.34E-06
4-12	5.140E-03	3.692E-04	8.952E-05	3.416E-05	2.137E-05	1.347E-05	2.16E-05
4-13	4.115E-02	2.432E-03	4.940E-04	3.098E-04	3.288E-04	3.641E-04	4.58E-05
4-14	3.108E-02	2.021E-03	5.986E-04	4.877E-04	5.430E-04	6.216E-04	8.07E-05
4-15	5.857E+00	8.834E+00	1.108E+01	1.312E+01	1.503E+01	1.717E+01	2.27E+00
4-16	8.655E-02	1.258E-01	1.328E-01	1.246E-01	9.695E-02	6.167E-02	4.26E-04
4-17	5.472E-02	7.134E-02	7.596E-02	7.272E-02	5.936E-02	4.253E-02	1.67E-03
4-18	1.125E-02	7.513E-04	1.557E-04	5.016E-05	3.262E-05	2.175E-05	4.00E-05
4-19	1.204E-01	1.753E-01	1.907E-01	1.945E-01	1.694E-01	1.171E-01	2.11E-01
4-20	1.975E-02	1.455E-02	1.777E-02	2.118E-02	2.443E-02	2.809E-02	3.86E-03
4-21	9.193E-03	1.013E-03	6.614E-04	7.231E-04	8.333E-04	9.619E-04	1.33E-04
5-6	2.561E-02	2.668E-03	5.457E-03	1.139E-03	9.322E-04	6.281E-04	1.08E-03
5-7	6.804E-02	8.860E-03	4.049E-04	4.661E-03	3.862E-03	2.609E-03	4.51E-03
5-8	5.546E-03	8.829E-04	1.115E-04	2.923E-04	2.442E-04	1.661E-04	2.76E-04
5-9	6.256E-03	4.819E-04	1.584E-04	3.597E-05	2.065E-05	1.273E-05	2.06E-05
5-10	6.567E-03	7.303E-04	9.358E-05	2.344E-05	4.362E-06	1.036E-06	1.18E-07
5-11	4.501E-03	3.268E-04	2.722E-04	4.833E-05	3.545E-05	2.322E-05	3.71E-05
5-12	1.050E-02	8.553E-04	1.067E-03	1.546E-04	1.173E-04	7.696E-05	1.29E-04
5-13	1.431E-02	1.567E-03	3.868E-03	1.122E-03	1.243E-03	1.387E-03	1.75E-04
5-14	9.394E-02	7.703E-03	1.663E+01	3.913E-03	4.364E-03	4.889E-03	6.19E-04
5-15	8.767E+00	1.326E+01	3.125E-02	1.969E+01	2.255E+01	2.579E+01	3.41E+00
5-16	2.418E-02	2.988E-02	1.089E-01	2.914E-02	2.245E-02	1.406E-02	3.80E-05
5-17	7.520E-02	1.033E-01	2.133E-01	1.020E-01	7.952E-02	5.181E-02	7.44E-04
5-18	1.439E-01	2.010E-01	2.334E-01	2.017E-01	1.611E-01	1.116E-01	3.49E-03
5-19	1.597E-01	2.152E-01	7.917E-03	2.377E-01	2.064E-01	1.431E-01	2.58E-01
5-20	3.055E-02	7.707E-03	6.277E-05	9.242E-03	1.062E-02	1.217E-02	1.66E-03
5-21	5.797E-03	3.891E-04	1.104E+01	1.956E-05	1.429E-05	9.644E-06	1.74E-05

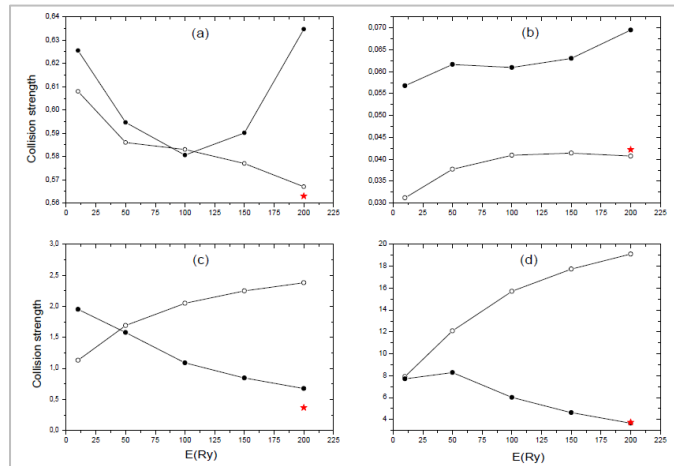


Figure 1: Collision strength as a function of electron energy for the 4 selected transitions: $3s^2 3p^2 \ ^2P_{1/2}^o - 3s^2 3p^2 \ ^2P_{3/2}^o$ (a: 1-2), $3s^2 3p^2 \ ^2P_{1/2}^o - 3s 3p^3 d^2 \ ^2D_{3/2}$ (b: 2-30), $3s^2 3p^2 \ ^2P_{1/2}^o - 3s 3p^3 d^2 \ ^2D_{3/2}$ (c: 1-6) and $3s^2 3p^2 \ ^2P_{1/2}^o - 3s 2^3 d^4 \ ^4D_{3/2}$ (d: 1-11). \circ : AS, \bullet : UCL, \star : infinite energy Born limits.

It is known that collision strengths are determined by summing over the total angular momentum J , consequently, it is important to ensure that we have included all the values of J that contribute to the collision strengths; i.e. check that as J increases its contribution for Ω decreases and approximately tends to zero. We examine here this convergence problem with the angular momentum J . For illustration, we present in Figure 2 the contributions of each angular momentum J to the partial collision strengths Ω_J at different electron energies for some transitions. As it is known for electric dipole transitions, collision strengths do not converge easily with J , and we have to take into account the contributions of higher partial waves especially at high energies. This case is illustrated in panels (c) and (d) of Figure 2 respectively for the $3s^2 3p^2 \ ^2P_{1/2}^o - 3s 3p^3 d^2 \ ^2D_{3/2}$ transition (1-6) and the $3s 3p^3 d^2 \ ^2D_{3/2}^o - 3p^3 2^3 d^4 \ ^4D_{3/2}$ one (30-52), where collision strengths start to converge for high J (90-100) at electron energy $E = 150$ Ry. The two forbidden transitions $3s^2 3p^2 \ ^2P_{1/2}^o - 3s 2^3 p^3 \ ^2P_{3/2}^o$ (1-2) and $3s^2 3p^2 \ ^2P_{1/2}^o - 3s 3p^3 d^2 \ ^2D_{3/2}$ (2-17) (panels a and b of Figure 2) converge easily (for $J = 35-45$) as it is expected even at high energies. A first conclusion can be drawn from the above discussions is that all the necessary angular momenta that contribute to the collision strengths are well introduced, and so our collisional calculations are sufficiently complete.

$3s^2 3p^2 \ ^2P_{1/2}^o - 3s 2^3 p^3 \ ^2P_{3/2}^o$ (1-2) and $3s^2 3p^2 \ ^2P_{1/2}^o - 3s 3p^3 d^2 \ ^4F_{5/2}^o$ (2-17) (panels a and b of Figure 2) converge easily (for $J = 35-45$) as it is expected even at high energies. A first conclusion can be drawn from the above discussions is that all the necessary angular momenta that contribute to the collision strengths are well introduced, and so our collisional calculations are sufficiently complete.

3.4. Effective collision strengths

In a hot plasma, electrons have a wide range of velocities (energies), then collision strength Ω are averaged over a given velocities distribution to provide effective collision strength Y . Assuming a thermodynamic equilibrium state, a Maxwellian distribution is chosen. Hence, effective collision strengths Y are obtained by convolving the collision strength Ω with the Maxwellian electron energy distribution as follows:

$$Y_{if}(T_e) = \int_0^\infty \Omega_{if}(E) e^{-E_f/kT_e} d(E_f/kT_e), \quad (17)$$

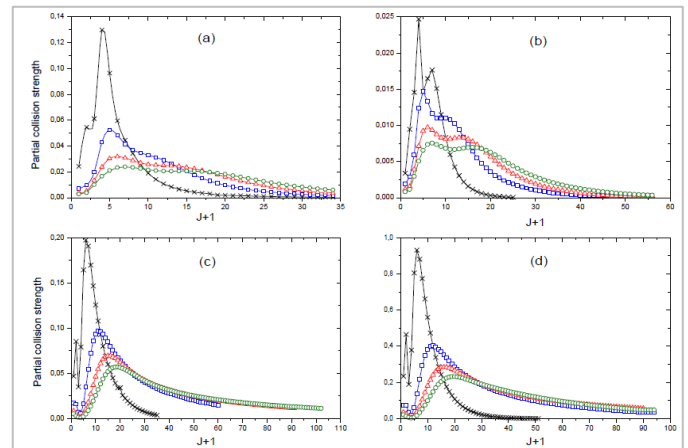


Figure 2: Partial collision strength as a function of the total angular momentum J for several electron energies for the 4 selected transitions: $3s^2 3p^2 \ ^2P_{1/2}^o - 3s 2^3 p^3 \ ^2P_{3/2}^o$ (a: 1-2), $3s^2 3p^2 \ ^2P_{1/2}^o - 3p^3 2^3 \ ^2P_{1/2}^o$ (b: 2-17), $3s^2 3p^2 \ ^2P_{1/2}^o - 3s 3p^3 d^2 \ ^2D_{3/2}$ (c: 1-6) and $3s 3p^3 d^2 \ ^2D_{3/2}^o - 3p^3 2^3 d^4 \ ^4D_{3/2}$ (d: 30-52) at energies 10 Ry (\times), 50 Ry (\bullet), 100 Ry (Δ) and 150 Ry (\diamond).

where k is the Boltzman constant, T_e is the electron temperature in K and E_f is the incident electron energy with respect to the final (upper) level. These quantities are dimensionless and are involved in astrophysical and solar applications through the excitation $q(i, f)$ and de-excitation $q(f, i)$ rate coefficients defined as:

$$q(i, f) = \frac{8.629 \times 10^{-6}}{g_i T_e^{1/2}} Y(T_e) e^{-\Delta E_{if}/kT_e} \text{ (cm}^3 \text{s}^{-1}) \quad (18)$$

$$\text{and } q(f, i) = \frac{8.629 \times 10^{-6}}{g_f T_e^{1/2}} Y(T_e) \text{ (cm}^3 \text{s}^{-1}) \quad (19)$$

where g_i and g_f are the statistical weights of the initial (i) and the final (f) levels, respectively, and $\Delta E_{if} = E_f - E_i$ is the corresponding transition energy. The integration in Equation 6 should be carried out using energy-dependent collision strengths from threshold to infinity. The collision strengths at higher energies are particularly important for the dipole allowed transitions, where they grow as $\ln(E)$. In the case of the electric quadrupole or magnetic dipole transitions, the collision strengths are approximately constant, whereas for intercombination transitions they rapidly decrease as $1/E^2$ in the asymptotic region[22].

Our effective collision strengths $Y_{ik}(T_e)$ are calculated with the code ADASEXJ¹ using the collision strengths Ω from the code AUTOSTRUCTURE. We present in Table 7 $Y_{ik}(T_e)$ with $i = 1 - 6$ and $k = 2 - 21$ over a wide temperature range from 7.2×10^3 K up to 3.6×10^5 K suitable for astrophysical and plasma applications. We compare with the results of [2] obtained by the Breit-Pauli R-matrix method (BPRM)². On the light of these comparison, there are several points that have to be stressed:

- Firstly, we remark that almost all transitions involving the levels from 16 to 21 ($3s3p3d \ ^4F_{3/2-9/2}$ and $3p^3 \ ^2P_{1/2-3/2}$) present effective collision strengths that are not in good agreement with our

results. We remark also that levels 16–21 have not the same order in our calculations as in the calculations of [2], and the disagreement can be due to the inversion of these levels.

- Secondly, Effective collision strengths of electric dipole transitions agree well with the results of [2]. This point is illustrated in Figure 3 (panel c) displaying effective collision strengths of the 1 – 8, 1 – 9, 1 – 11 and 4 – 15 allowed transitions. For the forbidden transitions (E2 and M1), the agreement is less than that of the allowed transitions. Figs. 2 (panels a and b) show our results and those of the [2] for four forbidden transitions (1 – 17, 2 – 20, 3 – 6 and 6 – 8).

- Thirdly, we remark that the agreement is as good as the transition is more probable (strong transition). Table 7 shows the fact that the ratio AS/BPRM is varying from 0.16 for the E2 transition 1 – 17 with a radiative decay rate $A(1 - 17) = 1.991 \times 10^{-2}$ to 0.95 for the E2/M1 transition 2 – 20 with $A(2 - 20) = 8.416 \times 10^4$. This is also true for allowed transitions where the agreement increases with the strength of the transition: the ratio AS/BPRM increases from 0.29 for the transition 1 – 4 with $A(1 - 4) = 4.343 \times 10^{+3}$ to 0.99 for the transition 1 – 11 with $A(1 - 11) = 1.651 \times 10^{+10}$. There are some exceptions that escape this conclusion.

- Finally, we note that for forbidden transitions, the agreement is better for high temperatures (Figure 3, panels a and b), but for electric dipole transitions, the agreement is better for low temperatures (Figure 3, panel c). This can be explained by the fact that for allowed transitions, the contribution of high energies (temperatures) to collision strengths is important, in contrast to intercombination transitions where collision strengths vary rapidly in the asymptotic region (low temperature). We illustrate this remark in the Table 8.

Table 7: Effective collision strengths Y_{ik} (Present) for transitions from the lowest 6 levels to the other 21 ones compared to BPRM results [2]. $a \pm b$ means $a \times 10^{\pm b}$.

$T_e(K)$	7.20+03		3.60+04		1.80+05		7.20+05		3.60+05	
	Present	BPRM								
1-2	8.86-01	6.33+00	8.72-01	6.42+00	8.15-01	4.73+00	7.18-01	2.26+00	6.28-01	3.39+00
1-3	4.94-02	2.95-01	4.85-02	2.39-01	4.42-02	1.55-01	3.32-02	7.25-02	1.54-02	2.50-02
1-4	6.99-02	3.77-01	6.86-02	4.07-01	6.24-02	2.64-01	4.63-02	1.21-01	2.03-02	4.55-02
1-5	4.34-02	5.76-01	4.26-02	5.39-01	3.87-02	3.23-01	2.87-02	1.34-01	1.25-02	4.46-02
1-6	7.96-01	1.72+00	8.03-01	1.62+00	8.38-01	1.34+00	9.66-01	1.14+00	1.30+00	1.37+00
1-7	1.65-01	1.53+00	1.62-01	1.23+00	1.48-01	7.13-01	1.14-01	3.17-01	6.75-02	1.24-01
1-8	1.66+00	1.57+00	1.68+00	1.52+00	1.79+00	1.52+00	2.16+00	1.79+00	3.02+00	2.67+00
1-9	2.28+00	2.77+00	2.31+00	2.63+00	2.47+00	2.77+00	3.00+00	3.46+00	4.19+00	5.21+00
1-10	1.67+00	1.94+00	1.69+00	1.85+00	1.80+00	1.89+00	2.17+00	2.25+00	3.01+00	3.30+00
1-11	4.71+00	4.37+00	4.84+00	4.72+00	5.42+00	5.25+00	6.71+00	6.78+00	9.33+00	1.06+01
1-12	1.40-01	5.29-01	1.38-01	5.61-01	1.31-01	4.35-01	1.10-01	2.51-01	9.08-02	1.51-01
1-13	1.97-01	2.99-01	2.00-01	2.77-01	2.15-01	2.45-01	2.31-01	2.56-01	2.61-01	3.06-01
1-14	1.30-01	2.98-01	1.32-01	2.65-01	1.41-01	1.99-01	1.50-01	1.81-01	1.69-01	2.03-01
1-15	1.03-03	2.64-02	1.01-03	3.63-02	8.89-04	2.25-02	6.49-04	9.08-03	4.07-04	3.57-03
1-16	4.36-02	1.35-01	4.27-02	1.06-01	3.85-02	7.25-02	2.80-02	4.08-02	1.21-02	1.56-02
1-17	5.04-02	1.90-01	4.94-02	1.42-01	4.46-02	9.30-02	3.24-02	5.03-02	1.40-02	1.87-02
1-18	3.87-02	1.60-01	3.79-02	1.23-01	3.42-02	7.75-02	2.48-02	4.08-02	1.07-02	1.48-02
1-19	6.62-04	8.78-02	6.38-04	5.61-02	5.30-04	2.76-02	3.34-04	9.97-03	1.30-04	2.31-03
1-20	1.13-01	1.94-01	1.15-01	1.83-01	1.24-01	1.57-01	1.35-01	1.58-01	1.55-01	1.89-01
1-21	1.13-03	5.86-02	1.11-03	5.58-02	1.03-03	3.37-02	8.45-04	1.82-02	6.18-04	1.25-02
2-3	3.01-02	4.70-01	2.95-02	3.77-01	2.69-02	2.23-01	2.02-02	9.12-02	9.42-03	2.66-02
2-4	8.70-02	7.28-01	8.54-02	7.43-01	7.77-02	4.69-01	5.80-02	2.05-01	2.60-02	7.66-02
2-5	1.93-01	1.23+00	1.90-01	1.19+00	1.73-01	7.64-01	1.29-01	3.48-01	5.89-02	1.32-01
2-6	3.22-01	1.91+00	3.19-01	1.64+00	3.06-01	1.04+00	2.81-01	5.53-01	2.69-01	3.57-01
2-7	1.50+00	3.94+00	1.51+00	3.62+00	1.56+00	2.86+00	1.75+00	2.23+00	2.27+00	2.47+00
2-8	6.49-01	1.45+00	6.56-01	1.42+00	6.93-01	1.22+00	8.29-01	1.18+00	1.15+00	1.58+00
2-9	2.40+00	2.81+00	2.43+00	2.39+00	2.59+00	2.41+00	3.12+00	2.91+00	4.34+00	4.36+00
2-10	8.00+00	7.93+00	8.11+00	7.97+00	8.68+00	8.58+00	1.05+01	1.07+01	1.47+01	1.62+01
2-11	1.22+00	1.61+00	1.24+00	1.69+00	1.35+00	1.65+00	1.59+00	1.75+00	2.11+00	2.44+00
2-12	8.69+00	8.44+00	8.92+00	9.10+00	9.99+00	9.95+00	1.23+01	1.26+01	1.70+01	1.95+01
2-13	1.80-01	4.06-01	1.83-01	3.62-01	1.95-01	2.77-01	2.08-01	2.54-01	2.34-01	2.85-01
2-14	4.36-01	7.40-01	4.43-01	6.94-01	4.74-01	5.83-01	5.08-01	5.85-01	5.72-01	6.83-01
2-15	1.82-03	5.14-02	1.77-03	6.98-02	1.56-03	4.35-02	1.13-03	1.76-02	7.01-04	7.11-03
2-16	1.21-02	1.36-01	1.19-02	9.07-02	1.07-02	5.36-02	7.73-03	2.36-02	3.33-03	7.12-03
2-17	3.31-02	2.73-01	3.25-02	1.82-01	2.92-02	1.09-01	2.12-02	5.07-02	9.13-03	1.63-02
2-18	7.28-02	2.90-01	7.13-02	2.25-01	6.43-02	1.47-01	4.66-02	7.77-02	2.01-02	2.85-02
2-19	1.38-01	3.77-01	1.35-01	3.11-01	1.22-01	2.19-01	8.86-02	1.27-01	3.83-02	4.81-02

¹ <http://amdpp.phys.strath.ac.uk/autos/ver/misc/>

² Data of effective collision strengths have been taken from the website <http://open.adas.ac.uk>

Table 7: Continued.

$T_e(K)$	7.20+03		3.60+04		1.80+05		7.20+05		3.60+05	
	Present	BPRM								
3-4	4.43-01	1.81+00	4.30-01	2.86+00	3.75-0	6.58+00	2.71-01	7.76+00	1.53-01	5.01+00
3-5	8.03-01	2.46+00	7.96-01	2.80+00	7.66-01	4.07+00	7.21-01	4.74+00	6.92-01	4.02+00
3-6	1.01-01	4.84-01	9.77-02	4.78-01	8.22-02	3.85-01	5.34-02	2.90-01	2.10-02	2.55-01
3-7	6.05-02	4.72-01	5.85-02	4.47-01	4.94-02	3.52-01	3.24-02	2.38-01	1.28-02	1.82-01
3-8	1.89-02	1.53-01	1.82-02	1.60-01	1.50-02	1.37-01	9.15-03	1.04-01	3.32-03	1.04-01
3-9	3.14-03	1.22-01	3.01-03	1.58-01	2.43-03	1.87-01	1.48-03	1.07+00	5.67-04	1.66+00
3-10	1.66-02	1.23-01	1.60-02	2.18-01	1.37-02	2.46-01	9.04-03	6.77-01	3.61-03	9.55-01
3-11	1.50-02	2.45-01	1.45-02	2.66-01	1.25-02	1.78-01	8.28-03	1.23-01	3.36-03	1.04-01
3-12	1.02-02	1.91-01	9.92-03	2.35-01	8.55-03	1.65-01	5.78-03	9.82-02	2.41-03	7.47-02
3-13	1.11-01	3.26-01	1.09-01	3.11-01	9.93-02	1.88-01	7.22-02	1.00-01	3.07-02	3.88-02
3-14	2.74-02	2.78-01	2.68-02	2.54-01	2.36-02	1.27-01	1.65-02	5.09-02	6.78-03	1.52-02
3-15	1.91+00	1.94+00	1.93+00	2.07+00	2.04+00	2.11+00	2.44+00	2.51+00	3.37+00	3.65+00
3-16	2.47-02	4.72-01	2.41-02	2.55-01	2.11-02	1.36-01	1.45-02	5.97-02	6.36-03	1.81-02
3-17	6.34-02	5.83-01	6.28-02	3.64-01	6.03-02	2.01-01	5.47-02	1.13-01	5.40-02	7.75-02
3-18	8.94-02	6.07-01	8.91-02	4.02-01	8.79-02	2.26-01	8.49-02	1.45-01	9.27-02	1.23-01
3-19	1.69-02	3.17-01	1.64-02	1.82-01	1.43-02	8.41-02	9.78-03	3.52-02	3.93-03	9.89-03
3-20	1.63-02	1.85-01	1.61-02	1.37-01	1.51-02	6.30-02	1.24-02	2.87-02	8.90-03	1.43-02
3-21	2.02-02	1.13-01	1.99-02	8.99-02	1.82-02	4.71-02	1.34-02	2.37-02	5.70-03	8.97-03
4-5	1.50+00	5.25+00	1.48+00	6.42+00	1.38+00	1.38+01	1.21+00	3.14+01	1.05+00	3.82+01
4-6	1.57-01	8.40-01	1.51-01	8.34-01	1.27-01	1.13+00	8.28-02	1.67+00	3.24-02	1.99+00
4-7	1.72-01	1.09+00	1.66-01	1.05+00	1.40-01	1.37+00	9.16-02	2.12+00	3.67-02	2.50+00
4-8	3.45-02	2.72-01	3.32-02	2.90-01	2.74-02	2.45-01	1.67-02	1.28-01	6.09-03	9.02-02
4-9	1.25-02	2.33-01	1.20-02	3.02-01	1.01-02	3.88-01	6.42-03	6.57-01	2.53-03	1.50+00
4-10	3.15-02	2.79-01	3.05-02	5.28-01	2.59-02	2.16+00	1.70-02	1.04+01	6.73-03	1.32+01
4-11	2.44-02	4.72-01	2.37-02	4.81-01	2.02-02	3.08-01	1.34-02	2.09-01	5.33-03	3.29-01
4-12	2.62-02	5.00-01	2.54-02	5.54-01	2.18-02	3.83-01	1.45-02	3.00-01	5.81-03	4.51-01
4-13	1.54-01	5.49-01	1.51-01	5.20-01	1.37-01	3.01-01	9.90-02	1.51-01	4.18-02	5.73-02
4-14	1.20-01	6.35-01	1.18-01	6.03-01	1.06-01	3.28-01	7.60-02	1.50-01	3.20-02	5.54-02
4-15	3.79+00	3.87+00	3.83+00	4.11+00	4.06+00	4.21+00	4.87+00	5.03+00	6.76+00	7.35+00
4-16	1.01-01	8.36-01	1.00-01	4.98-01	9.80-02	2.83-01	9.32-02	1.74-01	9.90-02	1.31-01
4-17	8.51-02	1.01+00	8.41-02	5.82-01	7.93-02	3.16-01	6.91-02	1.65-01	6.27-02	9.23-02
4-18	5.63-02	1.02+00	5.48-02	5.91-01	4.77-02	3.14-01	3.24-02	1.36-01	1.29-02	3.93-02
4-19	1.45-01	1.24+00	1.44-01	7.68-01	1.40-01	4.16-01	1.32-01	2.50-01	1.38-01	1.91-01
4-20	4.54-02	3.76-01	4.48-02	2.84-01	4.18-02	1.37-01	3.35-02	6.56-02	2.15-02	2.99-02
4-21	3.25-02	2.06-01	3.19-02	1.59-01	2.93-02	8.16-02	2.15-02	3.98-02	9.37-03	1.49-02

Table 7: Continued.

$T_e(K)$	7.20+03		3.60+04		1.80+05		7.20+05		3.60+05	
	Present	BPRM								
5-6	1.35-01	9.75-01	1.30-01	9.56-01	1.10-01	1.97+00	7.26-02	3.80+00	2.93-02	4.62+00
5-7	3.67-01	1.94+00	3.54-01	1.91+00	2.99-01	2.51+00	1.96-01	4.13+00	7.94-02	5.03+00
5-8	4.51-02	3.49-01	4.34-02	3.83-01	3.59-02	3.18-01	2.21-02	1.39-01	8.21-03	4.07-02
5-9	3.57-02	2.85-01	3.45-02	3.35-01	2.92-02	2.93-01	1.90-02	2.45-01	7.46-03	2.21-01
5-10	4.01-02	5.16-01	3.87-02	8.30-01	3.25-02	2.76+00	2.08-02	1.36+01	8.14-03	1.67+01
5-11	2.28-02	5.12-01	2.21-02	5.19-01	1.90-02	3.78-01	1.27-02	4.36-01	5.08-03	9.30-01
5-12	5.43-02	1.07+00	5.26-02	1.05+00	4.50-02	6.88-01	2.99-02	5.83-01	1.20-02	9.98-01
5-13	5.89-02	1.07+00	5.75-02	1.05+00	5.10-02	6.88-01	3.59-02	5.83-01	1.52-02	9.98-01
5-14	3.47-01	1.09+00	3.41-01	1.11+00	3.08-01	6.65-01	2.23-01	3.41-01	9.56-02	1.33-01
5-15	5.64+00	5.85+00	5.70+00	6.18+00	6.05+00	6.33+00	7.28+00	7.58+00	1.01+01	1.11+01
5-16	4.16-02	6.00-01	4.10-02	3.25-01	3.82-02	1.59-01	3.23-02	8.05-02	2.75-02	4.24-02
5-17	1.02-01	1.03+00	1.01-01	6.26-01	9.67-02	3.39-01	8.77-02	1.90-01	8.58-02	1.21-01
5-18	1.87-01	1.73+00	1.85-01	1.06+00	1.78-01	6.00-01	1.64-01	3.46-01	1.65-01	2.33-01
5-19	2.42-01	2.66+00	2.39-01	1.59+00	2.27-01	8.99-01	1.99-01	4.80-01	1.84-01	2.86-01
5-20	9.94-02	6.20-01	9.78-02	4.82-01	9.00-02	2.47-01	6.71-02	1.22-01	3.16-02	4.94-02
5-21	2.21-02	2.31-01	2.17-02	1.73-01	1.97-02	8.39-02	1.43-02	3.70-02	6.00-03	1.21-02
6-7	8.01-01	6.35+00	7.90-01	5.72+00	7.39-01	6.01+00	6.53-01	8.28+00	5.70-01	8.73+00
6-8	6.16-01	9.76-01	6.11-01	1.15+00	5.93-01	1.02+00	5.86-01	8.22-01	6.14-01	7.83-01
6-9	1.66-01	1.34+00	1.64-01	9.23-01	1.53-01	8.06-01	1.38-01	1.55+00	1.27-01	1.80+00
6-10	1.65-01	1.08+00	1.60-01	1.06+00	1.38-01	1.60+00	9.85-02	6.56+00	5.39-02	9.22+00
6-11	1.06-01	2.72+00	1.02-01	2.07+00	8.32-02	1.70+00	5.32-02	1.60+00	2.66-02	1.64+00
6-12	1.53-01	1.60+00	1.47-01	1.26+00	1.18-01	1.04+00	7.20-02	1.26+00	3.35-02	1.48+00
6-13	1.27+00	1.68+00	1.29+00	1.71+00	1.35+00	1.43+00	1.57+00	1.42+00	2.13+00	1.86+00
6-14	2.95-01	1.04+00	2.94-01	1.10+00	2.90-01	6.59-01	2.90-01	3.93-01	3.22-01	3.18-01
6-15	7.46-04	2.60-01	7.32-04	2.24-01	6.69-04	1.08-01	5.48-04	3.79-02	4.40-04	1.25-02
6-16	1.68-01	6.18-01	1.64-01	4.75-01	1.47-01	2.84-01	1.05-01	1.53-01	4.59-02	5.92-02
6-17	1.94-01	7.34-01	1.90-01	5.68-01	1.69-01	3.41-01	1.19-01	1.80-01	4.88-02	6.62-02
6-18	1.52-01	6.70-01	1.49-01	4.97-01	1.32-01	2.90-01	9.32-02	1.50-01	3.81-02	5.23-02
6-19	1.65-02	4.57-01	1.60-02	2.65-01	1.38-02	1.19-01	9.28-03	4.64-02	3.69-03	1.23-02
6-20	4.62-01	1.01+00	4.66-01	8.37-01	4.86-01	6.36-01	5.70-01	6.14-01	7.76-01	8.10-01
6-21	2.23+00	2.30+00	2.25+00	2.22+00	2.39+00	2.26+00	2.88+00	2.79+00	4.03+00	4.15+00

Table 8: Ratio of our effective collision strengths Υ (AS) to the BPRM [2] ones for some chosen forbidden transitions and their radiative decay rates.

Forbidden transitions			Allowed transitions		
$i - j$	$A_{ji}(s^{-1})$	AS/BPRM	$i - j$	$A_{ji}(s^{-1})$	AS/BPRM
1 - 17	1.991E-02	0.16	1 - 4	4.343E+03	0.29
3 - 6	1.211E-01	0.17	1 - 3	2.522E+05	0.37
1 - 16	2.945E+00	0.57	4 - 16	1.125E+06	0.43
6 - 8	4.969E+01	0.66	7 - 13	7.75E+07	0.65
2 - 20	8.416E+04	0.95	1 - 11	1.651E+10	0.99

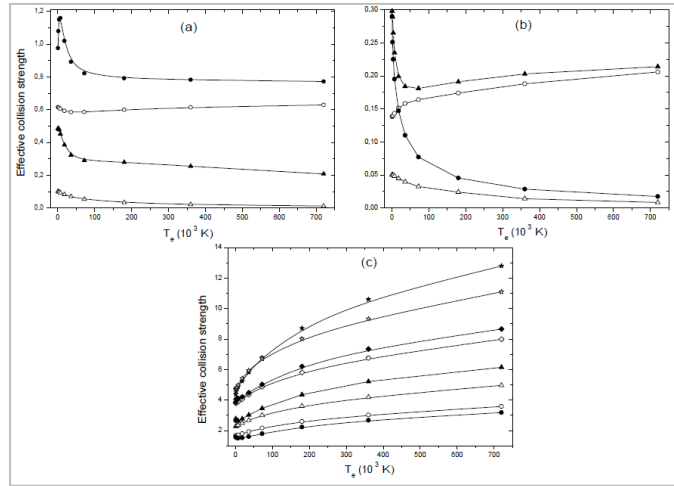


Figure 3: Effective collision strength Υ as a function of electron temperature T_e . Panel (a): the two forbidden transitions 3 - 6 (Δ) and 6 - 8 (\circ). Panel (b): the two forbidden transitions 1 - 17 (Δ) and 2 - 20 (\circ). Panel (c): the 4 electric dipole transitions 1 - 8 (\circ), 1 - 9 (Δ), 1 - 11 (\circ) and 4 - 15 (\star). Open symbols refer to our DW results and filled symbols to the BPRM ones [2].

4. Summary of the results and conclusion

Structure and collision calculations have been performed in the present work using the code AUTOSTRUCTURE [13]. We have used the 12 configurations: $3s^2 3p$, $3s3p^2$, $3s^2 3d$, $3p^3$, $3s3p3d$, $3s^2 4s$, $3s^2 4p$, $3p^2 3d$, $3s^2 4d$, $3s3p4s$, $3s3p4p$ and $3s3p4d$ yielding to 121 fine structure levels. Comparison of energy levels has been performed with the results of the multiconfiguration Hartree-Fock (MCHF) approach [8] and with the NIST values [11] for the lowest 60 levels. Agreement between the three results is about 3 % except for some levels belonging to the configuration $3s3p3d$ for which the difference reaches 5 %. We found disagreements in the term splitting energy between our results and those of MCHF and NIST. Lifetimes have also been reported. Radiative atomic data (line strengths, oscillator strengths and radiative decay rates) have been calculated for allowed (E1) transitions. We reported the results for transitions between the ground level and the lowest 43 ones. Comparisons for these allowed transitions have been performed with the calculations of [8]. The averaged difference between the two results was about 25 %, except transitions between the precedent levels which presented a high disagreement in their energies. Radiative decay rates and line strengths for forbidden electric quadrupole (E2), octopole (E3), magnetic dipole (M1) and quadrupole (M2) have been also provided. To the best of our knowledge, no other radiative data for forbidden transitions have been found in the literature, except the M1 transition $3s^2 3p^2 P_{1/2} - 3s^2 3p^2 P_{3/2}^o$ (1-2) where it has been presented by NIST [11]. The agreement for this transition was good (about 2 %). Excitation collision strengths between fine structure levels have been calculated at electron energies 10, 50, 100, 200, 400 and 800 Ry. To our best knowledge, there are no collision strength data in the literature to compare with. We presented collision strengths for transitions from the levels 1 - 5 to the levels 2 - 21. We have used also the UCL codes SST/DW/JAJOM to provide collision strengths, and we have compared with the AS results for some selected transitions. In general, our collision strengths match the infinite energy Born limited except for some dipole electric transitions. We perform a study of collision strength convergence with the total angular momentum J . We showed that the convergence behaviour depends on the transition type, but in general our collision strengths converge even for (E1) transitions and at high electron energies. Effective collision strengths, which are very important in astrophysical applications, have been evaluated for an electron

temperature ranging from 7.2×10^3 to 3.6×10^5 . A detailed comparison has been performed between our results obtained from the code ADASEXJ (using our distorted wave collision strengths) and those of the BPRM method [2]. Several conclusions have been drawn from this comparison: our effective collision strengths are in good agreement with those of the BPRM method for allowed transitions, but for forbidden transitions, the agreement is less. The agreement increases also with the strength of the transition. We hope that our results for allowing and especially for forbidden transitions (missing in the literature) will be helpful for astrophysical and solar plasmas modelling.

Acknowledgements: This work has been supported by the Tunisian Laboratory of Molecular Spectroscopy and Dynamics LR18ES02.

Conflicts of Interest: Declare conflicts of interest or state "The author declares no conflict of interest."

References

- [1] J. M. Munoz Burgos, C. P. Balance, S. D. Loch, R. F. Boivin. Electron-impact excitation of Ar^{2+} . *Astron. Astrophys.* **2009**, 500, 1253-1261. [10.1051/0004-6361/200911743](https://doi.org/10.1051/0004-6361/200911743)
- [2] J. A. Ludlow, C. P. Ballance, S. D. Loch, F. S. Pindzola. Breit-Pauli R-matrix electron-impact excitation calculations along the argon isonuclear sequence. *J. Phys. B: At. Mol. Opt. Phys.* **2010**, 43, 74029. [10.1088/0953-4075/43/7/074029](https://doi.org/10.1088/0953-4075/43/7/074029)
- [3] T. Rauch, M. Ziegler, K. Werner, J. W. Kruk, C. M. Oliveira, D. Vande Putte, R. P. Mignani, F. Kerber. High-resolution FUSE and HST ultraviolet spectroscopy of the white dwarf central star of Sh 2-216. *Astron. Astrophys.* **2007**, 470, 317-329. [10.1051/0004-6361:20077166](https://doi.org/10.1051/0004-6361:20077166)
- [4] L. W. Phillips, W. L. Parker. Spectra of Argon in the Extreme Ultraviolet. *Phys. Rev.* **1941**, 60, 301-307. [10.1103/PhysRev.60.301](https://doi.org/10.1103/PhysRev.60.301)
- [5] M. Raineri *et al.* Revised and extended analysis of five times ionized argon (Ar VI). *Phys. Scr.* **1992**, 45, 584-589. [10.1088/0031-8949/45/6/008](https://doi.org/10.1088/0031-8949/45/6/008)
- [6] M. Raineri, M. Gallardo, F. O. Borges, A. G. Trigueiros, J. Reyna Almandos. Extended analysis of the Al-like argon spectrum. *Phys. Scr.* **2009**, 79, 25302. [10.1088/0031-8949/79/02/025302](https://doi.org/10.1088/0031-8949/79/02/025302)
- [7] G. P. Gupta, A. Z. Msezane. Calculated Energy Levels, Oscillator Strengths and Lifetimes in Al-like Argon. *Phys. Scr.* **2004**, 69, 273. [10.1238/Physica.Regular.069a00273](https://doi.org/10.1238/Physica.Regular.069a00273)
- [8] C. Froese Fischer, G. Tachiev, A. Irimia. Relativistic energy levels, lifetimes, and transition probabilities for the sodium-like to argon-like sequences. *At. Data Nucl. Data Tables.* **2006**, 92, 607-812. [10.1016/j.adt.2006.03.001](https://doi.org/10.1016/j.adt.2006.03.001)
- [9] J. Colgan, H. L. Zhang, C. J. Fontes. Electron-impact excitation and ionization cross sections for the Si, Cl, and Ar isonuclear sequences. *Phys. Rev. A.* **2008**, 77, 62704. [10.1103/PhysRevA.77.062704](https://doi.org/10.1103/PhysRevA.77.062704)
- [10] H. Elabidi. Electron impact excitation for Ar VI. *Journal of Physics: Conference Series.* **2012**, 397, 012055. [10.1088/1742-6596/397/1/012055](https://doi.org/10.1088/1742-6596/397/1/012055)
- [11] A. Kramida, Yu. Ralchenko, J. Reader and NIST ASD Team. NIST Atomic Spectra Database (ver. 5.5.6), [Online]. Available: <https://physics.nist.gov/asd>. National Institute of Standards and Technology, Gaithersburg, MD. **2018**
- [12] N. R. Badnell. On the effects of the two-body non-fine-structure operators of the Breit-Pauli Hamiltonian. *J. Phys. B: At. Mol. Opt. Phys.* **1997**, 30, 1-11. [10.1088/0953-4075/30/1/005](https://doi.org/10.1088/0953-4075/30/1/005)
- [13] N. R. Badnell. A Breit-Pauli distorted wave implementation for AUTOSTRUCTURE. *Comput. Phys. Commun.* **2011**, 182, 1528-1535. [10.1016/j.cpc.2011.03.023](https://doi.org/10.1016/j.cpc.2011.03.023)
- [14] W. Eissner, M. Jones, H. Nussbaumer. Techniques for the calculation of atomic structures and radiative data including relativistic corrections. *Comput. Phys. Commun.* **1974**, 8, 270-306. [10.1016/0010-4655\(74\)90019-8](https://doi.org/10.1016/0010-4655(74)90019-8)
- [15] W. Eissner. The UCL distorted wave code. *Comput. Phys. Commun.* **1998**, 114, 295-341. [10.1016/S0010-4655\(98\)00082-4](https://doi.org/10.1016/S0010-4655(98)00082-4)
- [16] H. E. Saraph. Fine structure cross sections from reactance matrices. *Comput. Phys. Commun.* **1972**, 3, 256-268. [10.1016/0010-4655\(72\)90071-9](https://doi.org/10.1016/0010-4655(72)90071-9)
- [17] H. E. Saraph. Fine structure cross sections from reactance matrices, a more versatile development of the program JAJOM. *Comput. Phys. Commun.* **1978**, 15, 247-258. [10.1016/0010-4655\(78\)90095-4](https://doi.org/10.1016/0010-4655(78)90095-4)

- [18] H. A. Bethe, E. E. Salpeter. Quantum Mechanics of One- and Two-Electron Atoms. Berlin, Göttingen: Springer, 1957
- [19] R. D. Cowan, K. L. Andrew. Coupling Considerations in Two-Electron Spectra. *Journal of the Optical Society of America*. **1965**, 55, 502-516.
- [20] G. Racah. Theory of Complex Spectra. III. *Phys. Rev.* **1943**, 63, 367-333. [10.1103/PhysRev.63.367](https://doi.org/10.1103/PhysRev.63.367)
- [21] A. Burgess, V. B. Sheorey. Electron impact excitation of the resonance lines of alkali-like positive ions. *J. Phys. B: At. Mol. Phys.* **1974**, 7, 2403-2416. [10.1088/0022-3700/7/17/026](https://doi.org/10.1088/0022-3700/7/17/026)
- [22] A. Burgess, D. G. Hummer, J. A. Tully. Electron Impact Excitation of Positive Ions. *Philosophical Transactions of the Royal Society of London Series A*. **1970**, 266, 225-279. [10.1098/rsta.1970.0007](https://doi.org/10.1098/rsta.1970.0007)
- [23] M. C. Chidichimo. S. P. Haigh. Electron-impact excitation of quadrupole-allowed transitions in positive ions. *Phys. Rev. A*. **1989**, 39, 4991-4997. [10.1103/PhysRevA.39.4991](https://doi.org/10.1103/PhysRevA.39.4991)
- [24] M. C. Chidichimo. Electron-impact excitation of electric octupole transitions in positive ions: Asymptotic behavior of the sum over partial-collision strengths. *Phys. Rev. A*. **1992**, 45, 1690-1700. [10.1103/PhysRevA.45.1690](https://doi.org/10.1103/PhysRevA.45.1690)



Energies, and Transition Rates in Ga-like ions (Sn XX - I XXIII)

S. M. Attia^{a,b}

^a Physics Department, Faculty of Science, Kafrelsheikh University, Kafr El-Sheikh, Egypt.

^b Physics Department, Faculty of Applied Science, Umm Al-Qura University, Makkah, Saudi Arabia.

ARTICLE INFO

Article History:

Submission date: 04/11/2019

Accepted date: 16/11/2020

Keywords:

Energy Levels; Transition Probabilities; Oscillator Strengths; Line Strengths; Ga-Like Ions.

ABSTRACT

Energy levels, wavelengths, transition probabilities, oscillator strengths, and line strengths were calculated for electric dipole $4s^24p - 4s4p^2$, $4s^24p - 4s^24d$, and $4s4p^2 - 4p^3$ transitions of Gallium-like ions, Sn XX, Sb XXI, Te XXII, and I XXIII. The fully relativistic multiconfiguration Dirac-Fock method, taking into account both correlations within the $n = 4$ complex and the quantum electrodynamic effects, have been used in the calculations. The results were compared with the available experimental and other theoretical results.

1. Introduction

The spectra of highly ionized ions have a great interest in many fields of physics, such as plasma physics, astrophysics, and laser physics. The atomic data of Ga-like ions have been observed and calculated [1-30].

On the experimental side, the spectrum of Sn XX has been observed, and the spectral lines of $4s^24p - 4s^2ns$ and $4s^24p - 4s^2nd$ ($n=5-7$) have been reported by Khan [2]. Fournier *et al.* [11] measured the wavelengths for some transitions belonging to $4s^24p-4s4p^2$, and $4s^24p-4s4d^2$ transitions in the tokamak and the laser-produced plasma for Pr XXIX, Eu XXXIII, Gd XXXIV, Dy XXXVI, and Yb XL ions. The wavelengths of Xe XXIV have been observed in the extreme ultraviolet (EUV) wavelength range at the Berlin Electron Beam Ion Trap facility by Biedermann *et al.* [13], and the experimental wavelengths were compared with the HULLAC code results.

On the theoretical side, for Ga-like ions with $Z \leq 92$, the theoretical energy level values of $4s^24p \ ^2P_{3/2}^o$ state have been calculated using semiempirical (SE) and Dirac-Fock (DF) methods by Curtis [7], using the multiconfiguration Dirac Fock (MCDF) method by Ali [12], and using the relativistic many-body perturbation theory by Safronova *et al.* [15]. For I XXIII, the energy levels of $4s^24p \ ^2P_{3/2}^o$, $4s4p^2$ ($^4P^e$, $^2D^e$, $^2P^e$, $^2S^e$) terms have been calculated using the GRASP2K program [20], and wavelengths results were reported [20-21].

The atomic data for some ions in Ga-like ions, Ge II-Rb VII [22], Pt XLVIII [24], W XLIV [25, 30], Ag XVII [26], Xe XXIV-Pr XXIX [27], Nd XXX-Tb XXXV [28], Kr VI-Xe XXIV [29] are presented.

In this paper, the energy levels, wavelengths, transition probabilities, oscillator strengths, and line strengths of electric dipole (E1) transitions among the fine-structure levels of terms belonging to the $4s^24p$, $4s4p^2$, $4s^24d$, and $4p^3$ configurations are calculated for Ga-like ions from Sn XX to I XXIII, and the calculations have been performed using the multiconfiguration Dirac-Fock (MCDF) method.

2. Calculations

The present calculations were performed using the multiconfiguration Dirac-Fock (MCDF) method with the multiconfiguration Dirac-Fock and General Matrix Elements (MCDFGME) program [31]. This program is used to calculate a number of atomic quantities, such as energy levels, transition rates, photoionization cross sections, and hyperfine structure constants, taking into account the relativistic Breit-interactions (BI) and quantum

electrodynamics (QED), vacuum polarization and self-energy, contributions.

The wavelengths, transition probabilities, oscillator strengths, and line strengths for the $4s^24p - 4s4p^2$, $4s^24p - 4s^24d$, and $4s4p^2 - 4p^3$ electric dipole transitions were calculated for Sn XX, Sb XXI, Te XXII, and I XXIII, using MCDF method.

Most odd and even configurations with the $n = 4$ complex were included in the calculations. These configurations are $4s^24p$, $4p^3$, $4s4p4d$, $4p4d^2$, $4s^24f$, $4s4d4f$, $4p^24f$, $4d^24f$ and $4s4p^2$, $4s^24d$, $4s4d^2$, $4p^24d$, $4s4p4f$, $4p4d4f$, $4d^3$ for odd and even parities, respectively.

3. Results and Discussion

3.1. Energy Levels

The MCDF energy level values for the $4s^24p$, $4s4p^2$, $4s^24d$, and $4p^3$ configurations for Ga-like Sn XX – I XXIII were listed in Table 1, where each level was presented in both the *LS*-coupling and the *jj*-coupling schemes.

Table 1: MCDF energy levels (in cm^{-1}) for the $4s^24p$, $4s4p^2$, $4s^24d$, and $4p^3$ configurations for Ga-like ions with $Z=50-53$.

Index	Configuration	LSJ	JJ	Sn XX	Sb XXI	Te XXII	I XXIII
1	$4s^2 4p$	$^2P_{1/2}^o$	$4s^2 4p^*$	0	0	0	0
2	$4s^2 4p$	$^2P_{3/2}^o$	$4s^2 4p$	87,825	98,964	111,108	124,317
3	$4s 4p^2$	$^4P_{1/2}^e$	$4s4p^*2$	328,307	345,892	363,650	381,582
4	$4s 4p^2$	$^4P_{3/2}^e$	$4s4p^*4p$	380,110	405,793	432,600	460,607
5	$4s 4p^2$	$^4P_{5/2}^e$	$4s4p^*4p$	408,975	436,685	465,494	495,475
6	$4s 4p^2$	$^2D_{3/2}^e$	$4s4p^*4p$	462,433	492,964	522,242	553,917
7	$4s 4p^2$	$^2D_{5/2}^e$	$4s4p^*4p$	502,390	531,108	560,893	591,833
8	$4s 4p^2$	$^2D_{7/2}^e$	$4s4p^2$	499,093	536,554	574,184	615,028
9	$4s 4p^2$	$^2S_{1/2}^e$	$4s4p^2$	588,891	628,751	670,702	714,889
10	$4s 4p^2$	$^2P_{3/2}^e$	$4s4p^2$	598,757	638,581	680,406	724,359
11	$4s^2 4d$	$^2D_{3/2}^e$	$4s^2 4d^*$	720,294	760,253	801,254	843,393
12	$4s^2 4d$	$^2D_{5/2}^e$	$4s^2 4d$	735,274	777,267	820,471	864,976
13	$4p^3$	$^4S_{3/2}^o$	$4p^*24p$	842,694	889,465	937,391	986,571
14	$4p^3$	$^2D_{3/2}^o$	$4p^*4p^2$	910,964	968,029	998,140	1,057,713
15	$4p^3$	$^2D_{5/2}^o$	$4p^*4p^2$	888,669	992,478	1,001,399	1,061,050
16	$4p^3$	$^2P_{1/2}^o$	$4p^*4p^2$	945,434	1,025,953	1,062,679	1,124,782
17	$4p^3$	$^2P_{3/2}^o$	$4p^3$	1,001,697	1,103,932	1,136,270	1,222,964

It showed that the present MCDF energy levels were in an excellent agreement with the other theoretical results, where the agreement was within $\sim 0.07\%$ with DF [7] results, and was within 0.6% with [7, 12, 15] results (Table 2).

* Corresponding Author

Physics Department, Faculty of Applied Science, Umm Al-Qura University, Makkah, Saudi Arabia.

E-mail address: saidattia2004@yahoo.com (S. M. Attia).

1685-4732 / 1685-4740 © 2020 UQU All rights reserved.

Table 2. Comparison between MCDF and other theoretical $4s^24p^2P_{3/2}$ in Ga-like ions with $Z=50-53$.

Ion	MCDF	SE [7]	DF [7]	[12]	RMBPT [15]
Sn XX	87,825	88,356	87,850	88,411	88,357
Sb XXI	98,964	99,492	99,007	99,593	99,545
Te XXII	111,108	111,614	111,169	111,779	111,738
I XXIII	124,317	124,783	124,396	125,030	124,999

3.2. Wavelengths, Transition Probabilities, and Oscillator Strengths

Tables 3 and 4 present wavelengths λ (in Å), transition probabilities A in length gauge (in sec^{-1}), oscillator strengths f (dimensionless), and line strengths S (in a. u.) for electric dipole $4s^24p - 4s4p^2$, $4s^24p - 4s^24d$, and $4s4p^2 - 4p^3$ transitions for Sn XX, Sb XXI, Te XXII, and I XXIII.

For strong transitions ($f \geq 0.01$), the difference between transition probabilities in the Babushkin (length) and the Coulomb (velocity) gauges is within ~10%, except for $4s4p^2-4p^3$ ($^2D_{3/2}^o - ^4S_{3/2}^o$, $^2P_{1/2}^e - ^2P_{3/2}^o$, and $^2P_{1/2}^e - ^4S_{3/2}^o$) transitions for all ions, and for Sn XX, and Sb XXI, there are several transitions have difference greater than 25%,

Table 3: MCDF wavelengths λ (in Å), transition probabilities A (in sec^{-1}), oscillator strengths f , and line strengths S (in a. u.) for Sn XX, and Sb XXI.

Configuration	i	j	Sn XX				Sb XXI			
			λ	A	f	S	λ	A	f	S
4s24p - 4s4p2	2P1/2o	4P1/2e	306.42	1.66E+09	2.34E-02	4.72E-02	290.93	2.07E+09	2.63E-02	5.04E-02
	2P1/2o	4P3/2e	264.41	3.70E+07	7.76E-04	1.35E-03	247.73	4.71E+07	8.67E-04	1.41E-03
	2P1/2o	2D3/2e	217.11	2.08E+10	2.94E-01	4.20E-01	203.69	2.39E+10	2.97E-01	3.98E-01
	2P1/2o	2P1/2e	199.83	8.15E+10	4.88E-01	6.42E-01	189.06	8.99E+10	4.82E-01	6.00E-01
	2P1/2o	2S1/2e	170.36	6.15E+09	2.68E-02	3.00E-02	159.58	5.99E+09	2.29E-02	2.40E-02
	2P1/2o	2P3/2e	167.54	2.13E+10	1.79E-01	1.97E-01	157.11	2.40E+10	1.77E-01	1.84E-01
	2P3/2o	4P1/2e	419.32	9.09E+07	1.20E-03	6.62E-03	408.63	9.38E+07	1.17E-03	6.32E-03
	2P3/2o	4P3/2e	344.44	1.85E+08	3.29E-03	1.49E-02	328.23	2.21E+08	3.56E-03	1.54E-02
	2P3/2o	4P5/2e	313.27	1.45E+09	3.20E-02	1.32E-01	297.99	1.74E+09	3.48E-02	1.37E-01
	2P3/2o	2D3/2e	268.29	6.03E+08	6.50E-03	2.30E-02	255.15	9.01E+08	8.79E-03	2.95E-02
	2P3/2o	2P1/2e	242.39	2.77E+09	1.22E-02	3.89E-02	232.60	3.39E+09	1.37E-02	4.21E-02
	2P3/2o	2D5/2e	244.24	7.01E+09	9.41E-02	3.03E-01	229.59	7.45E+09	8.83E-02	2.67E-01
4s24p - 4s24d	2P3/2o	2S1/2e	200.35	5.99E+10	1.80E-01	4.75E-01	189.52	6.53E+10	1.76E-01	4.39E-01
	2P3/2o	2P3/2e	196.46	9.56E+10	5.53E-01	1.43E+00	186.05	1.04E+11	5.40E-01	1.32E+00
	2P3/2o	2D3/2e	138.87	1.61E+11	9.33E-01	8.53E-01	131.57	1.75E+11	9.09E-01	7.88E-01
4s4p2 - 4p3	2P3/2o	2D3/2e	158.17	3.48E+10	1.31E-01	2.72E-01	151.28	3.88E+10	1.33E-01	2.65E-01
	2P3/2o	2D5/2e	154.49	1.52E+11	8.16E-01	1.66E+00	147.47	1.63E+11	7.96E-01	1.55E+00
	4P1/2e	4S3/2o	195.16	2.42E+10	2.76E-01	3.55E-01	184.71	2.72E+10	2.78E-01	3.38E-01
	4P1/2e	2D3/2o	172.2	2.11E+09	1.88E-02	2.13E-02	161.30	2.31E+09	1.80E-02	1.91E-02
	4P1/2e	2P1/2o	162.51	4.79E+08	1.90E-03	2.03E-03	147.51	1.33E+09	4.35E-03	4.22E-03
	4P1/2e	2P3/2o	148.84	4.39E+09	2.92E-02	2.86E-02	132.28	3.53E+07	1.85E-04	1.61E-04
	4P3/2e	4S3/2o	217.13	1.66E+10	1.18E-01	3.36E-01	207.71	1.66E+10	1.07E-01	2.93E-01
	4P3/2e	2D3/2o	189.09	2.44E+10	1.31E-01	3.26E-01	178.56	2.87E+10	1.37E-01	3.23E-01
	4P3/2e	2D5/2o	197.27	8.37E+07	7.33E-04	1.90E-03	171.09	1.96E+08	1.29E-03	2.91E-03
	4P3/2e	2P1/2o	177.46	5.40E+08	1.27E-03	2.98E-03	161.82	4.24E+08	8.32E-04	1.77E-03
	4P3/2e	2P3/2o	161.29	2.82E+09	1.10E-02	2.33E-02	143.68	9.13E+08	2.82E-03	5.34E-03
	4P5/2e	4S3/2o	231.66	3.17E+10	1.70E-01	7.78E-01	221.97	3.32E+10	1.63E-01	7.16E-01
	4P5/2e	2D3/2o	200.01	5.20E+09	2.08E-02	8.21E-02	188.99	5.73E+09	2.04E-02	7.63E-02
	4P5/2e	2D5/2o	209.19	6.79E+09	4.45E-02	1.84E-01	180.65	2.11E+10	1.03E-01	3.68E-01
	4P5/2e	2P3/2o	169.17	9.41E+07	2.69E-04	8.99E-04	150.35	3.56E+08	8.04E-04	2.39E-03
	2D3/2e	4S3/2o	264.44	4.23E+09	4.44E-02	1.55E-01	253.70	4.89E+09	4.72E-02	1.58E-01
	2D3/2e	2D3/2o	223.99	1.24E+10	9.29E-02	2.74E-01	211.52	1.29E+10	8.67E-02	2.41E-01
	2D3/2e	2D5/2o	235.57	4.22E+09	5.26E-02	1.63E-01	201.12	1.83E+10	1.66E-01	4.40E-01
	2D3/2e	2P1/2o	207.85	4.37E+10	1.42E-01	3.88E-01	188.42	5.60E+10	1.49E-01	3.70E-01
	2D3/2e	2P3/2o	186.02	5.68E+09	2.95E-02	7.21E-02	164.27	1.24E+10	5.03E-02	1.09E-01
	2D5/2e	4S3/2o	292.86	5.60E+07	4.80E-04	2.78E-03	285.27	7.51E+07	6.11E-04	3.44E-03
	2D5/2e	2D3/2o	244.05	1.46E+10	8.68E-02	4.18E-01	233.03	1.60E+10	8.70E-02	4.01E-01
	2D5/2e	2D5/2o	257.86	1.10E+10	1.09E-01	5.57E-01	220.46	2.64E+10	1.92E-01	8.37E-01
	2D5/2e	2P3/2o	199.64	2.44E+10	9.71E-02	3.83E-01	176.96	2.16E+10	6.75E-02	2.36E-01
	2P1/2e	4S3/2o	295.57	5.47E+09	1.43E-01	2.79E-01	280.77	6.40E+09	1.51E-01	2.80E-01
	2P1/2e	2D3/2o	245.93	2.41E+10	4.38E-01	7.08E-01	230.01	2.74E+10	4.34E-01	6.57E-01
	2P1/2e	2P1/2o	226.61	3.30E+09	2.54E-02	3.79E-02	202.96	8.42E+09	5.20E-02	6.95E-02
	2P1/2e	2P3/2o	200.9	4.83E+09	5.84E-02	7.73E-02	175.21	3.01E+09	2.77E-02	3.20E-02
	2S1/2e	4S3/2o	397.2	1.66E+08	7.84E-03	2.05E-02	386.91	1.57E+08	7.06E-03	1.80E-02
	2S1/2e	2D3/2o	312.44	1.12E+09	3.28E-02	6.76E-02	296.69	1.01E+09	2.66E-02	5.19E-02
2S1/2e	2P1/2o	281.91	1.29E+10	1.53E-01	2.85E-01	253.16	2.79E+10	2.68E-01	4.48E-01	
2S1/2e	2P3/2o	243.19	3.00E+09	5.33E-02	8.53E-02	211.40	1.41E+10	1.90E-01	2.64E-01	
2P3/2e	4S3/2o	413.42	3.11E+08	7.97E-03	4.34E-02	402.24	3.09E+08	7.49E-03	3.97E-02	
2P3/2e	2D3/2o	322.39	4.72E+08	7.35E-03	3.12E-02	305.62	5.25E+08	7.35E-03	2.96E-02	
2P3/2e	2D5/2o	346.94	3.55E+09	9.61E-02	9.61E-02	284.37	1.53E+10	2.78E-01	1.04E+00	
2P3/2e	2P1/2o	289.99	8.76E+08	5.52E-03	5.52E-03	259.63	3.33E+09	1.68E-02	5.76E-02	
2P3/2e	2P3/2o	249.18	1.76E+10	1.64E-01	5.36E-01	215.90	5.94E+10	4.15E-01	1.18E+00	

these transitions are $4s4p^2-4p^3$ ($^4P_{1/2}^e - ^2D_{3/2}^o$, $^2P_{1/2}^e - ^2D_{3/2}^o$, $^2P_{3/2}^e - ^2D_{5/2}^o$, and $^2S_{1/2}^e - ^2D_{3/2}^o$).

Table A presents comparison between the present MCDF wavelengths with the available experimental and other theoretical results for I XXIII [20, 21].

Table A: Comparison between MCDF, experimental, and other theoretical wavelengths (in Å) of I XXIII ion.

Index	Transition	MCDF	Experimental [20]	GRASP2K [21]
1	$4s^24p^2P_{1/2}^o - 4s4p^2^4P_{1/2}^e$	263.89	267.7 ± 0.10	264.1
2	$4s^24p^2P_{3/2}^o - 4s4p^2^4P_{3/2}^e$	271.33	270.0 ± 0.10	271.8
3	$4s^24p^2P_{3/2}^o - 4s4p^2^4P_{3/2}^e$	299.70	296.3 ± 0.15	299.4

A comparison showed that the present MCDF wavelengths were in an excellent agreement with the available theoretical [21] and experimental [20] results, where the agreement was within ~ 1% -1.4 %.

Table 4: MCDF wavelengths λ (in Å), transition probabilities A (in sec⁻¹), oscillator strengths f , and line strengths S (in a. u.) for Te XXII, and I XXIII.

Configuration	i	j	Te XXII				I XXIII			
			λ	A	f	S	λ	A	f	S
4s ² 4p - 4s4p ²	² P _{1/2} ^o	⁴ P _{1/2} ^e	276.81	2.55E+09	2.93E-02	5.34E-02	263.89	3.10E+09	3.24E-02	5.63E-02
	² P _{1/2} ^o	⁴ P _{3/2} ^e	232.42	5.94E+07	9.62E-04	1.47E-03	218.33	7.43E+07	1.06E-03	1.53E-03
	² P _{1/2} ^o	² D _{3/2} ^e	192.31	2.76E+10	3.06E-01	3.87E-01	181.35	3.16E+10	3.12E-01	3.72E-01
	² P _{1/2} ^o	² P _{1/2} ^e	179.05	9.89E+10	4.75E-01	5.60E-01	169.72	1.09E+11	4.69E-01	5.24E-01
	² P _{1/2} ^o	² S _{1/2} ^e	149.62	5.86E+09	1.97E-02	1.94E-02	140.39	5.74E+09	1.69E-02	1.57E-02
	² P _{1/2} ^o	² P _{3/2} ^e	147.47	2.72E+10	1.78E-01	1.72E-01	138.53	3.12E+10	1.80E-01	1.64E-01
	² P _{3/2} ^o	⁴ P _{1/2} ^e	399.83	9.50E+07	1.14E-03	5.99E-03	392.78	9.44E+07	1.09E-03	5.65E-03
	² P _{3/2} ^o	⁴ P _{3/2} ^e	313.38	2.61E+08	3.84E-03	1.58E-02	299.70	3.05E+08	4.11E-03	1.62E-02
	² P _{3/2} ^o	⁴ P _{5/2} ^e	284.07	2.06E+09	3.75E-02	1.40E-01	271.33	2.41E+09	3.99E-02	1.43E-01
	² P _{3/2} ^o	² D _{3/2} ^e	244.59	1.13E+09	1.01E-02	3.27E-02	234.15	1.47E+09	1.21E-02	3.73E-02
	² P _{3/2} ^o	² P _{1/2} ^e	223.54	4.06E+09	1.52E-02	4.47E-02	215.13	4.78E+09	1.66E-02	4.69E-02
	² P _{3/2} ^o	² D _{5/2} ^e	217.00	8.02E+09	8.50E-02	2.43E-01	204.82	8.53E+09	8.05E-02	2.17E-01
4s ² 4p - 4s ² 4d	² P _{3/2} ^o	² S _{1/2} ^e	179.46	7.12E+10	1.72E-01	4.06E-01	170.08	7.76E+10	1.68E-01	3.77E-01
	² P _{3/2} ^o	² P _{3/2} ^e	176.38	1.13E+11	5.26E-01	1.22E+00	167.37	1.22E+11	5.12E-01	1.13E+00
	² P _{1/2} ^o	² D _{3/2} ^e	124.84	1.90E+11	8.86E-01	7.28E-01	118.61	2.04E+11	8.63E-01	6.74E-01
4s4p ² - 4p ³	² P _{3/2} ^o	² D _{3/2} ^e	144.96	4.33E+10	1.36E-01	2.61E-01	139.13	4.87E+10	1.41E-01	2.59E-01
	² P _{3/2} ^o	² D _{5/2} ^e	141.01	1.74E+11	7.78E-01	1.44E+00	135.06	1.86E+11	7.61E-01	1.35E+00
	⁴ P _{1/2} ^e	⁴ S _{3/2} ^o	175.03	3.06E+10	2.81E-01	3.24E-01	166.02	3.45E+10	2.85E-01	3.12E-01
	⁴ P _{1/2} ^e	² D _{3/2} ^o	158.15	1.34E+10	1.01E-01	1.05E-01	148.42	1.50E+10	9.90E-02	9.68E-02
	⁴ P _{1/2} ^e	² P _{1/2} ^o	143.50	5.71E+08	1.76E-03	1.67E-03	134.99	6.05E+08	1.65E-03	1.47E-03
	⁴ P _{1/2} ^e	² P _{3/2} ^o	129.72	2.02E+10	1.02E-01	8.70E-02	119.05	5.46E+10	2.32E-01	1.82E-01
	⁴ P _{3/2} ^e	⁴ S _{3/2} ^o	199.07	1.65E+10	9.82E-02	2.58E-01	191.11	1.65E+10	9.03E-02	2.27E-01
	⁴ P _{3/2} ^e	² D _{3/2} ^o	177.52	3.50E+10	1.66E-01	3.87E-01	168.16	3.88E+10	1.64E-01	3.64E-01
	⁴ P _{3/2} ^e	² D _{5/2} ^o	176.43	1.32E+08	9.23E-04	1.15E-03	167.15	1.64E+08	1.03E-03	2.27E-03
	⁴ P _{3/2} ^e	² P _{1/2} ^o	159.27	7.82E+08	1.49E-03	3.12E-03	151.12	9.32E+08	1.60E-03	3.18E-03
	⁴ P _{3/2} ^e	² P _{3/2} ^o	142.47	1.24E+09	3.78E-03	7.09E-03	131.42	3.03E+10	7.85E-02	1.36E-01
	⁴ P _{5/2} ^e	⁴ S _{3/2} ^o	213.03	3.46E+10	1.57E-01	6.61E-01	204.77	3.62E+10	1.52E-01	6.13E-01
	⁴ P _{5/2} ^e	² D _{3/2} ^o	188.53	1.77E+10	6.27E-02	2.34E-01	178.64	1.86E+10	5.94E-02	2.09E-01
	⁴ P _{5/2} ^e	² D _{5/2} ^o	187.31	9.62E+09	5.06E-02	1.87E-01	177.50	1.12E+10	5.27E-02	1.85E-01
	⁴ P _{5/2} ^e	² P _{3/2} ^o	149.48	8.17E+07	1.82E-04	5.39E-04	137.74	1.76E+09	3.34E-03	9.09E-03
	² D _{3/2} ^e	⁴ S _{3/2} ^o	242.37	5.72E+09	5.04E-02	1.61E-01	232.64	6.49E+09	5.27E-02	1.61E-01
	² D _{3/2} ^e	² D _{3/2} ^o	211.15	3.63E+09	2.43E-02	6.75E-02	199.49	3.68E+09	2.19E-02	5.76E-02
	² D _{3/2} ^e	² D _{5/2} ^o	209.61	5.56E+09	5.49E-02	1.52E-01	198.08	6.28E+09	5.54E-02	1.44E-01
	² D _{3/2} ^e	² P _{1/2} ^o	185.83	5.44E+10	1.41E-01	3.44E-01	175.96	6.05E+10	1.40E-01	3.25E-01
	² D _{3/2} ^e	² P _{3/2} ^o	163.36	3.33E+09	1.33E-02	2.87E-02	149.81	1.61E+10	5.41E-02	1.07E-01
	² D _{5/2} ^e	⁴ S _{3/2} ^o	277.31	6.06E+07	4.66E-04	2.55E-03	271.23	5.91E+07	4.34E-04	2.33E-03
	² D _{5/2} ^e	² D _{3/2} ^o	237.19	9.60E+09	5.40E-02	2.53E-01	227.21	1.07E+10	5.50E-02	2.47E-01
	² D _{5/2} ^e	² D _{5/2} ^o	235.25	1.18E+10	9.80E-02	4.56E-01	225.38	1.21E+10	9.25E-02	4.12E-01
	² D _{5/2} ^e	² P _{3/2} ^o	178.52	2.73E+10	8.70E-02	3.07E-01	164.92	2.51E+10	6.82E-02	2.22E-01
	² P _{1/2} ^o	⁴ S _{3/2} ^o	267.32	7.34E+09	1.57E-01	2.77E-01	255.05	8.27E+09	1.61E-01	2.71E-01
	² P _{1/2} ^o	² D _{3/2} ^o	229.84	6.04E+09	9.57E-02	1.45E-01	215.74	6.94E+09	9.68E-02	1.37E-01
	² P _{1/2} ^o	² P _{1/2} ^o	200.15	5.17E+09	3.10E-02	4.09E-02	188.48	6.33E+09	3.37E-02	4.18E-02
	² P _{1/2} ^o	² P _{3/2} ^o	174.32	6.58E+09	5.99E-02	6.88E-02	158.79	8.04E+08	6.08E-03	6.35E-03
	² S _{1/2} ^e	⁴ S _{3/2} ^o	378.50	1.46E+08	6.28E-03	1.57E-02	371.81	1.34E+08	5.53E-03	1.36E-02
	² S _{1/2} ^e	² D _{3/2} ^o	307.50	1.87E+08	5.29E-03	1.07E-02	293.79	1.69E+08	4.38E-03	8.46E-03
	² S _{1/2} ^e	² P _{1/2} ^o	256.58	1.47E+10	1.46E-01	2.46E-01	245.44	1.57E+10	1.42E-01	2.29E-01
	² S _{1/2} ^e	² P _{3/2} ^o	215.62	3.63E+09	5.05E-02	7.18E-02	197.39	2.58E+09	3.01E-02	3.91E-02
	² P _{3/2} ^o	⁴ S _{3/2} ^o	392.98	3.01E+08	6.98E-03	3.61E-02	385.45	2.90E+08	6.46E-03	3.28E-02
	² P _{3/2} ^o	² D _{3/2} ^o	316.98	8.14E+08	1.23E-02	5.12E-02	302.24	8.96E+08	1.23E-02	4.88E-02
	² P _{3/2} ^o	² D _{5/2} ^o	313.53	4.09E+09	9.03E-02	3.73E-01	299.01	4.35E+09	8.74E-02	3.44E-01
	² P _{3/2} ^o	² P _{1/2} ^o	263.15	7.88E+08	4.09E-03	1.42E-02	251.31	7.38E+08	3.49E-03	1.16E-02
² P _{3/2} ^o	² P _{3/2} ^o	220.25	1.94E+10	1.41E-01	4.09E-01	201.17	1.85E+10	1.12E-01	2.97E-01	

4. Conclusions

In the present work, the energy levels, wavelengths, transition probabilities, oscillator strengths, and line strengths for electric dipole (E1) 4s²4p - 4s4p², 4s²4p - 4s²4d, and 4s4p² - 4p³ transitions for Sn XX, Sb XXI, Te XXII, and I XXIII were calculated using the multiconfiguration Dirac-Fock (MCDF) method. The correlations within the n=4 complex and the quantum electrodynamic (QED) effects were taken into account in the calculations. The calculated MCDF energy levels and wavelengths were compared with the available experimental and other theoretical results, and the comparison showed an excellent agreement.

References

[1] E. Alexander, M. Even-Zohar, B. S. Fraenkel, S. Goldsmith. Classification of Transitions in the EUV Spectra of Y IX–XIII, Zr X–XIV, Nb XI–XV, and Mo XII–XVI. *J. Opt. Soc. Am.*, **1971**, 61, 508-514. <https://doi.org/10.1364/JOSA.61.000508>

[2] M. A. Khan. Spectra of Sn xx–Sn xxii in the extreme ultraviolet. *J. Opt. Soc. Am.*, **1982**, 72, 268-272. <https://doi.org/10.1364/JOSA.72.000268>

[3] J. Migdalek. Relativistic Hartree-Fock energies and oscillator strengths for some ions with ns²np (n=4-6) ground-state configuration. *J. Quant. Spectrosc. Radiat. Transf.*, **1983**, 30, 169-174. [https://doi.org/10.1016/0022-4073\(83\)90098-5](https://doi.org/10.1016/0022-4073(83)90098-5)

[4] L. J. Curtis, J. Reader, S. Goldsmith, B. Denne, and E. Hinnov. 4s²4p ²P intervals in the Ga isoelectronic sequence from Rb⁶⁺ to In¹⁸⁺. *Phys. Rev. A*, **1984**, 29, 2248-2250. <https://doi.org/10.1103/PhysRevA.29.2248>

[5] J. Reader, N. Acquista, and S. Goldsmith. 4s²4p–4s4p² and 4s²4p–4s²5s transitions of galliumlike ions from Rb VII to In XIX. *J. Opt. Soc. Am. B*, **1986**, 3, 874-878. <https://doi.org/10.1364/JOSAB.3.000874>

[6] E. Biémont, and J. E. Hansen. Calculations of transition probabilities for forbidden lines in 3pN and 4pN configurations. *Nucl. Instrum. Methods Phys. Res. B*, **1987**, 23, 274-277. [https://doi.org/10.1016/0168-583X\(87\)90460-5](https://doi.org/10.1016/0168-583X(87)90460-5)

[7] L. J. Curtis. Fine-structure intervals for the lowest P terms in the Cu, Zn, Ga, and Br isoelectronic sequences for Z≤92. *Phys. Rev. A*, **1987**, 35, 2089-2094. <https://doi.org/10.1103/PhysRevA.35.2089>

- [8] C. Breton, C. DeMichelis, W. Hecq, M. Mattioli, J. Ramette, B. Saoutic, C. Bauche-Arnoult, J. Bauche, and J. F. Wyart. Highly ionized xenon spectra (95-260 Å) excited in TFR tokamak plasmas. *Phys. Scripta*, **1988**, 37, 33-37. <https://doi.org/10.1088/0031-8949/37/1/004>
- [9] E. Biémont, and P. Quinet. Energy levels and oscillator strengths for gallium-like ions (Br V-In XIX). *J. Quant. Spectrosc. Radiat. Transf.*, **1990**, 44, 233-244. [https://doi.org/10.1016/0022-4073\(90\)90029-6](https://doi.org/10.1016/0022-4073(90)90029-6)
- [10] U. Litzén, and X. Zeng. The 4s24p-4s4p2 transition array and energy levels of the Ga-like ions Ru XIV-In XIX. *Phys. Scripta*, **1991**, 43, 262-265. <https://doi.org/10.1088/0031-8949/43/3/008>
- [11] K. B. Fournier, W. H. Goldstein, A. Osterheld, M. Finkenthal, S. Lippmann, L. K. Huang, H. W. Moos, and N. Spector. Soft x-ray emission of galliumlike rare-earth atoms produced by high-temperature low-density tokamak and high-density laser plasmas. *Phys. Rev. A*, **1994**, 50, 2248-2256. <https://doi.org/10.1103/PhysRevA.50.2248>
- [12] M. A. Ali. Fine-structure splitting and magnetic dipole and electric quadrupole transition probabilities between the ground levels of Ga-like ions. *Phys. Scripta*, **1997**, 55, 159-166. <https://doi.org/10.1088/0031-8949/55/2/007>
- [13] C. Biedermann, R. Radtke, G. Fußmann, J. L. Schwob, and P. Mandelbaum. EUV spectroscopy of highly charged xenon ions. *Nucl. Instrum. Methods Phys. Res. B*, **2005**, 235, 126-130. <https://doi.org/10.1016/j.nimb.2005.03.158>
- [14] M. J. May, P. Beiersdorfer, N. Jordan, J. H. Scofield, K. J. Reed, S. B. Hansen, K. B. Fournier, M. F. Gu, G. V. Brown, F. S. Porter, R. Kelley, C. A. Kilbourne, and K. R. Boyce. Measurement of electron impact collisional excitation cross sections of Ni to Ga-Like Gold. *Nucl. Instrum. Methods Phys. Res. B*, **2005**, 235, 231-234. <https://doi.org/10.1016/j.nimb.2005.03.179>
- [15] U. I. Safronova, T. E. Cowan, and M. S. Safronova. Relativistic many-body calculations of energies, E2, and M1 transition rates of 4s²4p states in Ga-like ions. *Phys. Lett. A*, **2006**, 348, 293-298. <https://doi.org/10.1016/j.physleta.2005.08.056>
- [16] P. Quinet, É. Biémont, P. Palmeri, and E. Träbert. Multiconfiguration Dirac-Fock wavelengths and transition rates in the X-ray spectra of highly charged Ga-like ions from Yb³⁹⁺ to U⁶¹⁺. *Atomic Data and Nuclear Data Tables*, **2007**, 93, 167-182. <https://doi.org/10.1016/j.adt.2006.09.001>
- [17] J. Zeng, G. Zhao, and J. Yuan. Electron impact collision strengths and oscillator strengths for Ge-, Ga-, Zn-, Cu-, Ni-, and Co-like Au ions. *Atomic Data and Nuclear Data Tables*, **2007**, 93, 199-273. <https://doi.org/10.1016/j.adt.2006.10.002>
- [18] P. Mandelbaum, and J. L. Schwob. Excitation-autoionization cross sections and rate coefficients for Ga-like ions. *Eur. Phys. J. D*, **2008**, 49, 173-184. <https://doi.org/10.1140/epjd/e2008-00159-2>
- [19] E. Charro, Z. Curiel, and I. Martin. Spontaneous radiative decay rates in Ga-like ions. *Inter. J. Quantum Chem.*, **2008**, 108, 744-753. <https://doi.org/10.1002/qua.21552>
- [20] E. Träbert. EUV beam-foil observations of Cu-like ions through Ge-like ions of iodine. *Phys. Scripta*, **2011**, T144, 014004. <https://doi.org/10.1088/0031-8949/2011/T144/014004>
- [21] J. Li, E. Träbert, and C. Dong. Energy levels, transition rates and lifetimes for low-lying levels in Cu-, Zn-, Ga- and Ge-like ions of iodine. *Phys. Scripta*, **2011**, 83, 015301. <https://doi.org/10.1088/0031-8949/83/01/015301>
- [22] F. Hu, J. Yang, C. Wang, L. Jing, S. Chen, G. Jiang, H. Liu, and L. Hao. Multiconfiguration Dirac-Fock calculations on multi-valence-electron systems: Benchmarks on Ga-like ions. *Phys. Rev. A*, **2011**, 84, 042506. <https://doi.org/10.1103/PhysRevA.84.042506>
- [23] Fan Jian-Zhong, Zhang Deng-Hong, Chang Zhi-Wei, Shi Ying-Long, and Dong Chen-Zhong. Energy-Crossing and Its Effect on Lifetime of the 4s²4p ²P_{3/2} Level for Highly Charged Ga-Like Ions. *Chinese Phys. Lett.*, **2012**, 29, 073102. <http://doi.org/10.1088/0256-307X/29/7/073102>
- [24] J. A. Santana, Y. Ishikawa, and E. Träbert. Relativistic MR-MP calculations of the energy levels and transition probabilities in Ni- to Kr-like Pt ions. *Atomic Data and Nuclear Data Tables*, **2014**, 100, 183-271. <https://doi.org/10.1016/j.adt.2013.05.001>
- [25] J. Clementson, P. Beiersdorfer, T. Brage, M. F. Gu. Atomic data and theoretical X-ray spectra of Ge-like through V-like W ions. *Atomic Data and Nuclear Data Tables*, **2014**, 100, 577-649. <https://doi.org/10.1016/j.adt.2013.07.002>
- [26] F. Hu, M. Mei, C. Han, B. Han, G. Jiang, J. Yang. Correlation effects for nl-n'l' transitions in nine isoelectronic sequences of silver ions. *J. Quant. Spectrosc. Radiat. Transf.*, **2014**, 133, 319-328. <https://doi.org/10.1016/j.jqsrt.2013.08.017>
- [27] F. El-Sayed. Energy Levels and Transition Rates for Ga-Like Ions (Xe XXIV-Pr XXIX). *J. Applied Spectrosc.*, **2015**, 82, 487-493. <https://doi.org/10.1007/s10812-015-0136-6>
- [28] Fatma El-Sayed, and S. M. Attia. Energies, Wavelengths, and Transition Rates for Ga-Like Ions (Nd XXX-Tb XXXV). *J. Appl. Spectrosc.*, **2016**, 83, 126-132. <https://doi.org/10.1007/s10812-016-0254-9>
- [29] E. Träbert, J. A. Santana, P. Quinet, and P. Palmeri. Intercombination transitions in the n=4 shell of Zn-, Ga-, and Ge-like ions of elements Kr through Xe. *Atoms*, **2018**, 6, 40. <https://doi.org/10.3390/atoms6030040>
- [30] N. Shukla, T. Das, R. Srivastava. Electron impact N-shell excitation of Se-like to Ga-like tungsten ions and polarization of their subsequent emissions. *J. Quant. Spectrosc. Radiat. Transf.*, **2019**, 222-223, 247-256. <https://doi.org/10.1016/j.jqsrt.2018.10.031>
- [31] J. P. Desclaux and P. Indelicato, MCDFGME, a MultiConfiguration Dirac Fock and General Matrix Elements program, ver (2005).



Investigation of the Effects of Various Navigation Patterns in the Design of Mobile Learning Applications within Saudi Higher Education

Ali Alowayr

Information Technology Department, College of Computer Science & Information Technology, Albaha University, Albaha, Saudi Arabia.

ARTICLE INFO

Article History:

Submission date: 28/03/2020

Accepted date: 22/06/2020

Keywords:

Application design, mobile learning, learning achievements, linear navigation, net (grid) navigation.

ABSTRACT

The aim of the present study is to investigate the effects of different navigation patterns for mobile learning (m-learning) application designs, on students' academic performance and skills development in the IT department of Albaha University, Saudi Arabia. Pre- and post-achievement tests to assess knowledge of theoretical concepts for online-learning application design and a pre-/post-observation card to measure the participants' skills were considered as a useful supplement. Thus, design-based research was conducted, using an experimental approach to examine students in their third year of a Platform-Based Development (PBD) course: a compulsory module in the University's IT department. Sixty male students registered in this course were recruited as a convenience sample for the investigation and then divided into two groups. The first experimental group studied how to design m-learning applications using linear navigation, while the second experimental group took the same class, but used net (grid) navigation. The findings indicate statistically significant differences between the mean scores of the first group (who used a linear navigation style), and the second group (who used a net [grid] navigation style), generating the p-values 0.03 and 0.01, respectively. This outcome was therefore in favor of the second group, who studied and applied a net navigation pattern; as shown in the results of the achievement test and observation card for m-learning application design skills. The findings suggest a need to train instructors intensively in how to simplify instruction in the design of smart phone learning applications.

1. Introduction

This current era is characterized by tremendous progress in the fields of enhanced learning technologies, communications technology, and m-learning applications [1,2]. Progress in these fields has posed many challenges to educational systems worldwide. This has demanded radical change and development through various technological innovations, in order to maximize their potential in the service of education and consequently enhance students' learning achievement [3]. Most segments of society have realized the importance of smartphones, such as those produced by iPhone, Galaxy, Huawei, etc. and are appealing for their use in sectors such as education [4].

The education sector has already been affected by curricula and courses run on device platforms, as encountered by most users with computer experience across the developed world. It should also be noted that if learning takes place with suitable technologies in the right environment and context, it can produce excellent results in many educational situations, particularly in terms of interaction and communication. Moreover, it effectively takes into account individual differences between learners [5,6]. This undoubtedly promotes the efficiency and quality of teaching and learning via the design of multiple e-learning applications for smart devices [7]. In the relevant context, [8] assert that ICT has led to the production of educational mobile applications, which have contributed to the development of teaching methods, and provided an opportunity to enhance instructional techniques that can promote an effective educational environment. In turn, this can help stimulate students' interest and motivation, as well as challenging them appropriately.

Multimedia educational software comprise one genre of educational application for smart devices, characterized by multiple image-processing on a single subject in various media, such as audio-content, still images, graphics, animation/video and text. This software is intended to enrich and diversify the processing of topics communicated via these applications [8,9]. M-learning applications of various types allow a learner to learn independently, without the need for in-depth knowledge of mobile-learning settings. Moreover, the use

of mobile and educational applications is perhaps the most appropriate form of e-learning program for teaching certain kinds of scientific material [10,11]. [12] argues that there are five interactive functions of multimedia software that can prove useful when studying subjects: confirmation, self-pacing, navigation, inquiry, and elaboration. Therefore, this study aims to experimentally investigate navigation patterns for designing an interactive m-learning application.

2. Research Model and Hypotheses

The skills required to design smartphone applications for interactive self-learning are complex. Continuous and coherent practical training is therefore required to be able to design an integrated electronic application [13]. To be specific, undergraduate students are faced with the task of learning difficult skills on the Platform-Based Development (PBD) course, as these will be fundamental to them attaining competence in designing for the online computer and technology environment. As a specialist in this field at Albaha University in Saudi Arabia, the present researcher has noted distinct difficulties in teaching these skills in the design of educational smartphone applications, pointing to the need for innovative and unconventional methods, which will enable instructors to develop these skills in their students [14].

Much of the existing educational technology literature emphasizes that the potential of application design to solve many educational problems is dependent on increasing students' participation and interaction [15]. Therefore, the present research aims to investigate the impact of different navigation patterns on skills in m-learning application design, and on the learning outcomes and performance of students on a mandatory IT program for third-year students at Albaha University. This study therefore seeks to develop teaching strategies for the University's PBD course. These consist of new, useful and effective methods of enhancing learners' motivation and facilitating their mastery of general application design skills, and more specifically, for designing m-learning applications. In recent years, there has been an increasing interest in the use of various types of navigation in e-learning for the benefit of electronic education and training, as these help determine the suitability of each pattern for

* Corresponding Author

Information Technology Department, College of Computer Science & Information Technology, Albaha University, Albaha, Saudi Arabia.

E-mail address: aalowayr@bu.edu.sa (Ali Alowayr).

1685-4732 / 1685-4740 © 2020 UQU All rights reserved.

specific electronic content. This is what [16] refers to as the need to assess the type of interaction, its appropriate content, its importance, and its impact on the development of average skill performance and knowledge acquisition. The design of m-learning applications requires a set of instructional procedures and plans to determine the learner's path and the conditions for transitioning from one unit of information to another [17].

E-learning programs consist of various types of navigation that enable learning and interaction with the tools provided. Interactivity is an effective component of e-learning applications, as it connects all elements of the content according to the specific navigation involved. Navigation styles in the design of e-learning applications include linear and net navigation [15]. A learning application with specific content that a student must study, together with related activities and questions, calls for linear navigation [18]. Therefore, the system/application has full control and the student cannot choose to omit any steps from the content. Conversely, net navigation is more complex and consists of multiple links, leading the learner in different directions, particularly when the application has a vast array of content [19]. Control lies with the learner in this type of navigation, as he or she can select preferred sequences of content.

Therefore, this current research aims to measure the impact of different navigation styles (linear and net) applied in the construction of e-learning on the enhancement of learning skills amongst IT students at Albaha University. The main hypotheses of this study are as follows:

H1: There are no statistically significant differences at the level $\alpha=0.05$ between the mean scores of the first group of IT students, who undertake a unit on m-learning application design using a linear navigation style, and the mean scores of the second Group, who undertake the same unit using a net (grid) navigation style, when the results of an achievement test on theoretical concepts of m-learning application design are compared.

H2: There are no statistically significant differences at the level $\alpha=0.05$ between the mean scores of the first Group of IT students, who undertake a unit on the m-learning application design using a linear navigation style, and the mean scores of the second group, who undertake the same unit using a net (grid) navigation style, when the results of a skills performance observation card are compared, revealing the students' m-learning application design skills.

3. Research Methods

This study explores approaches to designing an e-learning application based on different navigation styles (linear and net), with a view to enhancing Web and e-learning application design skills. This was achieved by investigating differences in the effectiveness of each style with an achievement test and skills development observation card. The findings of this investigation are expected to confirm which modern methods offer optimal time saving and resource investment, as well as enhancing communication and interaction between learners and the e-learning environment. Accordingly, an experimental research approach was adopted as the most appropriate means of meeting this research objective. Using this approach, the navigation styles for designing online learning applications were examined and the findings compared with similar studies in the extant literature. Moreover, a pre- and post-module observation card method was implemented to evaluate the learners' skills in designing an online interactive learning application. Furthermore, pre- and post-achievement tests were conducted to assess the learners' knowledge, acquired in practice while designing the application via either of the two navigation styles.

4. The Research Sample

This current research was carried out at Albaha University, a public university in Saudi Arabia. It is one of Saudi Arabia's most supportive and enthusiastic universities for the use of e-learning and distance learning to complement traditional learning approaches. Accordingly, there is a compulsory PBD module taught in its IT department. Once the students have completed this module, they are expected to be able to create online and mobile applications. However, the researcher noted the difficulties experienced by students registered on this module in Semester 1, 2019-2020. As a consequence, and in view of the manageable number and availability of this cohort, they were selected as the target sample in this research. The sample therefore

consisted of 60 male third-year undergraduate students, selected in a convenience sampling approach.

5. Development of the Instruments

At the beginning of the experiment, a brief description of the main objectives was presented to the targeted sample to ensure their informed consent, and to confirm that their data would be dealt with confidentially and used solely for the research purposes. Moreover, although the module was mandatory for their course, it was explained that they were free to request their withdrawal from this current study at any time before the data analysis, without compromising their academic grades. They would then continue the module without being observed or taking the pre- and post-achievement tests, whereupon any of their data relating to this experiment would be securely destroyed. The sample was split into two Experimental Groups: A and B, with 30 students in each. Group (A) was assigned to design a learning application using a linear navigation style and Group (B) were assigned to design a similar learning application using a net navigation style. Table 1 illustrates the study's experimental design.

Table 1: Experimental study design.

Tools Groups	Pre-evaluation	Experimental process	Post-evaluation
Group A	Observation card	Design using a linear approach	Observation card
Group B	Achievement test	Design using a net approach	Achievement test

The observation card was adapted slightly from previous studies to meet the main research objectives here. It comprised 40 items, formulated so that the observer could measure the learners' skills while they were designing the application. The items consisted of multiple-choice questions, using a three-point Likert scale that ranged across 1 (Students have no skills), 2 (Students have some of the necessary skills) and 3 (Students have all the required skills).

Conversely, an achievement test was prepared to evaluate the participants' knowledge, including their knowledge retention, understanding and implementation of electronic application design. This test comprised eight 35-part questions, designed to gather both qualitative and quantitative data. Moreover, the test began with a number of demographic questions to collect personal information about the participants, so that some data on their background could be provided. In addition, instructions and guidelines on how to answer these questions were clarified for the participants beforehand.

6. Data Collection Procedure

Both quantitative and qualitative data were subsequently collected in a pre- and post-achievement test using a three-point Likert scale observation card. Pre-assessment (with the observation card and achievement test) was conducted for the two Experimental Groups and the data were processed in preparation for statistical analysis. This pre-evaluation confirmed that the two groups were identical in their level of design skill and knowledge relating to the module. Group (A) then began designing the electronic application using a linear style, while group (B) used a net (grid) style. Meanwhile, the observers concentrated on the participants' implementation and scored their efforts with the observation card. Lastly, the participants were required to retake the same achievement test, so that the results for their knowledge could be compared, before and after the test.

The post-intervention scores for both the observation card and achievement test were entered into an Excel sheet in preparation for statistical analysis, as covered in the next section.

7. Data Analysis

The data collected in this research were analyzed using SPSS software. Statistical methods help a researcher to map mathematical expression relating to the research objectives. To ensure that there was no bias in the outcomes towards either the first group, taught how to design an m-learning application in a linear style, or the second group, taught the same class using a net (grid) style, the hypotheses were tested statistically; based on the participants' scores in the pre-achievement exam and on the design skills pre-observation card

completed by the observers. An independent sample t-test technique was used to compare the average scores from each Group (A and B) to give the P-value. The next section presents the findings from this analysis.

8. Results and Discussion

The results of validating the data collection tools in the pre-experimental data revealed no statistically significant differences between the averages of the two Groups: Group A designing an m-learning application in a linear style, and group B undertaking the same task in a net (grid) style, resulting in P-value = 0.71. Table 2, below, presents the statistical findings for the mean, standard deviation, t-test, and p-value differences between the two groups in the pre-achievement test.

Table 2: Pre-achievement test.

Tools Groups	Participants	Mean	Std. Error	t-Test	Sig.
Group A	30	2.70	1.09	2.47	0.71
Group B	30	2.62	1.39		

Table 2 shows that there are no differences between the two sets of results obtained from the pre-experimental data (Groups A and B), comparing the groups' achievement test scores. It is therefore likely that initially, all participants in both groups A and B were identical in terms of their knowledge, understanding and recall of theoretical concepts and skills for designing the m-learning application, as illustrated in Fig.1.

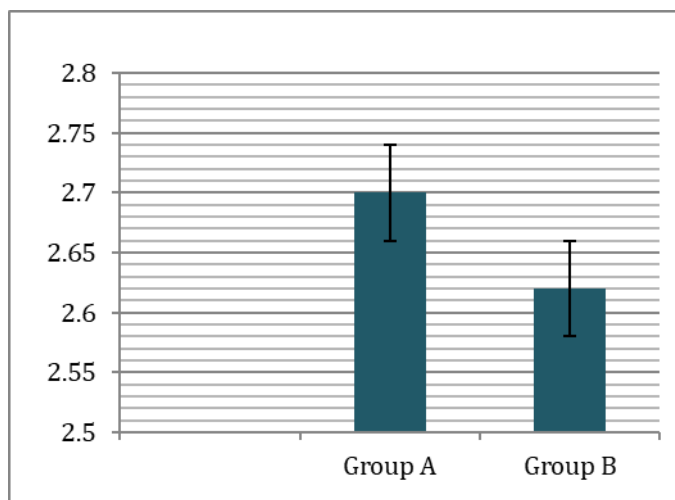


Figure 1: Mean difference between the pre-achievement tests

Conversely, the findings from the observation card were also tested to validate the card's implementation for both groups. The pre-observation cards were therefore analyzed, revealing no statistically significant differences between Groups A and B in terms of the participants' skills in designing m-learning applications (P-value = 0.32). Table 3, below, presents the statistical findings for the mean, standard deviation, t-test, and p-value differences between the two Groups for the observation card data. These results confirm the validity of the observation card used in this research.

Table 3: Pre-observation card.

Tools Groups	Participants	Mean	Std. Error	t-Test	Sig.
Group A	30	10.8	5.72	0.33	0.32
Group B	30	11.2	6.89		

Table 3 illustrates that in the results obtained from the pre-experimental data, there are no differences between the two Groups when comparing the scores from the observation cards. It is therefore likely that initially, all participants in Groups A and B were identical

in terms of their m-learning application design skills, as shown in Fig.2.

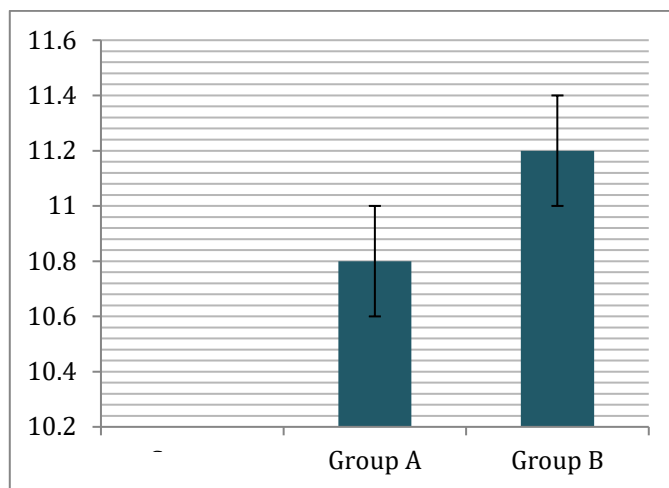


Figure 2: Mean differences for the pre-observation card

In this research, the validity of both the achievement test questions and observation items was confirmed. The results of the hypotheses tests will now be presented in the next section.

Result of the First Hypothesis (H1):

H1 states that there are no statistically significant differences at the level of significance ($\alpha=0.05$) between the mean score of Group (A) – who undertook the m-learning application design module using a linear navigation style – and the mean score of Group (B) – who took the same module using a net (grid) navigation style – in the post-achievement test on theoretical concepts and skills for designing m-learning applications. An independent sample t-test technique was applied to compare the means of Groups A and B. Table 4, below, presents the results for H1, relating to the participants' post-achievement test scores.

Table 4: Post-achievement test.

Tools Groups	Participants	Mean	Std. Error	t-Test	Sig.
Group A	30	25.86	5.42	2.03	0.03
Group B	30	28.65	5.49		

As Table 4 shows, H1 is rejected, as there is a significant difference between the two Groups: P-value = 0.03 in the participants' post-achievement test, in favor of students learning to design an m-learning application with net (grid) navigation. Fig.3 demonstrates the mean differences between the two Experimental Groups in the post-achievement test on theoretical concepts and knowledge of designing an online learning application.

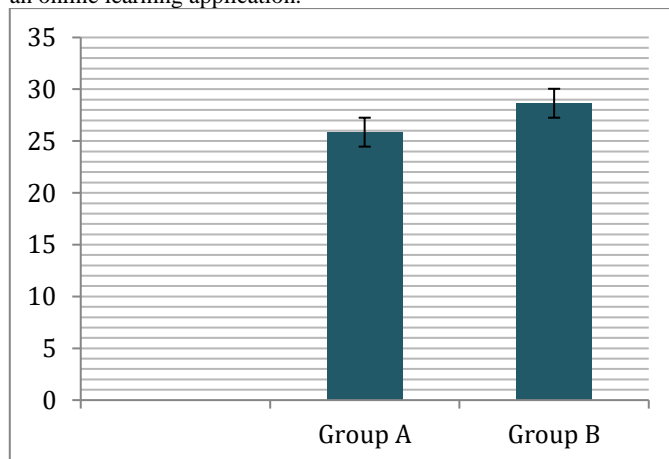


Figure 3: Mean differences for the post-achievement test

Results for the Second Hypothesis (H2):

H2 states that there are no statistically significant differences at the level of significance ($\alpha=0.05$) between the mean score of the first Group (A), undertaking the m-learning application design unit with a linear navigation style, and the mean score of the second Group (B), undertaking the same unit with a net (grid) navigation style, measured using a skills performance post-observation card for the IT students' m-learning application design skills. An independent sample t-test technique was applied to compare means between the two Experimental Groups. Table 5 presents the results for H2 in terms of the participants' observation card scores.

Table 5: Post-intervention observation card.

Tools Groups	Participants	Mean	Std. Error	t-test	Sig
Group A	30	56.56	6.82	2.85	0.01
Group B	30	65.55	8.83		

As Table 5 shows, H2 is rejected, as there is a significant difference between the two Groups, with P-value = 0.01; found using a post-intervention observation card to assess the participants. The observation found in favor of students learning to design an m-learning application using net (grid) navigation. **Fig.4** demonstrates the mean differences between the two Experimental Groups in the post-intervention observation card, completed by the observers for the participants' skills in designing an online learning application.

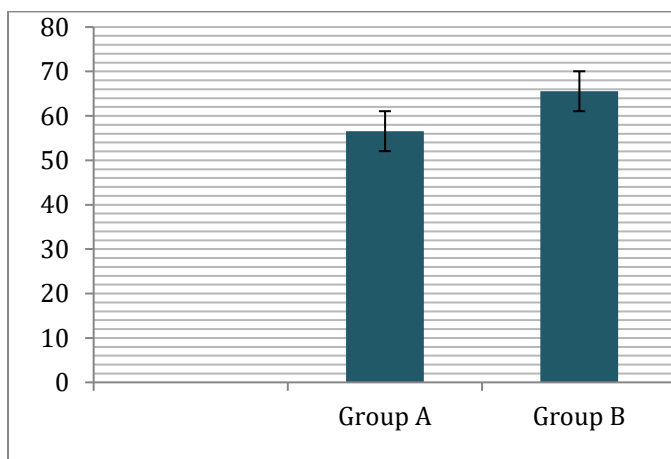


Figure 4: Mean difference for the post-intervention observation card

The most obvious finding to emerge from this study is that designing online learning applications via net (grid) navigation provides learners with broad scope for accessing and engaging deeply with learning content. It is possible that this approach assisted the IT students in increasing their skill in m-learning application design. The finding is consistent with those of previous studies, such as [20], who examined the effectiveness of different navigation patterns and their attractiveness. The above study generated similar results, with the learning achievements of students using net navigation being statistically higher than those of students using linear navigation, because the former appeared to feel free to navigate and learn without constraints. These findings enhance our understanding of multimedia use (video, image, audio- and text), since the use of grid navigation for designing interactive online learning applications has been proven to have a significant effect on learners' test performance and skills development.

It has also been shown that designing m-learning applications based on instant feedback for the learner clearly mitigate learners' weaknesses and capitalize on their strengths. In contrast, [21] demonstrated that the attitude of students using linear navigation was positive towards controlling and monitoring learning from the initial steps until the final screen, leading to optimal outcomes.

9. Conclusion

The present study was designed to determine the effect of different navigation patterns of m-learning application design on students' academic performance, and to explore ways of developing students' design skills. The contribution of this study is evident, as the outcomes

point to enormous potential for informing practitioners, researchers and instructors in higher education. The findings provide evidence that general awareness amongst these stakeholders of the importance of various types of navigation, especially net (grid) navigation, is highly recommended. Therefore, instructors need to design their lessons in an interactive way and provide different multimedia to enhance the learning and ensure that learners obtain real benefits in their learning performance. Additionally, higher education can exploit the advantages of this type of navigation (grid) to improving the delivery learning process.

Future research should therefore concentrate on investigating the design of various classes of student on different navigation styles, and other different universities based on the culture may provide more reliable results to be generalized. However, considerably more workshops and instructor-training courses should be undertaken to establish best practice in the design of m-learning applications. Moreover, students should be provided with practical training in particular learning design to reduce difficulties that they might face when undertaking the (PBD) course. In sum, the present study findings and accurate evaluation of the impact of m-learning in Saudi Arabia will help enhance policy making and the effectiveness of m-learning pedagogies for higher education.

Author Contributions: The author contributed to the study conception and design. Material preparation, data collection and analysis were performed by Ali Alowayr. The first draft of the manuscript was written by author and the proofreader commented on previous versions of the manuscript. The author read and approved the final manuscript.

Funding: This research was funded by Albaha University, grant number 23/1440.

Acknowledgments: I would like to express my sincere gratitude to Albaha University, Saudi Arabia for funding the project entitled 'Study of the Factors Influencing the Adoption of Mobile Learning Devices by Higher Education Students and Educators, and the Challenges to Such Utilization'. Special thanks are also due to all those who participated in this study for their time and enthusiasm.

References

- [1] V. Marta, M. Blasco, M. Sastre. Determinants of the acceptance of mobile learning as an element of human capital training in organizations. *Technological Forecasting and Social Change*, **2018**. <https://dx.doi.org/10.2139/ssrn.3225078>.
- [2] O. Pereira, and J. Rodrigues. Survey and analysis of current mobile learning applications and technologies. *ACM Computing Surveys*, **2013**, *46*, 35. <https://doi.org/10.1145/2543581.2543594>
- [3] C. J., Chung, G.J. Hwang, and C.L. Lai. A review of experimental mobile learning research in 2010–2016 based on the activity theory framework. *Computers and Education*, **2019**, *129*, 1-13. <https://doi.org/10.1016/j.compedu.2018.10.010>
- [4] H. Shava, W. Chinyamurindi, and A. Somdyala. An investigation into the usage of mobile phones among technical and vocational educational and training students in South Africa. *S. Afr. J. Inf. Manag.*, **2016**, *18*(1), 1-8. <http://dx.doi.org/10.4102/sajim.v18i1.716>
- [5] D. Metafas, A. Politi. Mobile-assisted learning: Designing class project assistant, a research-based educational app for project based learning. *IEEE Global Engineering Education Conference (EDUCON)*, **2017**, 667-675. DOI: [10.1109/EDUCON.2017.7942918](https://doi.org/10.1109/EDUCON.2017.7942918)
- [6] S. J. Baldwin, Y. Ching. Guidelines for Designing Online Courses for Mobile Devices. *Tech. Trends*, **2019**, *64*, 413–422. <https://doi.org/10.1007/s11528-019-00463-6>.
- [7] B. Gros. The design of smart educational environments. *Smart Learning Environments*, **2016**, *3*(15), 2-11. DOI: [10.1186/s40561-016-0039-x](https://doi.org/10.1186/s40561-016-0039-x)
- [8] M. Simonson, S. Smaldino. M. Albright, S. Zvacek. Teaching and learning at a distance. *Foundations of distance education*, 5th ed. Pearson, **2019**.
- [9] J. Stephenson. Teaching & learning online: New pedagogies for new technologies. Routledge, **2018**.
- [10] M. Alenezi. The effect of using computerized educational software designed according to the part-to-all teaching strategy in the immediate and postponed achievement of year one students in the Arabic language subject at the State of Kuwait. *PhD thesis, College of Graduate Studies, University of Jordan*, **2015**.

- [11] A. Chavoshi, and H. Hamidi. Social, individual, technological and pedagogical factors influencing mobile learning acceptance in higher education: A case from Iran. *Telematics and Informatics*, **2019**, 38, 133-165.
<https://doi.org/10.1016/j.tele.2018.09.007>
- [12] A. Richard. A taxonomy of interaction for instructional multimedia. *Annual Conference of the Association for Media and Technology in Education*, Vancouver, Canada, June, **1992**, 13-17. <https://files.eric.ed.gov/fulltext/ED352044.pdf>
- [13] K. N. Chee, N. Yahaya, N. Ibrahim. Effectiveness of mobile learning application in improving reading skills in Chinese language and towards post-attitudes. *International Journal of Mobile Learning and Organisation*, **2017**, 11(3), 210-222.
DOI: [10.1504/IJMLO.2017.10005992](https://doi.org/10.1504/IJMLO.2017.10005992)
- [14] I. Montiel, J. Delgado-Ceballos, N. Ortiz-de-Mandojana, R. Antolin-Lopez. New ways of teaching: Using technology and mobile apps to educate on societal grand challenges. *Journal of Business Ethics*, **2020**, 161, 243-251.
<https://doi.org/10.1007/s10551-019-04184-x>
- [15] Z. Zihui, and X. Yueshan. An improvement approach based on linear navigation law for mobile robot. *IEEE International Conference on Computer Science and Automation Engineering (CSAE)*, **2012**, 25-27, 495-498.
DOI: [10.1109/CSAE.2012.6273000](https://doi.org/10.1109/CSAE.2012.6273000)
- [16] M. De Silva, F. Rossi. The effect of firms' relational capabilities on knowledge acquisition and co-creation with universities. *Technological Forecasting and Social Change*, forthcoming, **2017**.
- [17] F. Alonso, G. López, D. Manrique, J.M. Viñes. An instructional model for web-based e-learning education with a blended learning process approach. *British Journal of Educational Technology*, **2005**, 36(2), 217-235.
<https://doi.org/10.1111/j.1467-8535.2005.00454.x>
- [18] D. Castilla, A. Garcia-Palacios, I. Miralles, J. Breton-Lopez, E. Parra, S. Rodriguez-Berges. Effect of Web navigation style in elderly users. *Computers in Human Behavior*, **2016**, 55, 909-920.
DOI: [10.1016/j.chb.2015.10.034](https://doi.org/10.1016/j.chb.2015.10.034)
- [19] D. A. Cook, D. M. Dupras. A practical guide to developing effective web-based learning. *Journal of General Internal Medicine*, **2004**, 19 (6), 698-707.
<https://doi.org/10.1111/j.1525-1497.2004.30029.x>
- [20] A. Alomdah. The effect of different types of navigation (linear - network) in e-learning on the development of database management skills for the Information and Statistics Unit specialist in Fayoum Governorate schools. *Educational Sciences*, **2014**, 2(1), 1-45.
- [21] A. Fouse, N. Weibel, E. Hutchins, J. D. Hollan. ChronoViz: A system for supporting navigation of time-coded data. CHI EA '11: CHI '11 *Extended Abstracts on Human Factors in Computing Systems*, **2011**, 7-12, 299-304



A Contribution To m-Power Closed Groups

Hasan Sankari, Mohammad Abobala*

Department of Mathematics, Faculty of Science, Tishreen University, Syria.

ARTICLE INFO

Article History:

Submission date: 03/02/2020

Accepted date: 22/06/2020

Keywords:

(m-group), (power central series), (m-normal factor), (Monic group).

ABSTRACT

The notion of (m-power closed) group was introduced Kappe et.al. We say that a group G is (m-power closed) if $G_m = \{g^m; g \in G\}$ with fixed integer m is a subgroup of G .

In this paper we study how the properties of G_m effects on G .

We focus on the case that m is a prime and G is a finite group, we prove that G is solvable if and only if G_m is solvable under the previous conditions, and we tried to determine a sufficient condition for a group G to be (m-power closed). Also, we studied the special case when a group G is (m-power closed) and (n-power closed) with relatively prime n, m which we call a Monic group and we determine some interesting properties.

1. Introduction

Date palm is a commonly edible fruit and has been known widely by the society of Kingdom of Saudi Arabia (KSA) and other Gulf countries. In KSA, there might be more than five hundred cultivars, and

A group G is said to be (m-power closed) if we have $G_m = \{g^m; g \in G\}$ which is a subgroup of G .

The previous definition is equivalent to the condition $\forall x, y \in G \exists z \in G$ such that $x^m y^m = z^m$.

The class of (m-power closed) groups is quotient and direct products are closed, but not subgroup closed see [1].

We will denote to (m-closed group) by (m-group).

1.1. Lemma

Let G be an (m-group) then:

(a) $G_m \triangleright G$ and G/G_m is (m-group)

(b) If H is a fully invariant (m-subgroup) of G then $H_m \triangleright H$

Proof:(a) Let φ be a homomorphism on G and x be an arbitrary element in G_m then $\exists y \in G$ such $x = y^m$, $\varphi(x) = \varphi(y^m) = (\varphi(y))^m \in G_m$ so G_m is a fully invariant subgroup so $G_m \triangleright G$ and $(G/G_m)_m = G_m/G_m = \{e\} \leq G/G_m$, the proof is complete.

(b) $\forall h^m \in H_m$ such $h \in H$ we have for a homomorphism φ on G that: $\varphi(h^m) = (\varphi(h))^m \in H_m$ so H_m is fully invariant and then normal according to [2].

1.2. Definition

Let G be a group and $H \triangleright G$, we say that H is (m-normal factor) of G if and only if the following condition is true: $\forall x, y \in G \exists z \in G$; $z^m x^m y^m \in H$, we denote that by $H \triangleright_m G$.

1.3. Theorem

Let G be a group then:

(a) If $H \triangleright_m G$ and $K \triangleright G$ then $HK \triangleright_m G$

(b) If $H \triangleright G$ then G/H is an (m-group) if and only if $H \triangleright_m G$

(c) If $H \triangleright G$ then $H \triangleright_m G$ if and only if $G_m H \leq G$

Proof:(a) Obviously $HK \triangleright G$, now suppose that $x, y \in G$ there is $z \in G$ such $z^m x^m y^m \in H \leq HK$ so $HK \triangleright_m G$

(b) Assume that G/H is an (m-group), let x, y be two arbitrary elements in G then $xH, yH \in G/H$ so $(xH)^m (yH)^m \in (G/H)_m$ that implies $x^m y^m H = z^m H$ for some $z \in G$ which means that $(z^{-1})^m x^m y^m \in H$ and $H \triangleright_m G$

Conversely assume that $H \triangleright_m G$, let xH, yH be two arbitrary elements in G/H , we have $x, y \in G$ so there is $z \in G$ such $z^m x^m y^m \in H$ that means $x^m y^m H = (z^{-1})^m H$ and G/H must be (m-group)

(c) suppose that $G_m H$ is a subgroup of G then for each $x, y \in G$ and $h_1, h_2 \in H$ we have: $(x^m h_1)(y^m h_2) = z^m h_3$; $z \in G$ and $h_3 \in H$ so, in addition to the normality of H we can write: $z^m h_3 = (x^m h_1)(y^m h_2) = x^m y^m (h_1 h_2)$; $(h_1 h_2)^{-1} \in H$

So $z^{-m} x^m y^m \in H$ and $H \triangleright_m G$

Conversely suppose that $H \triangleright_m G$ and $x, y \in G$, $h_1, h_2 \in H$

$(x^m h_1)(y^m h_2)^{-1} = x^m y^{-m} (h_1 h_2)^{-1}$; $(h_1 h_2)^{-1} \in H$

There is $z \in G$ such $(z^{-1})^m x^m y^{-m} = h \in H$ so $x^m y^{-m} = z^m h$ and we get that $(x^m h_1)(y^m h_2)^{-1} = (z^m h)(h_1 h_2)^{-1} \in G_m H$ this implies $G_m H \leq G$

1.4. Theorem

(a) If $N \triangleright_m G$ and G is a semi direct product of N and H then H is (m-group)

(b) If $H \triangleright G$ and $K \triangleright G$ and $G = HK$ then $N = H \cap K \triangleright_m G$ if and only if $N \triangleright_m H$ and $N \triangleright_m K$

Proof:(a) We have $G = HN$ with $H \cap N = \{e\}$ so $G/N \cong H$ and H must be (m-group)

(b) Suppose that $N \triangleright_m H$ and $N \triangleright_m K$, considering that $G/N \cong H/N \times K/N$ and $H/N, K/N$ are (m-groups) then G/N is (m-group) thus $N \triangleright_m G$

Conversely let $N \triangleright_m G$ then G/N is (m-group) so that $H/N, K/N$ are (m-groups), that means $N \triangleright_m H$ and $N \triangleright_m K$

2. Finite (m-groups)

In this section we consider a finite group G and we denote to (m-group) with prime m by (m^* -group)

2.1. Lemma

Let G be an (m-group) then:

(a) If G is (n-group) and (d-group) then $G_m G_n = G_d$; $d = \gcd(n, m)$

(b) If G is (n-group) with $\gcd(n, m) = 1$ then $G = G_m G_n$

(c) If $\gcd(m, |G|) = d$ then $G_m = G_d$

(d) If $\gcd(m, |G|) = 1$ then $G = G_m$

Proof:(a) there are two integers a, b such $d = am + bn$, $\forall x^d \in G_d$ then $x^d = (x^a)^m (x^b)^n \in G_m G_n$ so $G_d \leq G_m G_n$. Now $\forall x^m \in G_m$ then $x^m = (x^t)^d$; $m = td$ so $G_m \leq G_d$, according to the same argument we find that $G_n \leq G_d$ which means $G_m G_n \leq G_d$ and the proof is complete.

* Corresponding Author

Department of Mathematics, Faculty of Science, Tishreen University, Syria.
E-mail address: mohammadabobala777@gmail.com (Mohammad Abobala).
1685-4732 / 1685-4740 © 2020 UQU All rights reserved.

- (b) Holds directly from (a)
- (c) see [3]
- (d) Holds directly from (c)

2.2. Lemma

Let G be an (m-group) and an (n-group) ; gcd(n,m)=1 and let |G| = mnq ; q ∈ N then:

- (a) If $G_m = G_n = \{e\}$ then $G = \{e\}$
- (b) $G_n / (G_m \cap G_n) \cong G/G_m$ and $G_m / (G_n \cap G_m) \cong G/G_n$
- (c) $G / (G_m \cap G_n) \cong G/G_m \times G/G_n$
- (d) $(G_m \cap G_n)_q = \{e\}$
- (e) $n/|G_m|$ and $m/|G_n|$

Proof:

(a) there are two integers a,b such $1=an+bm$, let x be an arbitrary element of G then :

$$x = x^1 = x^{an} x^{bm} = e \cdot e = e \text{ so } G = \{e\}$$

(b) Holds by isomorphism theorem

(c) Holds directly from (b) and lemma 3.1

(d) Let $H = G_n \cap G_m$ then $H \leq G_n$ and $H \leq G_m$ so $H_{nq} \leq G_{mnq} = \{e\}$ and $H_{mq} \leq G_{mnq} = \{e\}$ thus $(H_q)_m = (H_q)_n = \{e\}$.Following the first condition, we can see that $H_q = \{e\}$

(e) We can find at least one element $x \in G$ such that $x^n = e$ because $n/|G|$ thus $G_n \neq G$, $(G/G_n)_m = G_n G_m / G_n = G/G_n$, using the previous argument we find that $\gcd(m, \frac{|G|}{|G_n|}) = 1$

, but $m/|G|$ so that $m/|G_n|$.The second proposition can be proved by the same way.

2.3. Theorem

Let G be an (m^* -group) with $m/|G|$, let $|G| = m^{k_1} p_2^{k_2} \dots p_s^{k_s}$; p_i are distinct primes for each $2 \leq i \leq s$ then :

- (a) $p_2^{k_2} \dots p_s^{k_s} / |G_m|$
- (b) G/G_m is a (p-group) with $m=p$
- (c) G is solvable if and only if G_m is solvable

Proof:

(a) for each prime p_i the (p_i -Sylow) subgroup H_i has order $p_i^{k_i}$ with $\gcd(p_i^{k_i}, m) = 1$

So $(H_i)_m = H_i \leq G_m$ then $p_i^{k_i} / |G_m|$ for each i ,thus $p_2^{k_2} \dots p_s^{k_s} / |G_m|$

(b) $|G/G_m| = m^k$; $k \leq k_1$ so G/G_m is a (p-group) with $m=p$

-we meant by (p-group) a group with order p^s ; $s \in N$ and p is prime-

(c) Assume that G_m is solvable then G/G_m is also solvable because it is a (p-group) according to [4] , this means that G is solvable, the converse is clear.

2.4. Theorem

Let G be an (m^* -group) with $m/|G|$ then:

- (a) If G simple, then it is cyclic of order m
- (b) If $H \triangleright G$ then $H / (H \cap G_m)$ is a (p-group) with $p=m$

Proof:(a) We have $m/|G|$ so that $G \neq G_m$, but $G_m \triangleright G$ so $G_m = \{e\}$ and G/G_m is a (p-group) and in this case $G/G_m \cong G$ which means that G is a simple (p-group) then G is cyclic with order m

(b) Suppose that $H \triangleright G$ then $G_m \cap H \triangleright H$ and $H / (H \cap G_m) \cong G_m H / G_m \leq G/G_m$ so $H / (H \cap G_m)$ is a (p-group)

2.5. Remark

If we consider that the finite group G is (m^k -group) with $|G| = m^{k_1} p_2^{k_2} \dots p_s^{k_s}$; $m, p_2, p_3 \dots p_s$ are distinct primes and $k \leq k_1$ then theorems (3.3) and (3.4) are still true.

3. Power central series

3.1. Definition

Let G be a group with center Z(G) we define the (m-center) of G by $Z_m(G) = (Z(G))_m$

3.2. Theorem

Let G be a group then G is (m-group) if and only if $G/Z_m(G)$ is (m-group)

Proof:

It is easy to see that $Z_m(G)$ is a characteristic subgroup so it is normal

If G is an (m-group), then $G/Z_m(G)$ is (m-group). Conversely suppose that $G/Z_m(G)$ is (m-group) and x , y be two arbitrary elements of G then there is $z \in G$ such $z^{-m} x^m y^m = k^m \in Z_m(G)$

thus $x^m y^m = z^m k^m$, we have $k \in Z(G)$ which implies that $z^m k^m = (zk)^m$ so $x^m y^m = (zk)^m$ and G is (m-group)

3.3. Definition

Let G be a group we define $Z_i^m(G)$ to be the subgroup of G such that $Z_i^m(G) / Z_{i-1}^m(G) = Z_m(G / Z_{i-1}^m(G))$ with $Z_0^m(G) = G$

By the previous definition, we get the series $\{e\} \leq Z_1^m(G) \leq Z_2^m(G) \leq \dots \leq Z_i^m(G) \leq \dots$

3.4. Theorem

Let G be a group then:

- (a) G is (m_group) if and only if there is an integer i such $Z_i^m(G) \triangleright_m G$
- (b) if there is an integer i such $Z_i^m(G) = G$ then G is (m-group)
- (c) if G is finite and there is an integer i such $\gcd(|G/Z_i^m(G)|, m) = 1$ then G is (m_group)

Proof:

(a) Assume that there is an integer i such $Z_i^m(G) \triangleright_m G$ then $G/Z_i^m(G) \cong (G/Z_{i-1}^m(G)) / Z_m(G/Z_{i-1}^m(G))$ is (m_group) so that $G/Z_{i-1}^m(G)$ is (m_group) , by the same argument we get $G/Z_m(G)$ is (m-group) so G is (m_group) by theorem 2.3

(b) Assume that there is an integer i such $Z_i^m(G) = G$ then $Z_i^m(G) \triangleright_m G$ so G is (m_group)

(c) Assume that G is finite and there is an integer i such $\gcd(|G/Z_i^m(G)|, m) = 1$ then $(G/Z_i^m(G))_m = G/Z_i^m(G)$ so $Z_i^m(G) \triangleright_m G$ and G is (m_group)

4. Monic groups

4.1. Definition

Let G be a finite (m-group) with $m/|G|$ then we say that it is a monic group if and only if G is an (n-group) with $n/|G|$ and $\gcd(n,m)=1$

4.2. Lemma

Let G be a monic group then:

- (a) $G = G_m G_n$
- (b) The homomorphic image of G is also monic

Proof:

(a) Holds from lemma 1.2

(b) Since the homomorphic image of (m-group) is also (m-group) the proof is complete

4.3. Lemma

Let G be a group and $H \triangleright G$ then G/H is monic if and only if $H \triangleright_m G$ and $H \triangleright_n G$

Proof:

Since G/H is (m-group) if and only if $H \triangleright_m G$ then the proof is complete

4.4. Theorem

Let G be a monic group then:

- (a) G is solvable if and only if G_m, G_n are solvable
- (b) If G_m, G_n are nilpotent groups then G is nilpotent
- (c) If G_m, G_n have an abelian automorphism group then G has an abelian automorphism group

Proof: (a) Since $G = G_m G_n$ then G is solvable if and only if G_m, G_n are solvable

(b) Suppose that G_m, G_n are nilpotent groups then $G_m G_n$ is nilpotent so G is.

(c) Suppose that G_m, G_n have an abelian automorphism group , G_m and G_n are characteristic subgroups of G then for each $f \in \text{aut}(G)$ we have $f \in \text{aut}(G_m) \cap \text{aut}(G_n)$, now there are two integers a,b such $am+bn=1$ and $\forall f, g \in \text{aut}(G)$ and for an arbitrary element $x \in G$ we have $f \circ g(x) = f \circ g(x^{am} x^{bn}) = f \circ g((x^a)^m) f \circ g((x^b)^n) = g \circ f((x^a)^m) g \circ f((x^b)^n) = g \circ f(x^{am} x^{bn}) = g \circ f(x)$ so G has an abelian automorphism group

4.5. Theorem

Let G be a monic group then G is cyclic if and only if G_m, G_n are cyclic

Proof: If G is cyclic then it is monic with cyclic G_m, G_n . Conversely suppose that G_m, G_n are cyclic then they are nilpotent so G is nilpotent and G is a direct product of its Sylow subgroups, let P_i be the (i-th) Sylow subgroup of this product with order p^s then P_i is (m-cyclic) and (n-cyclic) , because p is a prime we find that $\gcd(m,p)=1$ or $\gcd(n,p)=1$, without affecting the generality we assume that $\gcd(m,p)=1$

so $(P_i)_m = P_i$ and P_i must be cyclic. By cyclicity of G_m, G_n we find that they have an abelian automorphism group so G is a direct product of cyclic groups with abelian automorphism group then G must be cyclic.

4.6. Theorem

Let G be a monic group then G is abelian if and only if G_m, G_n are abelian

Proof: If G is abelian then it is monic with abelian G_m, G_n . Conversely suppose that G_m, G_n are abelian then they are nilpotent so G is nilpotent and G is a direct product of its Sylow subgroups, let P_i be the $(i$ -th) Sylow subgroup of this product with order p^s then P_i is $(m$ -abelian) and $(n$ -abelian), because p is a prime we find that $\gcd(m, p) = 1$ or $\gcd(n, p) = 1$, without affecting the generality we assume that $\gcd(m, p) = 1$ so $(P_i)_m = P_i$ and P_i must be abelian. So G is a direct product of abelian groups so G is abelian

4.7. Theorem

Let G be a finite nilpotent group then G is monic [5]

Proof: Assume that G is nilpotent then $G = P_1 \times P_2 \times \dots \times P_n$ where P_i is a Sylow subgroup with order $p_i^{k_i}$, we put $m = p_1^{k_1}$ and $n = p_2^{k_2}$ then $G_m = P_2 \times \dots \times P_n$ and $G_n = P_1 \times P_3 \times \dots \times P_n$ so G is a monic group since $\gcd(n, m) = 1$

[6]

4.8. Theorem

The direct product of two monic groups is again a monic group.

Proof: Holds directly from theorem (1.2)

5. Conclusions

In this article, we have studied m -groups and determined the sufficient condition of a group G to be an m -group. Also, we have defined and studied Monic groups in particular.

Funding "This research received no external funding"

Conflicts of Interest: "The authors declare no conflict of interest."

References

- [1] L. Kappe, J. Ying. On exact power margin groups. *Rend. Sem. Mat. University of Padova.*, **1992**, 87, 245-265. DOI:10.5486/PMD.1992.4779
- [2] J. Rotman, "The Theory of Groups", University of Illinois, Urbana., **1971**, 120-173. DOI:10.1007/978-1-4612-4176-8
- [3] F. Levi. Notes on Group Theory, *J. Indian Math. Soc.*, **1944**, 8, 1-7. DOI: [10.4153/CJM-1969-136-1](https://doi.org/10.4153/CJM-1969-136-1)
- [4] M. Hushi. The Algebraic Structures. Tishreen university press., **2004**, 217-233.
- [5] K. Dorek, T. Hawkes. Finite Soluble Groups", Walter de Gruyter, Berlin, **1992**.



Study on Adjacency Matrix for Flow

Hend El-Morsy

Department of Mathematics, Umm Al-Qura University, Mecca, Kingdom of Saudi Arabia.

ARTICLE INFO

Article History:

Submission date: 15/09/2019

Accepted date: 11/08/2020

Keywords:

Adjacency matrix, flow.

ABSTRACT

In this paper, we introduced the adjacency matrix for flow problems and its cases, then we discussed how could we computed max flow by using this matrix.

1. Introduction

Adjacency matrix: In graph theory and computer science, an adjacency matrix is a square matrix used to represent a finite graph. The elements of the matrix indicate whether pairs of vertices are adjacent or not in the graph [1].

Max flow: In optimization theory, maximum flow problems involve finding a feasible flow through a single-source, single-sink flow network that is maximum [2,3].

2. Results and discussion

The adjacency matrix for flow problems take the shape:

$$\begin{bmatrix} A_{11} & A_{21} & A_{31} & \dots & A_{n1} \\ A_{12} & A_{22} & A_{23} & \dots & A_{n2} \\ A_{13} & A_{23} & A_{33} & \dots & A_{n3} \\ \vdots & \vdots & \vdots & \ddots & \vdots \\ A_{1n} & A_{2n} & A_{3n} & \dots & A_{nn} \end{bmatrix}$$

Where all values of this matrix take values as follow:

$$\begin{bmatrix} 0 & 0 & 0 & 0 & 0 \\ A_{12} & 0 & 0 & 0 & 0 \\ A_{13} & A_{23} & 0 & 0 & 0 \\ \vdots & A_{24} & \vdots & 0 & 0 \\ 0 & 0 & A_{3n} & A_{4n} & 0 \end{bmatrix}$$

Values of A_{1n-1} , A_{1n} , A_{2n} equals 0.

- Each path of flow can be illustrated as the same matrix.
- We can compute max flow from this matrix by eliminating all other columns from the matrix except the columns of associated path, and

then subtract the lowest flow from each weight of the associated matrix.

We can write these computations as algorithm as follows:

Algorithm:

Input: Adjacency matrix M_i of flow F .

1. Let P_1 be the first path from source (S) to sink (T), M_1 is the adjacency matrix for P_1 .

a. Select the lowest flow X_1 on P_1 .

b. Subtract X_1 from all elements on M_1 .

2. IF there exist P_i from S to T,

Return to step 1,

Else,

Output P,

End algorithm.

Example 1:

For graph shown in Fig.(1) draw the associated adjacency matrix, then find max flow.

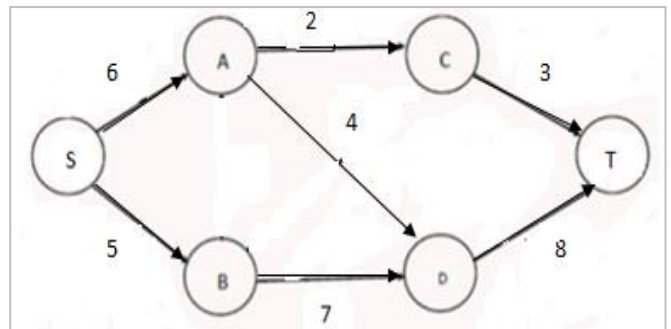


Figure 1:

The adjacency matrix will be:

$$\begin{bmatrix} S & A & B & C & D & T \\ 0 & 0 & 0 & 0 & 0 & 0 \\ 6 & 0 & 0 & 0 & 0 & 0 \\ 0 & 2 & 0 & 0 & 0 & 0 \\ 5 & 0 & 0 & 0 & 0 & 0 \\ 0 & 4 & 0 & 7 & 0 & 0 \\ 0 & 0 & 3 & 0 & 8 & 0 \end{bmatrix}$$

Subtract 2 from P_1 (SABT)

* Corresponding Author

D Department of Mathematics, Umm Al-Qura University, Mecca, Kingdom of Saudi Arabia.

E-mail address: hendelmorsy@yahoo.com (Hend El-Morsy).

1685-4732 / 1685-4740 © 2020 UQU All rights reserved.

$$\begin{vmatrix} S & A & B & T \\ 0 & 0 & 0 & 0 \\ 4 & 0 & 0 & 0 \\ 0 & 0 & 0 & 0 \\ 0 & 0 & 1 & 0 \end{vmatrix}$$

Subtract 4 from P₂ (SADT)

$$\begin{vmatrix} S & A & D & T \\ 0 & 0 & 0 & 0 \\ 0 & 0 & 0 & 0 \\ 0 & 0 & 0 & 0 \\ 0 & 0 & 4 & 0 \end{vmatrix}$$

Subtract 4 from P₃(SCDT)

$$\begin{vmatrix} S & C & D & T \\ 0 & 0 & 0 & 0 \\ 1 & 0 & 0 & 0 \\ 0 & 3 & 0 & 0 \\ 0 & 0 & 4 & 0 \end{vmatrix}$$

Then max flow = 2 + 4 + 4 = 10.

Example 2:

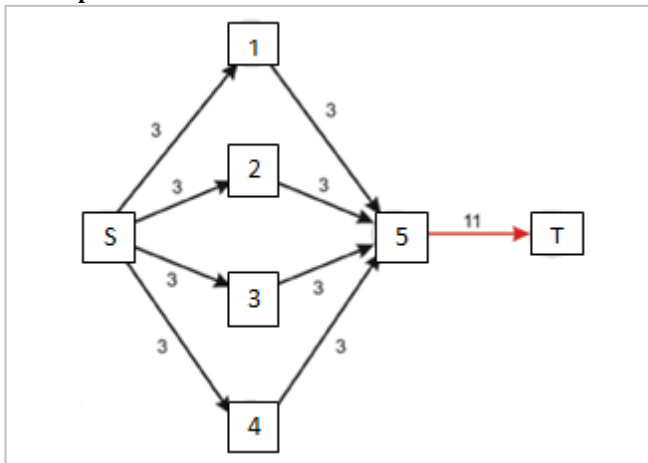


Figure 2:

The adjacency matrix for graph in Fig.(2) is:

$$\begin{vmatrix} S & 1 & 2 & 3 & 4 & 5 & T \\ 0 & 0 & 0 & 0 & 0 & 0 & 0 \\ 3 & 0 & 0 & 0 & 0 & 0 & 0 \\ 3 & 0 & 0 & 0 & 0 & 0 & 0 \\ 3 & 0 & 0 & 0 & 0 & 0 & 0 \\ 3 & 0 & 0 & 0 & 0 & 0 & 0 \\ 0 & 3 & 3 & 3 & 3 & 0 & 0 \\ 0 & 0 & 0 & 0 & 0 & 11 & 0 \end{vmatrix}$$

Subtract 3 from P₁(S15T),

$$\begin{vmatrix} S & 1 & 5 & T \\ 0 & 0 & 0 & 0 \\ 0 & 0 & 0 & 0 \\ 0 & 0 & 0 & 0 \\ 0 & 0 & 0 & 0 \\ 0 & 0 & 8 & 0 \end{vmatrix}$$

Subtract 3 from P₂(S25T)

$$\begin{vmatrix} S & 2 & 5 & T \\ 0 & 0 & 0 & 0 \\ 0 & 0 & 0 & 0 \\ 0 & 0 & 0 & 0 \\ 0 & 0 & 5 & 0 \end{vmatrix}$$

Subtract 3 from P₃(S35T)

$$\begin{vmatrix} S & 3 & 5 & T \\ 0 & 0 & 0 & 0 \\ 0 & 0 & 0 & 0 \\ 0 & 0 & 0 & 0 \\ 0 & 0 & 2 & 0 \end{vmatrix}$$

Subtract 2 from P₄(S45T)

$$\begin{vmatrix} S & 4 & 5 & T \\ 0 & 0 & 0 & 0 \\ 1 & 0 & 0 & 0 \\ 0 & 1 & 0 & 0 \\ 0 & 0 & 2 & 0 \end{vmatrix}$$

Then max flow = 3 + 3 + 3 + 2 = 11.

Theorem1:

In flow problems, if there exist a cycle flow in a sink such that the addition of two flows equal to the third, then the adjacency matrix of path containing these nodes have negative numbers.

Example 3:

The adjacency matrix for graph shown in Fig. (3) is:

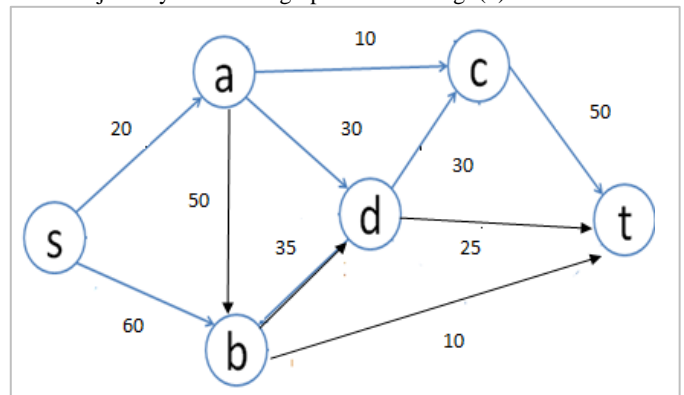


Figure 3:

$$\begin{vmatrix} S & a & b & d & c & t \\ 0 & 0 & 0 & 0 & 0 & 0 \\ 20 & 0 & 0 & 0 & 0 & 0 \\ 60 & 50 & 0 & 0 & 0 & 0 \\ 0 & 30 & 35 & 0 & 0 & 0 \\ 0 & 10 & 0 & 30 & 0 & 0 \\ 0 & 0 & 10 & 25 & 50 & 0 \end{vmatrix}$$

Subtract 10 from path (sact)

$$\begin{vmatrix} S & a & c & t \\ 0 & 0 & 0 & 0 \\ 10 & 0 & 0 & 0 \\ 0 & 0 & 0 & 0 \\ 0 & 0 & 40 & 0 \end{vmatrix}$$

Subtract 10 from (sbt)

S	b	t
0	0	0
50	0	0
0	0	0

Then subtract 10 from (sadt)

S	a	d	t
0	0	0	0
0	0	0	0
0	20	0	0
0	0	15	0

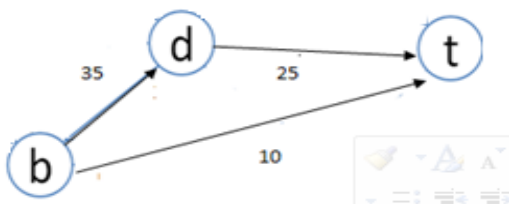
Then subtract 15 from (sbd)

S	b	d	t
0	0	0	0
35	0	0	0
0	20	0	0
0	0	0	0

Finally, subtract 20 from (sbdct)

S	b	d	c	t
0	0	0	0	0
15	0	0	0	0
0	0	0	0	0
0	0	10	0	0
0	-20	-20	20	0

From the above theorem,
The flow graph contain a cycle such that:



$bt + dt = bd$
Then there exist negative numbers (of red colour) in the adjacency matrix containing nodes b, d, t.

Example 4:

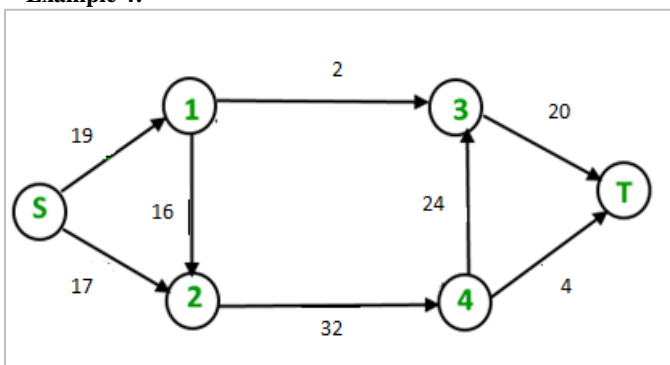


Figure 4:

The adjacency matrix is:

S	1	2	4	3	t
0	0	0	0	0	0
19	0	0	0	0	0
17	16	0	0	0	0
0	0	32	0	0	0
0	2	0	24	0	0
0	0	0	4	20	0

Subtract 2 from (s13T)

S	1	3	T
0	0	0	0
17	0	0	0
0	0	0	0
0	0	18	0

Then subtract 4 from (S24T)

S	2	4	T
0	0	0	0
13	0	0	0
0	28	0	0
0	0	0	0

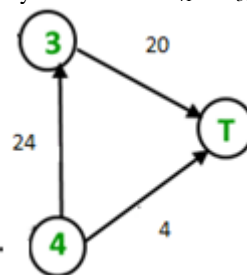
Subtract 13 from (S243T)

S	2	4	3	T
0	0	0	0	0
0	0	0	0	0
0	15	0	0	0
0	0	11	0	0
0	0	-13	5	0

Finally subtract 5 from (S1243T)

S	1	2	4	3	T
0	0	0	0	0	0
12	0	0	0	0	0
-5	11	0	0	0	0
0	0	10	0	0	0
0	-5	0	6	0	0
0	0	0	-5	0	0

There exist cycle such that $x_{4T} + x_{3T} = x_{43}$



References

- [1] R. J. Wilson. Introduction to graph theory. Oliver and Boyd, Edinburgh 1972.
- [2] V. Goldberg, É. Tardos, R.E. Tarjan, Network flow algorithms, Tech. Report STAN-CS-89-1252, Stanford University CS Dept., 1989
- [3] Schrijver, On the history of the transportation and maximum flow problems. Mathematical Programming, 2002, 91, 437–445. (DOI) [10.1007/s101070100259](https://doi.org/10.1007/s101070100259)